DESIGN, CONTROL, AND EVALUATION OF A SPATIAL

ACTIVE HANDREST FOR PROVIDING ERGONOMIC

SUPPORT AND GRAVITY COMPENSATION OVER A

LARGE WORKSPACE

by

Hamidreza Najafi Sani

The University of Utah Graduate School

STATEMENT OF DISSERTATION APPROVAL

The dissertation of   **Hamidreza Najafi Sani**

has been approved by the following supervisory committee members:

William Provancher	, Chair	**8/11/2014** Date Approved
Jake Abbott	, Member	**8/11/2014** Date Approved
Andrew Merryweather	, Member	**8/11/2014** Date Approved
Donald S. Bloswick	, Member	**8/11/2014** Date Approved
David E. Johnson	, Member	**8/11/2014** Date Approved

and by   **Tim Ameel**   , Chair/Dean of

the Department/College/School of   **Mechanical Engineering**

and by David B. Kieda, Dean of The Graduate School.

ABSTRACT

Most humans have difficulty performing precision tasks, such as writing and painting, without additional physical support(s) to help steady or offload their arm's weight. To alleviate this problem, various passive and active devices have been developed. However, such devices often have a small workspace and lack scalable gravity compensation throughout the workspace and/or diversity in their applications.

This dissertation describes the development of a Spatial Active Handrest (SAHR), a large-workspace manipulation aid, to offload the weight of the user's arm and increase user's accuracy over a large three-dimensional workspace. This device has four degrees-of-freedom and allows the user to perform dexterous tasks within a large workspace that matches the workspace of a human arm when performing daily tasks. Users can move this device to a desired position and orientation using force or position inputs, or a combination of both. The SAHR converts the given input(s) to desired velocities and commands corresponding motors using an admittance controller. This work builds on research of a previous two-degree-of-freedom robotic handrest.

To achieve this goal, the Vertical Active Handrest (VAHR), a one degree of freedom (DOF) handrest, was designed and constructed to investigate the benefit of providing support in only the vertical direction. Providing support in the vertical axis is more challenging than the horizontal plane since one must account for the effect of gravity. A series of experiments were conducted to develop various control strategies and evaluated

the user's performance with these controllers versus other unassisted support conditions. The Vertical Active Handrest was found to reduce participants mean absolute tracing error and improve their skill level.

Next, the Enhanced Planar Active handrest (E-PAHR) was developed, which extended the workspace of the prior two-degree-of-freedom planar Cartesian handrest (PAHR) and better matched the kinematics of the human arm. This was achieved by adding a rotational DOF to allow for forearm rotation within the horizontal plane. Various control strategies were examined through a series of human-subject experiments and found multiple controllers that provided more natural interaction with the device than the PAHR while matching the PAHR's skill level.

Finally, the Spatial Active Handrest (SAHR) was developed by adding an elevation axis to the E-PAHR to extend its workspace to the third dimension. The effect of various control strategies and virtual fixtures were investigated and a controller that permits natural user interaction, high accuracy, and low muscle fatigue was identified. The SAHR was shown to improve a user's accuracy beyond unassisted support conditions while preventing fatigue compared to the unassisted support conditions.

TABLE OF CONTENTS

LIST OF TABLES

ACKNOWLEDGMENTS

CHAPTER 1

INTRODUCTION

Humans have traditionally used various supports during tasks that require dexterous hand motions to increase stability and reduce muscle fatigue. For instance, humans use a table surface to stabilize the wrist while writing as a way to increase precision and reduce fatigue resulting from the person's arm weight. One of drawbacks of static supports is the need for repositioning them during tasks that have a large workspace. For this reason, movable supports are developed to enlarge the user's dexterous workspace. An example of a movable support is a maulstick, which is used by painters to reduce fatigue and to steady their hands in order to increase accuracy over a large canvas. Research has shown such repositionable static supports reduce muscle fatigue by eliminating the weight of a user's arm [1] or a grasped tool [2]. In order to utilize the aforementioned, many passive supports have been designed with the purpose of reducing muscle fatigue. These devices use either a spring and linkage mechanism [3] or cable suspension [4] to support the weight of the user's arm. Some of the most widely used passive devices – e.g. Balanced Forearm Support [5] and Mobile Arm Support [6] – do not allow for convenient scalable gravity compensation. However, in recent years a few passive devices have been developed using counterweights [7] or a spring system [8] to provide scalable gravity compensation. Compared to passive supports, active supports allow for convenient scalable gravity

compensation that could automatically adjust to a new user with no required adjustments [9]. Robotic devices with active support are commonly used for rehabilitation purposes and assisting in tasks that require dexterous motions.

Another area of research related to our device design is rehabilitation robots, which are designed to help users regain lost motor functions. Riener et al. have shown that a repetitive task-oriented motion is an effective means of upper arm rehabilitation [10]. Traditionally, a therapist is used to support and guide the patient through each rehabilitation session. However, robotic devices are becoming more popular as it is easier to motivate patients using virtual environments and games to achieve high intensity rehabilitation, which is shown to statistically improve rehabilitation of stroke patients [11]. Other benefits of such rehabilitation devices are improving ADL and grip strength throughout the first year after stroke [12] and increasing elbow extensions in the horizontal plane using active gravity support of the arm [9].

Common designs of rehabilitation robots include end point manipulation and powered exoskeletons. Examples of popular endpoint manipulation devices used for rehabilitation include MIT Manus [13], GENTLE/S [14], and PUMA 560 [15], which help to guide a user's arm along a predefined trajectory to regain lost motor skills in their arm. In contrast to end point manipulation interfaces, exoskeletons are anthropomorphic robots that are tightly connected to the human arm and its joint angles fully define a human arm's pose. An example of such a robotic device is the ARMin III [16], which can be attached to a chair or wheelchair to supply gravity compensation [17].

Another area of related research is the use of robotic devices to assist able bodied and disabled users in performing dexterous tasks. The Steady Hand, a robotic system developed

at Johns Hopkins University, helps users with submillimeter manipulation tasks by simultaneously taking force input from the user and a robot to move the tool accordingly [18]. Cobot is another example of a device that collaborates with a human to manipulate an object, assisting the operator by constraining motion to a desired trajectory, which requires foreknowledge of its environment [19].

Active and passive devices that have been developed throughout the years to help users with tasks that require dexterous motions have certain limitations. Such devices often suffer from a lack of large workspace, scalable gravity compensation throughout the workspace, and/or diversity in their applications.

This dissertation describes the development of the Spatial Active Handrest (SAHR), which is a four-degree-of-freedom (4-DOF) human-robot cooperative device that improves a user's accuracy, provides ergonomic localized support, and matches the kinematics of human arm over a large three-dimensional workspace. These factors will allow this device to be used in a wide range of applications such as robotic surgery, surgery training, human rehabilitation, and painting. The user can control the SAHR using either the applied force to the force sensor and position inputs from a stylus. It can also use the combination of the two. Admittance control is used to convert the applied input force to a desired velocity to move the stage. Three studies helped us to develop the SAHR from the original Planar Active Handrest (PAHR).

Our first study investigated the effect of providing support in the vertical direction. I designed and constructed a Vertical Active Handrest (VAHR), a one-degree-of-freedom handrest that provided wrist and forearm support over a vertical workspace. In an earlier assessment of VAHR [20], I found users to have significantly higher accuracy using the

position controller with an isotonic elastic controller compared to the force-based admittance controller. I improved the performance of the VAHR under force input by using a forearm support to provide local support and allow force inputs to be provided by small muscle groups in the wrist and hand. This method ensures that only the weight of the hand is applied to the force sensor as the forearm and shoulder are supported by the device's forearm support. However, introducing a forearm support led to a new problem that was mitigated by adapting the controller to account for user hand mass or use of a hand strap after tuning gains. For the pure force-based and position-based controllers, I conducted an experiment to select the controller with the combination of the smallest median tracing error and the shortest completion time, which was the force-based admittance controller with the added forearm support and hand strap. Lastly, I compared this selected controller with other unassisted cases such as unsupported (freehand) and fixed-support (fixed elbow) and found the force-based admittance controller to improve user's skill level beyond other unassisted conditions.

The primary goal of the second study was to develop the Extended Active Handrest E-PAHR, which extends the workspace of PAHR to better match the planar kinematics of human arm in the horizontal plane. To achieve this goal, I added a third DOF to the PAHR to allow for forearm rotation. I used a capstan drive to implement this rotational DOF, which increased the torque of the motor and reduced its angular velocity similar to a pair of gears, but without the vibration and backlash that occurs with meshing gears. Adding a third DOF to control a two DOF human arm, assuming that the shoulder is fixed (a widely used assumption in upper limb motion tracking literature [21],[22]), resulted in an overdefined system. Using such a system with additional joints allowed us to increase the

workspace of the device, reduce its size, increase robustness to singularities, and increase dexterity compared to alternative solutions [23]. I added a second six-axis ATI force sensor under the user's elbow to allow a rotation about the elbow and allow full control of this device and its three DOF. I conducted a series of experiments to compare the performance of developed control strategies and eliminate unnecessary control methods. Finally, I conducted an experiment to identify the trade-offs of matching the kinematics of the human arm by comparing the performance of the selected E-PAHR control strategy to unsupported (freehand), fixed support (elbow support), and best PAHR control strategy.

In our last study, I investigated further extending the workspace of E-PAHR to the third dimension. The resultant device, the SAHR, is a four-DOF assistive robotic device that provides localized support to the user's wrist and elbow over a large three-dimensional workspace.

I conducted a motion capture study to understand the elbow elevation relative to the hand elevation to ensure that the SAHR movement matches the kinematics of human arm within its workspace. Using the results of this experiment, the SAHR was designed to couple the elbow and hand elevation using a single linear lead-screw mechanism.

I conducted a series of experiments to identify the controller paradigms and virtual fixtures that allowed users to have a balance of performance characteristics, with the least tracing error, fastest trial completion time, and most natural arm movement. The addition of virtual fixtures to the SAHR guides users along an intended path [24], prevents them from entering a predefined forbidden region in surgeries [25], and simplifies the task. Lastly, I conducted an experiment to test the SAHR's utility with the best controller strategies and virtual fixtures versus unassisted support conditions. In this experiment, I

also recorded electromyography signals from users' large muscle groups to investigate the claim that SAHR would prevent shoulder fatigue and take the load off large muscle groups in the shoulder.

The combination of all of these studies showed that human-robot cooperative devices, such as the SAHR, could be useful for various applications. One common application is rehabilitation, to help users regain lost motor function, similar to current end point manipulators [26] and powered exoskeletons [27] that assist therapists. Another application suitable for the SAHR is use with surgery robots and assisting surgeons with dexterous tasks [28].

1.1 Contributions

Three main contributions were made throughout this research. This work established and refined a device and control methods for providing support in the vertical direction, identified the trade-offs of allowing more natural arm movements, and extended the workspace of active handrest to the third dimension.

1. Established and refined a device and control methods for providing support in the vertical direction.

> An assistive device for supporting vertical motions was designed, fabricated, and refined. A force-based admittance controller was implemented, improved upon, and proven to be as accurate and have faster completion time than the position-based controller with an isometric admittance term. Three modifications were made to demonstrate the force-base controller's usability. The first modification was adding a forearm support to offload the large muscle

groups in the shoulder. The second modification was strapping the user's arm to the stage to allow them to apply upward forces to improve control in the upward direction. The third modification was to implement a weight-based admittance controller to allow the stage to adjust admittance gains based on the user's arm weight. These modifications demonstrated that the force-based admittance controller could match or improve the user's performance while operating the VAHR compared to the position-based controller. This allows the VAHR to be operated without tracking the user's hand position.

2. Implemented and evaluated a rotary degree of freedom on a planar, Cartesian assistive device to facilitated more natural arm movement.

    The 2-axis Cartesian Active Handrest was retrofitted with a rotary axis to accommodate forearm rotation. Several control input paradigms were implemented and evaluated where user performance was best and was preferred by users when the device motion was modeled as a free body moving with viscous resistance. The addition of natural arm movement was shown to increase participant's comfort level and workspace without degradation in their performance relative to the prior 2-axis Cartesian design.

3. Created and evaluated a spatial assistive device to extend the workspace of the active handrest to the third dimension.

    The workspace of the Active Handrest was extended beyond the planar dimension. The elbow and wrist elevations were found to be significantly coupled, which ruled out the need for an independent control of the elevation at both locations. The device design takes advantage of this finding to couple the

motion of the user's hand and elbow elevation to make a simpler 4-DOF design possible. Of the controllers implemented, the free body controller again performed the best and was preferred by users. Further improvements in user performance were made by implementing virtual fixtures to confine the handrest motions to a tangent plane or path. The resulting device led to statistically improved performance; however, users preferred the unrestricted spatial active handrest movements to the use of virtual fixtures despite this improvement.

1.2 Chapter Overview

Chapter 2 explains the development of the Vertical Active Handrest (VAHR) and how this device was used to investigate the complications of applying gravity compensation to the user. To investigate this I explored the use of a forearm rest to support the user's arm throughout its workspace and reduced muscle activity of large muscle groups in the shoulder. Our second goal of this work was to determine if the force-based admittance controller could be improved to be as good as or better than a position controller with isotonic elastic stylus coupling. Doing so would increase the device's utility, as it would remove the need for a specialized tool with a known position relative to the stage. Chapter 2 describes various experiments that were conducted to optimize the controllers used in combination with the VAHR and the results obtained from each. The final experiment of this chapter compares the device's utility when compared to other nonassisted support conditions and identifies changes in skill levels across each support condition.

Chapter 3 demonstrates the enhancements of the Planar Active Handrest's (PAHR's)

workspace by adding a third degree-of-freedom to allow for forearm rotation in an attempt to better match the kinematics of a human arm. While increasing the user's comfort was an important goal of Chapter 3, it was also important to ensure that these improvements did not decrease the user's accuracy or skill level while using the stage. Seven different control strategies are proposed to control the device. An experiment was conducted to determine the controller strategy with the most effective user performance and preference based on subjective feedback. In the final experiment, the selected best controllers were compared to various unassisted support conditions to demonstrate the devices utility. Furthermore, a Planar Active Handrest condition is also among the tested support conditions to ensure that the added improvements did not degrade our main goal of developing a device that allows users to improve their task accuracy.

Chapter 4 demonstrates a further improvement of the Active Handrest and adding a vertical-degree-of-freedom that extended its workspace to the third dimension. This chapter combines our results and findings from previous chapters in the following ways: the Spatial Active Handrest (SAHR) will provide an ergonomic localized support over a large workspace, only force input will be used to control the device to improve device utility and reduce cost, and all the improvements are built on top of the previous Enhanced Planar Active Handrest (E-PAHR) from Chapter 3. To design a device that provides an ergonomic support over a large three-dimensional workspace I conducted an arm motion study. This study investigates whether the elbow elevation could be coupled with hand elevation or if a fifth-degree-of-freedom should be included. The most efficient controllers from Chapter 3 and other virtual fixtures were tested on the device through multiple experiments. The last experiment of this chapter compares the best control strategy and

virtual fixtures from the previous experiments versus unassisted support conditions. An electromyography (EMG) signal of the users' upper arm was recorded during this experiment to investigate whether using the device reduces muscle activity of the large muscle groups in the shoulder.

Chapter 5 summarizes and presents the results of this research and talks about future plans to commercialize the SAHR.

1.3 References

[1]   A. Erdelyi, T. Sihvonen, P. Helin, and O. Hanninen, "Shoulder strain in keyboard workers and its alleviation by arm supports," *Int. Arch. Occup. and Environ. Health*, vol. 60, no. 2, pp. 119–124, 1988.

[2]   Equipois. ZeroG. Available: "http://www.equipoisinc.com".

[3]   G. Kramer, G. R. B. E. Römer, and H. J. A. Stuyt, "Design of a Dynamic Arm Support (DAS) for gravity compensation," in Proc. *IEEE 10th Int. Conf. Rehabilitation Robotics*, Noordwijk, The Netherlands, 2007, pp. 1042–1048.

[4]   A.H.A. Stienen, E.E.G. Hekman, F.C.T. Van der Helm, G. B. Prange, M. J.A. Jannink, A.M.M. Aalsma, and H. Van der Kooij, "Freebal: dedicated gravity compensation for the upper extremities," in Proc. *IEEE 10th Int. Conf. Rehabilitation Robotics*, Noordwijk, The Netherlands, 2007, pp. 804–808.

[5]   S. B. Chyatte, C. Long 2nd, and P. J. Vignos Jr., "The balanced forearm orthosis in muscular dystrophy," *Arch. Phys. Med. Rehabil.*, vol. 46, pp. 633–636, 1965.

[6]   Y.L. Yasuda, K. Bowman, and J. Hsu. "Mobile arm supports: criteria for successful use in muscle disease patients," *Arch. Phys. Med. Rehabil.*, vol. 67, pp. 253–256, 1986.

[7]   J.L. Herder, "Development of a Statically Balanced Arm Support: ARMON," in Proc. *IEEE 9th Int. Conf. Rehabilitation Robotics*, Chicago, 2005, pp. 281–286.

[8]   R. J. Sanchez, J. Liu, S. Rao, P. Shah, R. Smith, T. Rahman, S. C. Cramer, J. E. Bobrow, and D. Reinkensmeyer, "Automating arm movement training following severe stroke: functional exercise with quantitative feedback in a gravity-reduced environment," IEEE Trans. Neural. Sci. Rehabil. Eng., vol. 1, pp. 378–389, 2006.

[9]   R. F. Beer, M. D. Ellis, B. G. Holubar, J. P.A. Dewald. "Impact of gravity loading on post-stroke reaching and its relationship to weakness." *Muscle. Nerve.*, vol. 36, no. 2, pp. 242–250, 2007.

[10]   R. Riener, T. Nef, and G. Colombo. "Robot-aided neurorehabilitation of the upper extremities." *Med. Biol. Eng. Comput.*, vol 43, no. 1, pp. 2–10, 2005.

[11]   G. Kwakkel, R. Wagenaar, T. Koelman, G. Lankhorst, and J. Koetsier. "Effects of intensity of rehabilitation after stroke: a research synthesis," *Stroke,.* vol. 28, no. 8, pp. 1550–1556, 1997.

[12]   B. Langhammer, B. Lindmark, and J. K. Stanghelle. "Stroke patients and long-term training: is it worthwhile? A randomized comparison of two different training strategies after rehabilitation," *Clinical Rehabil.*, vol. 21, no. 6 pp. 495–510, 2007.

[13]   Hogan N., "Impedance control : an approach to manipulation," *J. Dyn. Sys. Meas. Control*, vol. 107, no. 1, p. 1, 1985.

[14]   R. Loureiro, F. Amirabdollahian, M. Topping, B. Driessen, and W. Harwin. "Upper limb robot mediated stroke therapy—GENTLE/s approach," *Auto. Robots.*, vol. 15, no. 1, pp. 35–51, 2003.

[15]   P. S. Lum and C. G. Burgar, "Robot-assisted movement training compared with conventional therapy techniques for the rehabilitation of upper-limb motor function after stroke." *Arch. Phy. Med., Rehabil.*, vol. 83, no. 7, pp. 952–959, 2002.

[16]   T. Nef, M. Guidali, and R. Riener. "ARMin III – Arm therapy exoskeleton with an ergonomic shoulder actuation," *Applied Bionics and Biomech.*, vol, 6, no. 2, pp. 127–142, 2002.

[17]   S. Moubarak, M. Pham, R. Moreau, and T. Redarce. "Gravity compensation of an upper extremity exoskeleton," *Conf. Proc. IEEE Eng. Med. Biol. Soc. (EMBC)*, pp. 4489–4493, 2010.

[18]   R. Taylor, P. Jensen, L. Whitcomb, A. Barnes, R. Kumar, D. Stoianovici, P. Gupta, Z. Wang, E. Dejuan, and L. Kavoussi, "A Steady-Hand robotic system for microsurgical augmentation," *Int. J. Robotics Research*, vol. 18, pp. 1201–1210, 1999.

[19]   J. Colgate, W. Wannasuphoprasit, and M. Peshkin, "Cobots: robots for collaboration with human operators," *Proc. Int. Mech. Eng. Cong. Exhib.*, vol. DSC-58, pp. 433–440, 1996.

[20]   C. A. Stewart, "A Vertical Active Handrest to aid in dexterous tasks and to

provide gravitational support." M.S. thesis, Dept. Mech. Eng., Univ. Utah, Salt Lake City, UT, 2012.

[21]   L. Goncalves, E. Di Bernardo, E. Ursella, and P. Perona, "Monocular tracking of the human arm in 3D," *Proc. Fifth Int. Conf. Computer Vision*, pp. 764–770, 1995.

[22]   T. B. Moeslund and E. Granum, "Multiple cues used in model-based human motion capture," *Proc. Fourth IEEE Int. Conf. Auto. Face and Gesture Recognition*, pp. 362–367, 2000.

[23]   M. Ueberle, N. Mock, and M. Buss. "VISHARD10, a novel hyper-redundant haptic interface." *12th Int Symp. Haptic Interf. Virt. Environ. Teleop. Sys.*, pp. 58–65, 2004.

[24]   A. Bettini, P. Marayong, S. Lang, A.M. Okamura, and G.D. Hager, "Vision-assisted control for manipulation using virtual fixtures," *IEEE Trans. Robotics*, vol. 20, pp. 953-966, 2004.

[25]   J. Abbott, P. Marayong, and A. Okamura, "Haptic virtual fixtures for robot-assisted manipulation," *Robotics Research*, vol. 28, pp. 49-64, 2007.

[26]   N. Hogan, H. I. Krebs, A. Sharon, and J. Charnnarong, Interactive robotic therapist. US Patent 5,466,213, Massachusetts Institute of Technology, 1995.

[27]   T. Nef, M. Guidali, and R. Riener. "ARMin III – Arm therapy exoskeleton with an ergonomic shoulder actuation." *Applied Bio. Biomech.,* vol 6, no. 2, 127–142, 2009.

[28]   R. Taylor, P. Jensen, L. Whitcomb, A. Barnes, R. Kumar, D. Stoianovici, P. Gupta, Z. Wang, E. Dejuan, and L. Kavoussi, "A Steady-Hand robotic system for microsurgical augmentation," *Int. J. Robotics Research*, vol. 18, pp. 1201-1210, 1999.

CHAPTER 2

VERTICAL ACTIVE HANDREST FOR GRAVITY

COMPENSATION AND LOCAL SUPPORT

Dynamic handrests such as the Planar Active Handrest have been shown to be beneficial for large workspace planar tasks. However, providing precision support in the vertical direction proves to be challenging. The Vertical Active Handrest (VAHR) is designed to add gravitational support over a large workspace for tasks that require dexterous motions. Two input methods have been proposed for controlling the motion of the VAHR: tool position input and force input, measured at the handrest. This chapter presents several modified force input controllers with improved performance compared to a stylus position input controller. User performance with these control schemes is evaluated using a precision two-dimensional drawing task that includes vertical and lateral motions. The best VAHR support condition, which uses a forearm support and hand strap on the force sensor, is benchmarked against user performance under freehand and fixed elbow support conditions using the same vertical two-dimension drawing task. The results show a significant reduction in error when using the VAHR under force input control with a hand strap and forearm support.

2.1 Introduction

Performing a task that requires precision manipulation or holding a heavy tool for a long period can result in poor performance and upper extremity fatigue. Static supports, such as a table, have been used as hand or arm rests to help steady one's motions. Ito and Yokokohji [1] suggest that resting upper extremities on a support reduces muscle fatigue. However, the drawback to using a static support is that the workspace is limited to the wrist's range of motion, and intermittent repositioning of the arm is required for larger workspace tasks.

In a prior study at the University of Utah, a Planar Active Handrest was developed to assist with large workspace precision manipulation in the horizontal plane [2]. This device was shown to improve a user's precision versus their performance under freehand and fixed hand/elbow support conditions. However, this device is currently limited to horizontal planar tasks, and our end goal with designing the Vertical Active Handrest (VAHR) is to extend the workspace of the current device to the vertical dimension.

The VAHR is a single-degree-of-freedom (DOF) human-robot cooperative interface that adds gravitational and ergonomic support to aid in dexterous tasks over a large vertical workspace, similar to that achieved when moving the hand from a fixed elbow rest (going beyond this range also requires repositioning the user's torso). This device measures the desired motion of the user to provide appropriate wrist and/or forearm support. Two input methods have been proposed for controlling the motion of the VAHR: tool position input and force input, measured at the handrest. Both of these inputs are used to specify a desired velocity to reposition the device. In a previous study of this device, a position-based controller, which measured the position of the input stylus, was shown to reduce error in

dexterous tasks compared to freehand [3]. I propose to improve the performance of the VAHR under force input by using the following modifications: 1) add a forearm support to provide local support, 2) implement a hand-weight-based admittance gain, or 3) strap the user's arm to the handrest to allow the user to apply tensile forces to the force sensor at the handrest.

This chapter presents two preliminary and two main experiments to evaluate the performance of the VAHR in assisting users with precision tasks throughout its workspace. I used the preliminary experiments to fine-tune the gains of VAHR controllers in order to improve their performance in a two-dimensional vertical tracing task. The first main experiment compares various VAHR controllers against each other to determine the controller with the best speed-accuracy performance, with the main objective of high accuracy. The second experiment evaluates the performance of the best support condition from the first experiment versus fixed support (fixed elbow) and unsupported (freehand) conditions.

Our future goal is to integrate the results of this research and that of prior work with a Planar Active Handrest [2] into a three dimensional Spatial Active Handrest. Potential applications of this and similar devices are to assist persons with disabilities such as cerebral palsy or spinal muscular atrophy in performing basic activities of daily life (eating, lifting the arm, etc.) and to aid in upper extremity rehabilitation [cf., 4, 5]. This device could also be used by healthy users to increase their accuracy and precision and reduce fatigue in dexterous tasks such as surgery, painting, or holding a tool for an extended period.

2.2 Background

Different tools and methods have been used throughout the years to add support to a person's arm while he/she performs a dexterous task. A simple example of such support is the use of a table while writing to stabilize the wrist, increase precision, and reduce fatigue resulting from the person's arm weight. Another example is a maulstick, which is used by painters to reduce fatigue and steady their hands in order to increase accuracy for fine details over a large canvas.

Several studies have shown the benefits of using a static and/or moving arm support. Cook and Burgess-Limerick [6] demonstrated that while using mouse and keyboard, a forearm support is preferable and reduces musculoskeletal discomfort compared to a nonsupported posture. Repositionable supports are shown to reduce muscle fatigue by eliminating the weight of the arm [7],[8]. In addition to reducing the gravity load on the user, Ito and Yokokohji [1] demonstrated that an armrest reduces muscle fatigue by decreasing the grip force.

With these advantages, there has been many passive devices developed to help users with performing daily tasks. The EZ Rest painting hand rest is an example of a repositionable passive device that takes the place of a maulstick to aid with painting and reduces fatigue caused by holding the brush for a long period of time [9]. In a combined research project, the University of California and Lawrence Berkeley National Laboratory developed a three-DOF passive arm support with the goal of reducing muscle load for static and dynamic tasks [10]. This spring-loaded support succeeded in reducing muscle activity for tasks requiring horizontal arm motions, but was unsuccessful at lowering muscle load for tasks requiring vertical arm motions. Similarly, many robotic devices have been

developed over the years with the potential goals of increasing precision, reducing muscle fatigue, aiding disabled users, and providing a rehabilitation interface. I evaluate the potential for the first of these objectives, increased precision, herein.

Admittance-type robotic devices are used for human interaction with precise control. Such devices are nonbackdriveable and measure the input forces of the user to determine the desired velocity of the admittance device. The Planar Active Handrest [2], developed at the University of Utah, is an example of an Admittance-type human-robot cooperative manipulator that can be used in applications that require precision hand motion. The steady-hand, another admittance-type robotic system developed at Johns Hopkins University to help users with submillimeter manipulation tasks, simultaneously uses force input from the user and virtual constraint information and moves the tool accordingly [11]. This device cooperatively controls the tool to increase precision while the user performs a task, but it does not support the user's arm to reduce fatigue.

When controlling an admittance-type device, Nambi et al. [12] demonstrate that although the velocity limit and admittance gain of a device affects the force control accuracy, the input force is the most important factor. However, human force control and precision deteriorate at very low forces. This can be avoided by using a force deadband to stop the stage's motion at force levels below a certain threshold. After considering the effect of the input force, admittance gain and velocity are both important as the users find it more difficult to control how much force is being applied when the device is too responsive (i.e., has too high of an admittance gain). Nambi et al. [12] suggest that a low admittance gain is required to achieve the highest level of precision. However, Wise and Shadmehr [13] have shown that while a low admittance gain results in the highest level of

precision, a sluggish device results in the user exerting higher forces than necessary and thus in operator fatigue. These findings suggest that there is an ideal range of forces, admittance gains, and velocities for optimal human control and that every controller needs to be tuned appropriately to achieve admittance gains that have optimal performance and is least fatiguing on the user.

Researchers have developed various methods and tasks to evaluate the performance of assistive devices. Virtual environments are often used to assess the benefits and drawbacks of using robotic devices and their control methods for interacting with humans. Some examples of such environments are line tracing [14], labyrinth navigation [15], membrane piercing [16], pursuit tracking [17], pick and place [15], and grip tasks [18]. In a previous assessment of the VAHR [3], the device's performance was evaluated using a pursuit-tracking task, which is often used in aviation research to analyze pilot behavior [19]–[21]. However, this task was found to be biased by the user's reaction time and frequency response [3], which did not fully capture the accuracy improvements of the VAHR over the unassisted support conditions due to its time-based nature. The VAHR was designed with a low admittance gain to damp out a user's motions; hence, a task that focuses mostly on user's accuracy while keeping time as an evaluating factor is required. As a result, I believe that a tracing task is a more suitable task in evaluating the VAHR's ability in improving accuracy similar to what is shown by Fehlberg et al. [2].

2.3 VAHR Device Design

The VAHR (Figure 2.1) uses a single-axis linear stage that is oriented vertically. The operator can control the motion of the vertical stage using two possible input strategies:
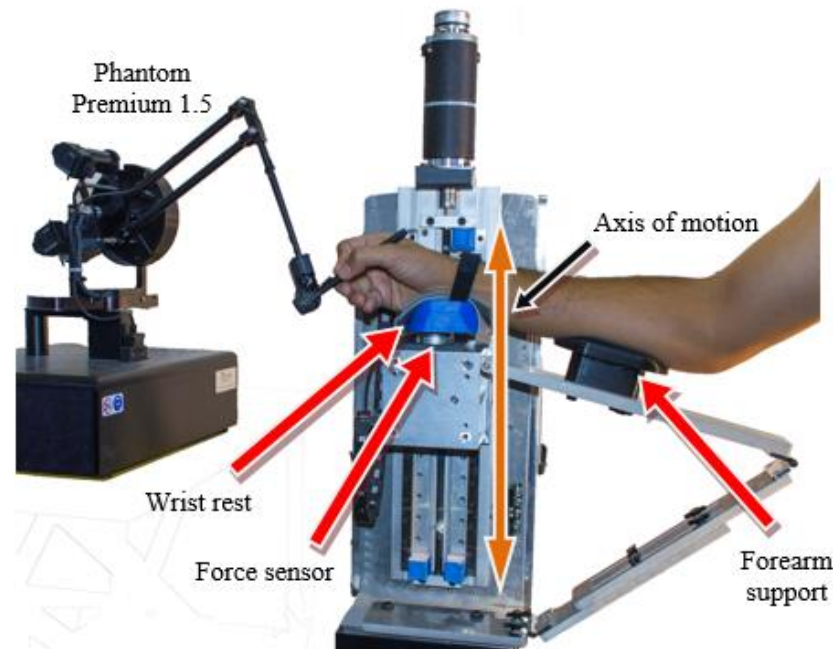
Figure. 2.1 The Vertical Active Handrest and its component.

force or position. The force input is provided by measuring the user's interaction forces with the force sensor under the wrist rest. The position input is provided by tracking the position of the stylus held by the user. An admittance controller takes these two inputs, calculates the desired velocity, and provides the appropriate electrical outputs to the stage's motor, thus adjusting the velocity of the wrist support to provide dynamic support to the arm accordingly. Further details of the device controller are given in Section 2.4.

The motion of the VAHR is provided by an Electrocraft RDM 103 brush-type DC motor (continuous stall torque of 0.3884 N-m) mounted to a 305 mm travel low-profile single-axis linear stage with a 6.35 mm pitch, antibacklash lead screw assembly provided by Servo Systems (model LPS 12-20). The workspace of the device is limited to 193 mm as a precaution to protect the carriage from running into its hard stops. The stage is mounted vertically to an aluminum frame with the motor located at the top. The total height of the

VAHR from the base of the frame to the top of the motor is 680 mm. Attached to the motor shaft is an Accu-Coder 15T-01SF-1000N5DHV-F00 incremental encoder with 1000 counts per revolution providing approximately 23 μm resolution for position feedback, when operated in quadrature.

A force sensor housing is mounted to the top of the stage's actuated carriage, with a wrist support plate attached directly above it. This force sensor housing consists of a 76.2 mm x 101.6 mm aluminum box-beam to support the user's arm weight. Even though only the vertical axis of force is used in the experiments presented in this chapter, based on the future goals of our project, a six-axis force sensor (ATI Mini40 calibrated to 60 N full scale) is used to measure input forces.

The VAHR is capable of supporting a user's arm through a combination of wrist and/or forearm support. The wrist rest, located directly above the force sensor, is contoured to the shape of a user's wrist and covered with 3-mm thick foam tape. This rest was designed to provide ergonomic support to users while allowing the user's wrist to be secured with a strap if desired. I ensured that users could still rotate their hand to complete drawing tasks while their wrist was strapped down. The forearm support is attached to a linkage mechanism that follows the natural motion of the user's forearm in order to provide ergonomic support of the forearm. The linkage mechanism is adjustable to accommodate small differences between users' arm sizes and kinematics.

A SensAble Phantom Premium 1.5 serves as a position input device for our experiments, with test participants grasping its stylus with their right hand. This device was chosen for its low inertia (< 0.75 g) and large workspace (381 W x 267 H x 191 D mm), which matches the vertical workspace of the VAHR and the requirements of our two-axis

tracing task. Microsoft Visual Studio C++ and the Chai3D libraries [22] are used to control the device and interface with the Phantom Premium and sensors. A Sensory Model 626 PCI Multifunction I/O Board measures input positions of the VAHR stage, and a National Instruments PCIE-6320, X-Series card measures input forces from the user's arm at a frequency of 2 kHz. The digital-to-analog converter on the Sensory 626 board outputs a voltage signal to an Advanced Motion Controls 12A8 Brush Type PWM amplifier, which in turn drives the stage's motor under current control at a maximum of 5 Amps full scale.

2.4 VAHR Control Design

I investigated several controller designs for setting the desired motion of the VAHR (Table 2.1). These control strategies can be divided into force-based and position-based admittance control, based on the input method. Each controller uses a measured or virtual force as its input to proportionately set the desired velocity of the vertical stage. A PID controller is then used to maintain the desired velocity. I limited the desired velocity of the device to ±110 mm/sec in all control modes for the safety of the user and the device.

2.4.1 Admittance Control

A linear admittance control law [cf., 11] is used to set the desired velocity of the stage, where the desired velocity (V_{des}) is equal to the admittance gain (K_a) multiplied by the combined input force (F_b):

$$V_{des} = K_a \cdot F_b \qquad (2.1)$$

Modifying (2.1) allows us to control the motion of the VAHR based on the relative applied force and/or position inputs. This can be achieved by changing the proportion p,

Table 2.1. VAHR admittance controller categories.

Input Method	Name
Force-based	Force
	Weight-based
Position-based	Position
	Elastic

which is the proportion of applied force to the handrest (F_{HR}) and/or the Phantom's end-effector position relative to the position of the stage (F_{sty}) as described below.

$$F_b = (1 - p) \cdot F_{HR} + (p) \cdot F_{sty} \qquad (2.2)$$

In the tests described herein, the value of p is set to either zero or one. Based on the value of p, (2.1) becomes either a force-based or position-based admittance controller. Figure 2.2 shows system diagram of this controller's governing equation and each contribution to the controller is now explained in detail.

2.4.2 Force-based Admittance Controller

The force-based control mode uses the measured force relative to resting hand weight applied to the wrist rest (as measured by the force sensor) to set the desired velocity. Our admittance control law (1) along with (2) results in a force admittance controller that accepts only force as an input when p is set to zero.

2.4.2.1 Force Controller

This controller is the most commonly used linear force admittance controller, where the combined input force (F_b) is equal to the applied force to the handrest (F_{HR}), which is then calculated as follows:
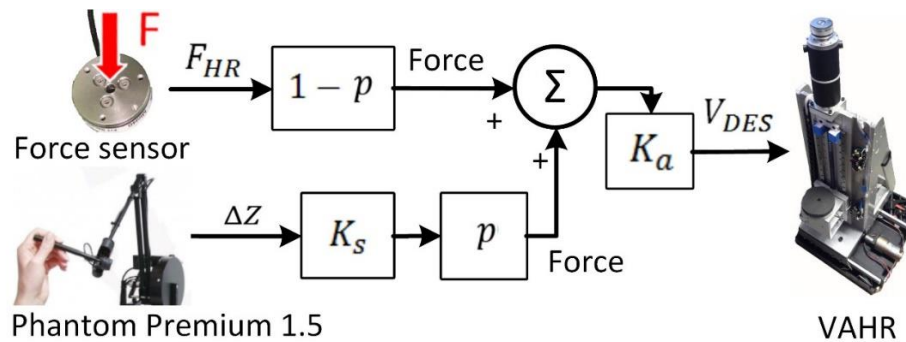
Figure 2.2. VAHR admittance controller categories.

$$F_{HR} = W_{arm} - F \qquad (2.3)$$

For our experiments, a force deadband value of 5% of the user's resting arm weight is used, which is roughly 0.5 N for the average user [23]. This value is selected such that the force inputs are always above levels where poor device performance occurs, as suggested by Nambi et al. [12]. This value ensures that the stage velocity is maintained at zero unless the user applies a force beyond the deadband range. The governing equation of the force controller can be obtained by combining (2.1), (2.2), and (2.3):

$$V_{des} = K_a \cdot (W_{arm} - F) \qquad (2.4)$$

Applying an input force (F) greater than the user's tared arm weight (W_{arm}) and the added deadband results in a negative desired velocity (V_{des}), which moves the stage downward, and applying a force less than the tared arm and deadband moves the stage upward with a positive desired velocity.

2.4.2.2 Weight-based Controller

Under the force controller described above, users with low arm weight could struggle with achieving high velocities in the upward direction and could break contact with the

device's wrist rest and force sensor. The weight-based controller fine tunes the force controller to each user and allows users with different arm weights to achieve similar maximum desired velocities in the upward direction (users with low arm weights would experience higher admittance gains and vice-versa). This controller modifies the force controller by scaling the admittance gain relative to each user's arm weight. The governing equation of our weight-based admittance controller is

$$V_{des} = K_a \cdot (W_{arm\_average}/W_{arm}) \cdot F \qquad (2.5)$$

where K_a is the fixed admittance gain (in mm/s/N), $W_{arm\_average}$ is the average weight of human arm (set to 4.5 N based on [23]), and W_{arm} (in N) is the resting weight of the user's arm. Note that the effective admittance gain ($K_a \cdot (W_{arm\_average}/W_{arm})$) for each user will be different based on their respective arm weight.

2.4.3 Position-based Admittance Controller

The position-based admittance controller uses the Phantom Premium's relative stylus position to set the desired velocity. This type of controller is achieved when proportion p is set to one in admittance control law (2.1) and (2.2).

2.4.3.1 Position Control

Similar to what is done in [2], the position control uses the position of the Phantom's stylus (Z_{sty}) relative to the position of the wrist rest (Z_{HR}) and transforms this relative displacement into a virtual input force (F_{sty}) using a virtual spring (K_s).

$$F_{sty} = K_s \cdot \Delta Z = K_s \cdot (Z_{sty} - Z_{HR}) \qquad (2.6)$$

A position deadband of ±2 mm is used around the position of the stylus relative to the

stage's position, which allows the VAHR to remain stationary when the stylus is within this range. When $p = 1$, substituting (2.5) into (2.1) results in the position controller's governing equation:

$$V_{des} = K_a \cdot K_s \cdot \left(Z_{sty} - Z_{HR} \pm Z_{db}\right) \qquad (2.7)$$

The stage's admittance gain was held at $K_a = 10$ mm/s/N for all position-based controllers described herein. The justification for this action will be explained in the preliminary position-based experiment section (Section 2.7).

2.4.3.2 Elastic Controller

After investigating the position controller, I sought to further improve the stability of the user's hand motions while using the VAHR with the addition of an elastic control term. Researchers have previously found that users can steady their hand motions and improve precision using these elastic forces [24]. Our implementation of the elastic controller is similar to the position controller, but with the addition of a spring force that pulls the stylus toward a set position of the wrist rest.

The governing equation of position input controller is also used in our elastic control mode with the addition of a spring force rendered through the Phantom to the user's hand. This spring force pulls the stylus toward the relative position of the wrist rest (Z_{HR}):

$$F_{elastic} = -K_e \cdot \Delta Z = -K_e \cdot (Z_{sty} - Z_{HR}) \qquad (2.8)$$

where K_e is the elastic spring constant and different from the virtual spring constant (K_s).

<u>2.5 Experimental Methods</u>

This section describes the general methods used in our experiments. Later sections focus on *specific* methods, results, and discussion for each particular experiment. It should be noted that the words controller and support conditions are used interchangeably throughout this chapter.

For all experiments, I asked each participant to sit in front of the monitor, grasp the Phantom's stylus with their right hand while maintaining a neutral writing posture, and interact with the device as instructed for a particular support condition (Figure 2.3). The proctor would then adjust the position of the forearm support based on what felt most comfortable to each participant, tare the force sensor to the user's hand/wrist weight, and tare the stylus position base on the initial centered posture of the participant's hand. Table 2.2 shows all support conditions used in this chapter, and their respective abbreviation is used for convenience throughout this chapter.

Before starting the experiment, I allowed every participant to practice with all support conditions for a total of 5 minutes. Longer experiments were broken into 2 days to prevent participant fatigue. On one day, I instructed the participant to complete the tracing task as accurately as possible (referred to as "accuracy" instruction) and on the other day to draw
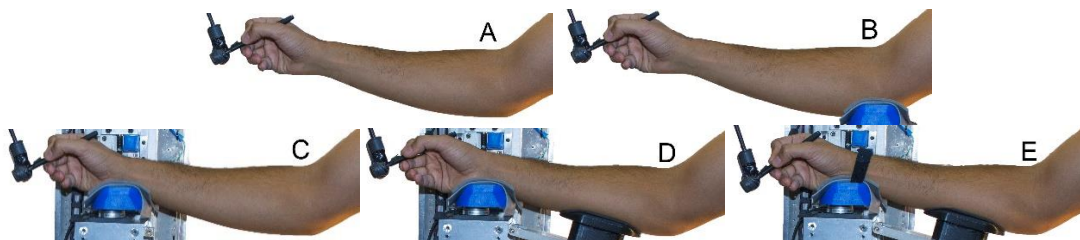

Figure 2.3. VAHR support conditions: a) Freehand; b) fixed elbow; c) force, position, and elastic; d) force support, and weight-based; and e) force strap.

Table 2.2. Support conditions used in experiments and their simplified abbreviations.

Support Condition Abbr.	Support Condition	Modification
Force	Force Admittance Control	—
Force support		Forearm Support
Weight-based		Forearm support + weight-based admittance gain
Force strap		Forearm support + strap
Position	Position Admittance Control	—
Elastic		Elastic Control
Freehand	Freehand	—
Fixed elbow	Fixed elbow	—

with a balance between accuracy and speed (referred to as "balanced" instruction). The accuracy test took slightly longer than the balanced test to complete, and the order of these sessions was balanced across participants.

All participants wore headphones playing white noise to reduce distractions and to mask ambient noise. They also used their right hand regardless of hand dominance. In order to minimize the effects of test order, such as fatigue and learning, I used a Latin squares approach to generate the order in which participants experienced each support condition. To further reduce the effects of fatigue, participants were given a 2-minute break between support conditions.

The shapes of the traced paths are composed of various piecewise linear and continuous shapes that were chosen based on prior research (Figure 2.4). All shapes were closed with the exception of the sine wave, which was only used for training purposes. Our test utilized asymmetric lemniscates (figure-eight) and oblate limacons (cartioids) due to their continuously changing radii of curvature as used by Viviani and Flash [25]. The other used shape was a rectangle, a piecewise linear shape, which is similar to the square shape used in [15], [26], and [27]. All shapes were stretched vertically to match VAHR's vertical

Shape		Description
Oblate Limacon (Cartioid)		Closed, Continuous, Changing curvature w/o change in direction
Asymmetric Lemniscate (figure-eight)		Closed, Continuous, Changing curvature with change in direction
Sine Wave		Open, Continuous, Changing curvature with change in direction
Rectangle		Closed, Piecewise linear, Discrete changes in curvature w/o change in direction

Figure 2.4. Virtual Environment shape types and their descriptions.

workspace of 193 mm. Each shape was approximated using a limited number of piecewise line segments to simplify the rendering, and ease of evaluation and reduce the computer processing time.

All paths contained a small green square as a starting location and a red square as the end location. A trial would start upon the participant passing through the start square and end when he/she crossed the end square. Their traced path was shown overlaid on top of the original path throughout the trial, starting from when the participant crossed the green start square. The participant would press the spacebar after completing a trial to proceed to the next trial. After finishing a set number of trials for a particular support condition, a tone was played and a text was displayed on the monitor to signal the end of the support condition. The proctor then prepared the stage for the next support condition while the user rested.

I recorded data at 2 kHz and examined error and time for our analysis. I normalized the

completion time data by the path length due to the different traced path lengths (see Figure 2.4). I selected the median absolute value of error as the best metric to evaluate participants' performance. This metric was selected among several suggested by Jagacinski and Flach [28], such as mean absolute value of error and the root-mean-squared error. The reasons for selecting median absolute value of error over the other metrics were 1) exact same trend as mean while being an unbiased estimator and not sensitive to outliers and 2) better cross comparison between our results and the test results of Fehlberg et al. [2].

I used a factorial two-way repeated measures ANOVA model to examine predictors for all following experiments, unless stated otherwise. Based on the results of ANOVA, I used a Bonferroni's post hoc analysis to perform a t-test on all pairs. The error bars in each figure indicate a 95% confidence interval, and a "*" identifies statistically significant support condition(s) from others.

2.6 Preliminary Force-based Experiment

In our first preliminary experiment, I explored a range of admittance gains that further improve the performance of the force controller (shown in Figure 2.3 c) to match this chapter's experiment design (i.e., shape tracing).

2.6.1 Methods

The participants' accuracy with a range of different admittance gains was explored with K_a = 5, 10, 15, and 20 mm/s/N. All eight participants completed six trials per admittance gain, tracing three cartioids and three figure-eight paths. The participants had an average age of 23 (ages 21 to 28), and there was one left hand-dominant participant by self-report.

This experiment took 45 minutes on average to complete, and the participants were instructed to trace the path as accurately as possible. I used a one-way repeated measures ANOVA model to examine whether admittance gain predicts median error.

2.6.2 Results and Discussion

Figure 2.5 shows participants' median tracing error across the range of tested force controller admittance gains while tracing as accurately as possible. The results demonstrate that admittance gain significantly predicts median error ($F(3,45) = 5.181$, $p = 0.021$), and the participants' median tracing error is significantly lower with $K_a = 10$ mm/s/N than with the other tested admittance gains ($p \leq 0.038$).

From these results, I selected the admittance gain (K_a) of 10 mm/s/N for all support conditions (force-based and position-based support conditions) in the following experiments for more comparability across controllers.
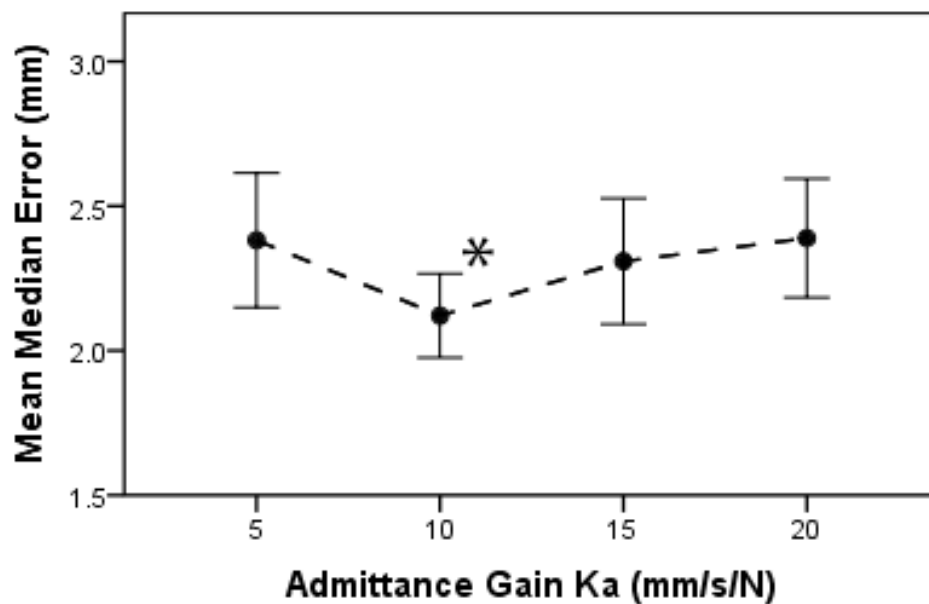
Figure 2.5. Participants' median absolute error vs. admittance gain (K_a).

2.7 Preliminary Position-based Experiment

In the second preliminary test, I explored a range of virtual (K_s) and elastic spring constant (K_e) to further improve the performance of the position and elastic controllers to match the task for our current experimental design.

2.7.1 Methods

In order to fine tune the position and elastic controllers, I tested various combinations of virtual and elastic spring constants that were found to work best in prior testing (Table 2.3). In the previous assessment of VAHR [3], I learned that adding a high elastic spring constant (K_e) in the elastic controller improves accuracy over a position controller. With this knowledge, I decided to test the elastic controller with three different virtual spring constants and a high elastic spring constant (K_e = 0.9 N/mm) and include a standard position controller case as a basis of comparison. I selected a virtual spring constant (K_s) range from 0.1 to 0.5 N/mm, as values outside this range were either too sluggish or too responsive/unstable.

Eight participants completed the preliminary position-based experiment. Each participant completed nine trials per support condition, with cartioids, figure eights, and rectangles as the possible path shapes for each trial. The participants' average age was 23 (ages 21 to 33), and all were right hand-dominant by self-report. This experiment took 90

Table 2.3. Virtual and elastic spring constants used in the preliminary position-based admittance control test.

Condition	1	2	3	4
K_s (N/mm)	0.1	0.3	0.5	0.3
K_e (N/mm)	0.9	0.9	0.9	0.0

minutes on average to complete, so it was broken into two sessions on different days.

2.7.2 Results and Discussion

A plot of median tracing error of the four position-based controllers is shown in Figure 2.6. The results demonstrate that the support condition statistically predicts median error ($F(3,12) = 3.959$, $p = 0.036$). The post hoc analysis shows the elastic controller with virtual spring constant (K_s) of 0.1 N/mm and elastic spring constant (K_e) of 0.9 N/mm to have significantly lower median error than other tested controller gains ($p \leq 0.008$). In other words, participants performed best with the least responsive of the tested controllers. I selected these controller gains as the best position-based controller among the tested spring constants, despite having numerically slower mean completion time per unit distance than others ($F(3,12) = 1.974$, $p = 0.172$). In addition, as expected, adding the elastic spring constant significantly reduces the median absolute tracing error over position controller ($p \leq 0.039$).
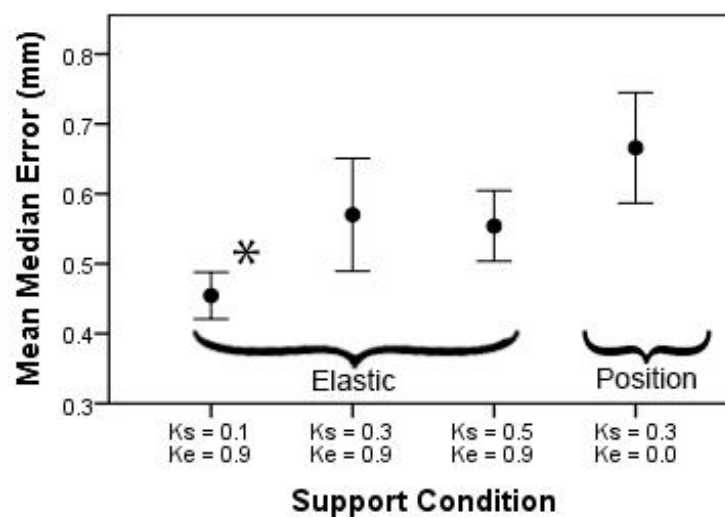
Figure 2.6. Participants' median tracing error based on tested position-based spring constants.

Figure 2.7 shows the tracing accuracy based on the shape, where tracing rectangles had significantly lower median tracing error than tracing cartioids and figure eights (p < 0.001). This is likely due to the decoupling of the motion into one-axis motions when tracing the rectangle. For the main experiments in this chapter, I selected the rectangle and figure-eight shapes as the tested shapes and eliminated cartioids. This was due to the performance similarities between figure eights and cartioids and that I preferred figure eights due to their inflection in addition to changing curvature. Eliminating cartioids allowed us to have fewer shapes in order to increase the number of repetitions per shape (increase the power of the experiment) without increasing the length of the experiment.

2.8 Experiment 1

I chose to compare participants' tracing performance using various VAHR controllers to select the best controller. I proposed to improve the performance of the VAHR under force input by using a forearm support to provide localized support, which allows force inputs to be provided by small muscle groups in the wrist and hand. With this method, only
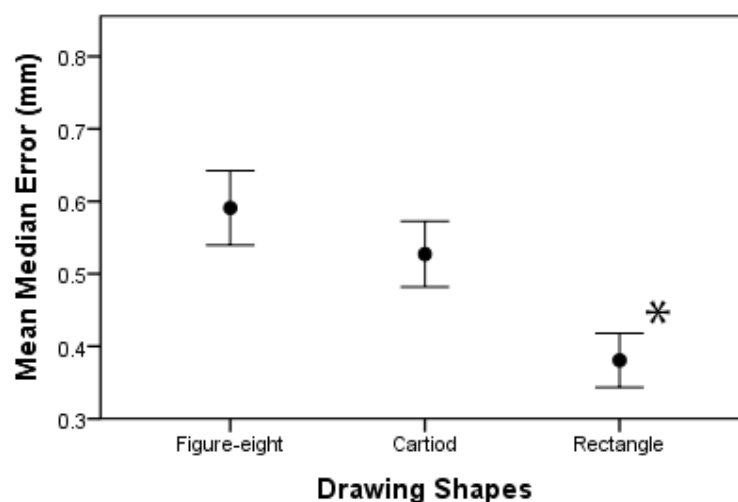
Figure 2.7. Participants' median tracing error based on traced shapes.

the weight of the hand is applied to the force sensor as the forearm and shoulder are supported by the forearm rest. However, I hypnotize that introducing a forearm support could lead to a new issue due to the much smaller forces being supported by the VAHR's force sensor. While participants can provide high downward forces to move the VAHR downward, the maximum upward speeds can be quite limited since once they lifted their hand off the force sensor under the handrest, no additional force input is possible. To address this issue, the weight-based and force strap controllers are introduced.

2.8.1 Methods

This experiment evaluated five VAHR support conditions to find the VAHR-assisted support condition with the lowest median tracking error. Two of these five support conditions were the force ($K_a = 10$ mm/s/N) and elastic ($K_s = 0.1$ N/mm, $K_e = 0.9$ N/mm) controllers from the two preliminary tests that had the lowest median tracing error and best speed-accuracy trade-off. The other three support conditions included modifications to the force controllers that I hypothesized could improve its performance. These modifications included the addition of a forearm support (force support), implementing a weight-based admittance gain (weight-based), and strapping the participants arm to the handrest to allow him/her to apply tensile forces on the handrest and force sensor (via force strap).

Every participant completed four trials per support condition and shape, with the shape of each path being either rectangular or a figure eight (asymmetric lemniscate), for 80 trials. Half of these trials were completed under the "accuracy" condition and half were completed under the "balanced" condition.

This experiment included 10 participants (three females), with an average age of 24

(ages 21 to 31), and one participant left-hand dominant by self-report. This experiment took 80 minutes on average to complete and was broken up into two sessions.

After the experiment, I asked participants to rate whether each support condition "felt natural." Their answer could be an integer from 1 (strongly disagree) to 5 (strongly agree).

2.8.2 Results and Discussion

The participants' median tracing error under "accuracy" and "balanced" instructions is shown in Figure 2.8, where support condition statistically predicts median error ($F(4,40) = 21.121$, $p < 0.001$). Adding a forearm support to the force controller (force support) results in a significant reduction in median tracing error ($p < 0.001$). This confirms our hypothesis that adding such a support would improve tracing performance. The elastic controller and modified force controllers (weight-based and force strap) result in further significant accuracy improvements over the force support controller ($p < 0.001$). However, no significant difference in median tracing error is seen between these support conditions ($p = 1.000$). Hence, force and force support were eliminated from consideration in Experiment
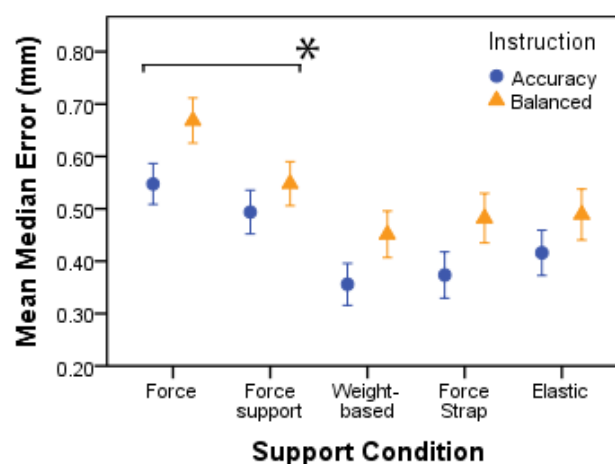
Figure 2.8. Mean of participants' median error versus the four tested force-based admittance controllers and an elastic controller.

2 due their significantly higher median error.

Figure 2.9 shows the mean time it took to complete each trial per support condition. Support condition is found to significantly predict completion time per unit distance $(F(4,41) = 7.505, p < 0.001)$. While the post hoc analysis shows no statistical difference between the four force-based admittance controllers based on completion time per unit distance $(p \geq 0.816)$, they were all found to be significantly faster than the elastic controller $(p \leq 0.001)$. This is partially because of the low effective admittance gain used in the elastic controller that was selected in the preliminary experiment (described in Section 2.7) that is based solely on an accuracy criterion. However, given that the accuracy of the elastic controller is comparable to the modified force-based controllers (Figure 2.8), its speed-accuracy performance is simply not as good. For this reason, the elastic support condition was also eliminated from consideration in Experiment 2.

Lastly, I used the subjective results from the questionnaire to make a final selection between the weight-based and force strap support conditions. Based on the questionnaire's result, most participants chose the force strap to be the most natural (mean of 3.67 out of
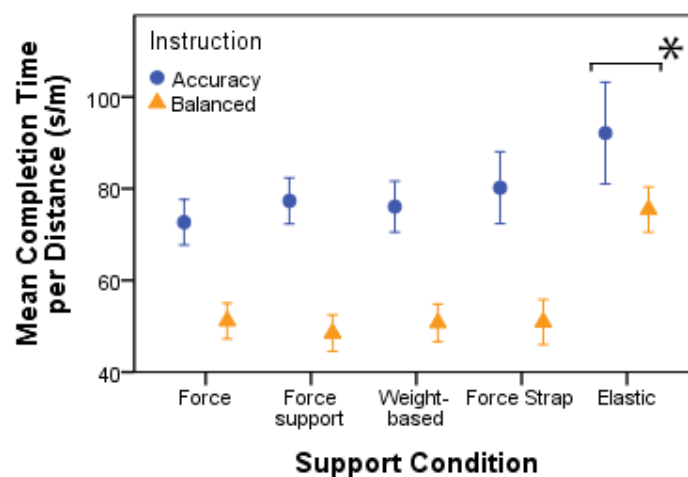
Figure 2.9. Mean completion time versus the four force-based and the elastic support conditions.

5, which was significantly higher than the other controllers tested) over the weight-based support condition (mean of 2.56 out of 5).

The force strap was selected as the best VAHR support condition among the tested support conditions (despite having slightly higher median tracing error than weight-based controller) and to be compared against unassisted support conditions in Experiment 2.

2.9 Experiment 2

This section compares the results of the chosen VAHR support condition from Experiment 1 to nonassisted support conditions.

2.9.1 Methods

I selected the force strap support condition to be compared against freehand and fixed elbow support conditions (i.e., unassisted drawing conditions). The fixed elbow condition is considered the best one would expect to perform without purchasing an assistive device. Each participant completed five trials per support condition and shape, tracing both rectangles and figure eights, for 60 trials (half with "accurate" and half with "balanced" instructions). This experiment included 12 participants (three females), with an average age of 24 (ages 19 to 33), and all participants were right-hand dominant by self-report. It took 70 minutes on average to complete Experiment 2, which was broken into two sessions on separate days.

After the experiment, I asked participants the following questions per support condition: "This condition felt natural to control" and "This condition allowed me to perform well." Participants could rank answers from 1 (strongly disagree) to 9 (strongly

agree). The reason for increasing the number scale was to allow for a wider range of answers and more accuracy as suggested by Nunnally and Bernstein [29].

2.9.2 Results and Discussion

Figure 2.10 shows the resultant mean of participants' median error grouped by "accurate" and "balanced" test instructions per support condition, where support condition is found to significantly predict the median tracing error ($F(2,20) = 29.067$, $p < 0.001$). Furthermore, the participants' tracing task performance using the force strap controller is significantly more accurate than the unassisted cases ($p < 0.001$).

The support condition is found to significantly predict completion time per unit distance ($F(2,20) = 6.091$, $p = 0.009$) (see Figure 2.11). Additionally, the completion time per unit distance of the force strap controller is significantly slower than other support conditions when participants are instructed to focus on drawing as accurately as possible ($p \leq 0.035$). However, this is not the case when participants are instructed to focus on a balance of accuracy and speed ($p = 1.000$).
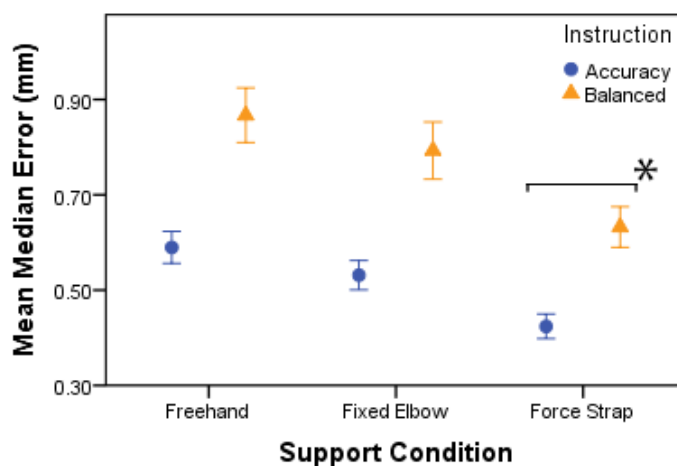
Figure 2.10. Mean of participants' median error for freehand, fixed elbow, and force strap support conditions.
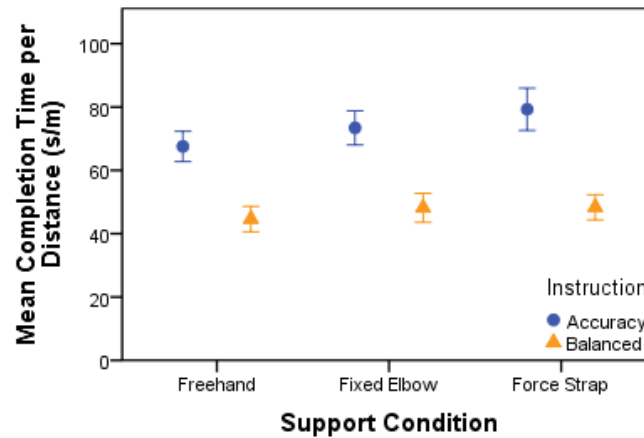
Figure 2.11. Mean completion time per unit distance for freehand, fixed elbow, and force strap support conditions.

I used a hierarchical regression analysis to further investigate the performance of the force strap controller, as well as the freehand and fixed elbow support conditions. This was done to better understand the speed-accuracy trade-off of each support condition. This analysis shows whether this controller helps to improve accuracy over all tested completion times or whether the VAHR simply slows down the user's motion. Figure 2.12 shows the correlation between completion time per unit distance and median absolute error. A loess smoother curve [30] is overlaid on the data purely for visual purposes.

Using the regression analysis, I can see that after accounting for the effect of trial completion time per unit distance (accounting for 58.4% of the variance in median error
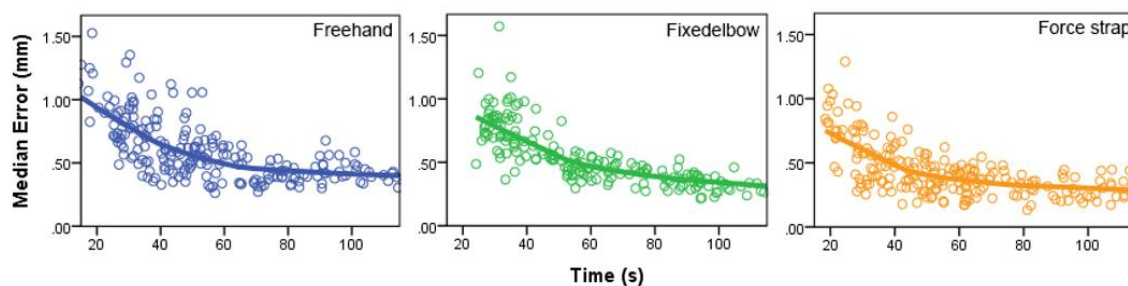
Figure 2.12. Mean completion time per unit distance for freehand, fixed elbow, and force strap support conditions.

$R^2 = 0.584$, $F(2,621) = 436$, $p < 0.001$), adding a support (adding forearm and wrist support in the force strap support condition and elbow support in fixed elbow support condition compared to freehand) improves drawing accuracy over the freehand case (R^2 change = 0.032, $F(3,620) = 331$, $p < 0.001$). Additionally, using the force strap controller results in even better drawing accuracy than other support conditions (R^2 change = 0.04, $F(4,619) = 295$, $p < 0.001$). It should be noted that the effect of adding a support was small, accounting for 3.2% of the remaining variance, while the effect of using an assisted force input support condition (force strap) was slightly higher, accounting for 4% of the remaining variance.

Figure 2.13 collects the plots from Figure 2.12 to provide a better visual comparison between support conditions. As seen from this figure, the participants were more accurate while using the force strap controller than the other two unassisted support conditions at all drawing speeds.

In agreement with the objective results, the questionnaire's subjective results show that every participant rated the force strap support condition higher, in both "how natural it felt" and on "how well they thought they performed," than the unassisted support conditions
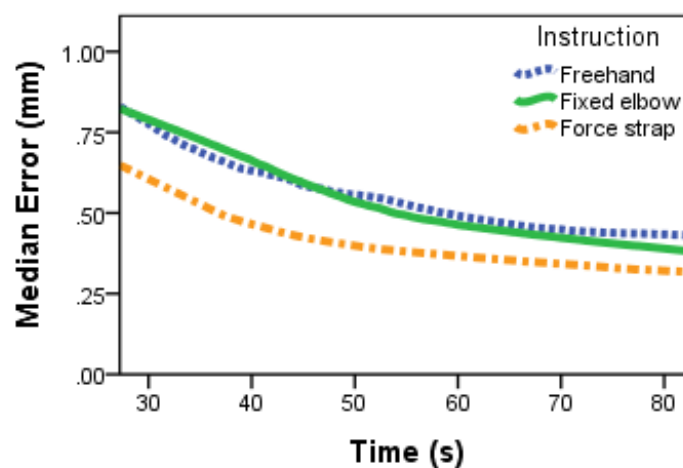
Figure 2.13. Regression analysis showing speed-accuracy data for each support condition.

(Table 2.4). In addition, participants reported a lower natural rating for Freehand and Fixed Elbow support conditions due to high fatigue levels, which they associated with an unnatural feeling.

These results demonstrate that a force-based admittance controller when used on the VAHR can be improved beyond other assisted and unassisted conditions by 1) tuning the admittance gains, 2) adding a forearm support to allow small muscle groups in the wrist and hand to provide motion input, and 3) allowing the participant to apply tensile forces on the force sensor to move the stage upward.

2.10 Conclusion

I presented the Vertical Active Handrest (VAHR), a novel device that provides gravitational and ergonomic support to the user's arm over a large vertical workspace to aid in dexterous tasks. Participants' tracing accuracy in a vertical two-axis tracing task was tested using various device control strategies. The best VAHR support condition, the "force strap," was then compared against freehand and fixed elbow support conditions. This support condition used a force-based linear admittance controller and held the user's hand against the wrist rest with a strap, which allowed them to exert tensile forces on the force sensor during upward motions.

Table 2.4. Mean completion time per unit distance for freehand, fixed elbow, and force strap support conditions.

	How natural it felt?		How well you performed	
	Accuracy	Balanced	Accuracy	Balanced
Freehand	3.49	3.74	3.03	3.18
Fixed Elbow	4.94	5.42	4.15	4.31
Force Strap	7.81	7.77	7.44	7.64

The experiment results show that the use of the VAHR with a force-based controller, a forearm support, and force sensor with wrist strap had significantly lower median absolute error while not hindering the user's speed when compared to the other tested conditions. Users found the hand strap to be nonintrusive and preferred it to other support conditions. However, if there was a case where a user did not want to be strapped to the VAHR's wrist rest, the use of a force-based controller with a weight-based admittance gain (weight-based support condition) was recommended, as this controller showed very similar performance to the force strap controller.

In the future I intend to integrate the understanding of controlling the motions on the vertical axis from this chapter into making a three dimensional Spatial Active Handrest. This device would match the three dimensional kinematics of the human arm and allow the user to naturally explore a large workspace.

2.11 Acknowledgment

2.12 References

[1]   S. Ito and Y. Yokokohji, "Maneuverability of master control devices considering the musculo-skeletal model of an operator," *World Haptics*, pp. 57–62, 2009.

[2]   M. A. Fehlberg, B. T. Gleeson, and W. R. Provancher, "Active Handrest: A large workspace tool for precision manipulation," *Int. J. Robotics Research*, vol. 31, no. 3, pp. 289–301, 2012.

[3]   C. A. Stewart, "A Vertical Active Handrest to aid in dexterous tasks and to provide gravitational support." M.S. thesis, Dept. Mech. Eng., Univ. Utah, Salt Lake City, UT, 2012.

[4]   Rancho Rehabilitation Engineering Program, Active Mobile Arm Support Project, 2005. http://www.ranchorep.org/project-3.html

[5]   A. Stienen, E. Hekman, F. Van der Helm, G. Prange, M. Jannink, A. Aalsma, and H. van der Kooij, "Freebal: dedicated gravity compensation for the upper extremities," *J. Med. Devices*, vol. 3, no. 4, pp. 804–808, 2009.

[6]   C. Cook and R. Burgess-Limerick, "The effect of forearm support on musculoskeletal discomfort during call centre work," *Applied Ergo.*, vol. 35, no. 4, pp. 337–342, 2004.

[7]   A. Erdelyil, T. Sihvonen, P. Helin, and O. Hänninen, "Shoulder strain in keyboard workers and its alleviation by arm supports," *Int. Arch Occup Environ Heath*, vol. 60, no. 2, pp. 119–124, 1988.

[8]   Equipois. ZeroG. Available: http://www.equipoisinc.com

[9]   "EZ Rest Painting Handrest," date accessed: 02/23/2011. http://www.jerrysartarama.com/discount-art-supplies/Painting-Supplies/Mahl-Sticks/EZ-Rest-Painting-Handrest.html

[10]   D. Odell, A. Barr, R. Goldberg, J. Chung, and D. Rempel, "Evaluation of a dynamic arm support for seated and standing tasks: a laboratory study of electromyography and subjective feedback," J. Ergo, vol. 50, no. 4, pp. 520–535, 2007.

[11]   R. Taylor, P. Jensen, L. Whitcomb, A. Barnes, R. Kumar, D. Stoianovici, P. Gupta, Z. Wang, E. Dejuan, and L. Kavoussi, "A Steady-Hand robotic system for microsurgical augmentation," *Int. J. Robotics Research*, vol. 18, no. 12, pp. 1201–1210, 1999.

[12]   M. Nambi, W. Provancher, and J. Abbott, "On the ability of humans to apply controlled forces to admittance-type devices," *Adv. Robo.*, vol. 25, no. 5, pp. 629–650, 2011.

[13]   S. P. Wise and R. Shadmehr, "Motor Control," *Encyclo. Human Brain*, vol. 3, pp. 137–157, 2002.

[14]   B. Brewer, S. McDowell, and L. Worthen-Chaudhari, "Poststroke upper extremity rehabilitation: a review of robotic systems and clinical results," *Stroke Rehabil.*, vol. 14, no. 6, pp. 22–44, 2007.

[15]   A. Bardorfer, M. Munih, A. Zupan, and A. Primozic. "Upper limb motion analysis using haptic interface." *IEEE/ASME Trans. Mechatronics*, vol. 6, no. 3, pp. 253-

260, 2001.

[16] C. Sewell, N. H. Blevins, S. Peddamatham, and H. Z. Tan, "The effect of virtual haptic training on real surgical drilling proficiency," *World Haptics*., pp. 601–603, 2007.

[17] D. Feth, R. Groten, A. Peer, and M. Buss, "Control-theoretic model of haptic human-human interaction in a pursuit tracking task," *IEEE Int. Symp Robot Human Inter. Com.*, pp. 1106–1111, 2009.

[18] M. Munih, G. Kurillo, M. Veber, J. Perdan, J. Podobnik, U. Mali, J. Cinkelj, M. Mihelj, T. Koritnik, R. Kamnik, and T. Bajd, "Analysis and synthesis of human and machine motion at UL FE," *IEEE Int. Conf. Rehabil. Robotics*, pp. 504–512, 2007.

[19] D. McRuer and H. Jex, "A review of quasi-linear pilot models," *IEEE Trans. Human Factors Elec.*, vol. 8, pp. 231–249, 1967.

[20] D. Kleinman, S. Baron, and W. Levison, "A control theoretic approach to manned-vehicle systems analysis," *IEEE Trans. Auto. Control*, vol. 16, pp. 824–832, 1971.

[21] R. A. Hess, "Pursuit tracking and higher levels of skill development in the human pilot," *IEEE Trans. Sys. Man. Cyber.*, vol. 11, pp. 262–273, 1981.

[22] F. Conti, F. Barbagli, D. Morris, and Sewell, "CHAI 3D: an open-source library for the rapid development of haptic scenes," *IEEE World Haptics,* 2005.

[23] C.E. Clauser, J.T. McConville, and J.M. Young. "Weight, volume, and center of mass of segments of the human body." Tech. Report AMRL-TR-69-70, Aerospace Medical Research Laboratory, Wright-Patterson Air Force Base, Dayton, OH. pp. 42–45, Aug 1969.

[24] S. Zhai, "Investigation of feel for 6DOF inputs: isometric and elastic rate control for manipulation in 3D environments," *Proc. Human Factors and Ergo. Soci.*, vol. 37, no. 4, pp. 323–327, 1993.

[25] P. Viviani and T. Flash, "Minimum-jerk, two-thirds power law, and isochrony: converging approaches to movement planning," *J. Exp. Psy. Human Perception and Performance*, vol. 21, no. 1, pp. 32–53, 1995.

[26] H. Burger, D. Brezovar, S. Kotnik, A. Bardorfer, and M. Munih, "Can haptic interface be used for evaluating upper limb prosthesis in children and adults." Proc. Med. Conf. Med. Bio. Eng. Comput., vol. 16, pp. 965–968, 2007.

[27] E. Lovquist and U. Dreifaldt, "The design of a haptic exercise for post-stroke arm rehabilitation." Proc. 6th Int. Conf. Disability, Virtual Reality and Associated Technology, pp. 309–315, 2006.

[28]   R. J. Jagacinski and J. Flach, *Control Theory for Humans: Quantitative Approaches to Modeling Performance*. Mahwah, NJ.: Erlbaum Associates, 2003.

[29]   J. C. Nunnally and I. H. Bernstein, *Psychometric Theory*. New York: McGraw-Hill, 1994.

[30]   Cleveland, William S. "Robust locally weighted regression and smoothing scatterplots." J. Am. Stat. Asso., vol. 74, no. 368, pp. 829–836, 1979.

CHAPTER 3

ENHANCEMENTS TO THE PLANAR ACTIVE HANDREST

The Planar Active Handrest (PAHR) is a large workspace assistive robotic device that has been shown to improve user performance for precision manipulation. The PAHR is somewhat restricted in its use because it does not rotate in the horizontal plane. This restriction limits the reachable workspace size and reduces user comfort. This chapter evaluates an improved assistive device, the Enhanced Planar Active Handrest (E-PAHR), which provides robotically controlled lateral/medial rotation of the upper arm. Under the E-PAHR design, a user is able to reach their desired hand position with redundant arm and device configurations. As such, I gave careful consideration to a variety of controller input choices and resultant robotic motor outputs/device motions that are available because of the redundant degree-of-freedom (DOF) available on the E-PAHR device. A series of experiments evaluated these controller designs to select the most effective method to control our device. I conclude that a rotational DOF allows the PAHR to better follow the kinematics of a user's planar arm movements while allowing skill level equal to the PAHR, but with reduced user force input and lower perceived exertion.

3.1 Introduction

The previous version of the Planar Active Handrest was a Cartesian two degree-of-freedom (DOF) human-robot cooperative interface that provided support while performing dexterous tasks over large workspaces. The PAHR provided user support from a 2-axis computer controlled motorized x-y stage that allowed planar movements with a fixed forearm orientation. Previous studies with this device demonstrated that use of the PAHR provides increased task accuracy and user skill level compared to freehand, fixed, and passive repositionable supports [1]. Additional studies showed that user skill level could be further improved by adding virtual fixtures to the device's controller [2]. In the research presented herein, I endeavor to improve the PAHR device to better match human arm kinematics by adding a rotational degree-of-freedom and to investigate its effect when interacting with this device.

Humans tend to have difficulty performing precision tasks without additional physical support. To alleviate this problem, static supports have been used to steady a human's arm or hand motions in performing activities of daily life. For instance, traditionally humans use the surface of a table to support their wrist while writing, which has been shown to reduce muscle activity and may reduce fatigue [3]. However, the inability to reposition the stationary support and being limited to the workspace of the hand is a major drawback of static supports. Traditional tools used to solve this issue, such as a maulstick used by painters, require the user to reposition the device, which does not fully solve the problem.

For our work described here, I developed an Enhanced Planar (E-PAHR) to provide additional ergonomic/kinematic support over a larger planar workspace (see Figure 3.1). This device has three degrees-of-freedom: two in translation and one in rotation. Through
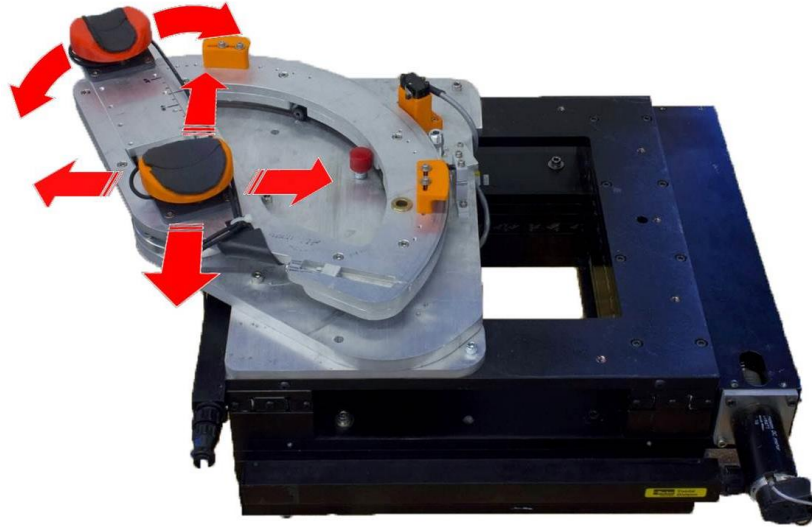
Figure 3.1. The controller and support conditions examined.

our investigations of this new device, I will enhance the workspace of the current PAHR to better match the kinematics of the human arm by developing a variety of methods to control the E-PAHR's redundant degrees-of-freedom.

This chapter presents three experiments evaluating the utility of E-PAHR controller methods and their effect on human movement. The first experiment examines preliminary controller methods to down select the most effective input/controller strategies based on participant performance and subjective feedback. The second experiment examines improvements/modifications to the three most effective strategies from the first experiment. The third experiment compares E-PAHR's controller strategies to the original PAHR design and the freehand drawing condition to evaluate the trade-off between speed and accuracy and the effectiveness of each condition, where effectiveness is expressed in terms of total applied force, efficiency, and perceived exertion of test participants.

The following section provides a brief background concerning the literature relevant to our research. The background section is followed by a description of the Enhanced Planar

Active Handrest and the control strategies I investigated. Next, I outline the general methods used in all our experiments. Each of the three experiments is then presented in turn, with individual methods and results subsections. Finally, results from all experiments are summarized and future work is discussed.

3.2 Background

Various methods of hand and arm support have been used to increase precision and reduce fatigue while performing dexterous tasks. A simple example of a fixed static support is using a table to stabilize the wrist while writing. Repositionable static supports reduce muscle fatigue by reducing the weight of the arm while typing [4] and using tools [5]. Passive [6],[7] and active [8] mechanical supports are also designed to reduce muscle fatigue through gravity compensation of the user's arm.

Robotic arm support devices have been used for both to rehabilitate and assist healthy users in performing dexterous tasks. In rehabilitation, robotic devices are often used in conjunction with virtual environments to motivate patients to achieve a higher intensity rehabilitation, which has been shown to improve rehabilitation of stroke patients [9]. Robot-assisted repetitive task-oriented motion has been used as an effective means of upper arm rehabilitation [10]. Other benefits of such rehabilitation devices are improving grip strength throughout the first year after stroke [11] and increasing elbow extensions in the horizontal plane using active gravity support of the arm [12].

Robotic devices have also been used to assist healthy users to perform dexterous tasks with a higher skill level. The Steady Hand, a robotic system developed at Johns Hopkins University, helps users with submillimeter manipulation tasks by simultaneously taking

force input from the user and a robot to move the tool accordingly [13]. A "Cobot" is a human-robot cooperative device that assists the user by constraining motion to a desired trajectory [14].

Common designs of robotic arm supports include end point manipulation and powered exoskeletons. Endpoint manipulation rehabilitation devices guide a user's hand along a predefined trajectory to regain lost motor skills in their arm [15]–[17]. In contrast, exoskeletons are typically anthropomorphic robots that are tightly connected to the user's arm and its joint angles fully define the arm's pose [18],[19]. The E-PAHR is a hybrid of these designs where our focus is to provide highly accurate end point motions without the constraints found in typical exoskeletons.

Another consideration in the design of robotic arm supports is the controller choice, which is often coupled to the device's design. The two major categories of robotic controllers are impedance and admittance control. Impedance control is used on lightweight, highly back-drivable devices that exert a force on the user based on the device's position [20].

Admittance control is used on heavier, nonbackdrivable devices. Admittance devices allow the user to move in a particular direction relative to the input force exerted by the user on a force sensor. The governing control law of a linear admittance controller is the following:

$$V = K_a \cdot F_{input} \qquad (3.1)$$

where V – velocity

K_a – admittance gain (~inverse of damping)

F_{input} – force input

Admittance control has been used in many robotic applications, such as commercial haptic interfaces [21], rehabilitation robotics [22], and eye surgery with the Johns Hopkins' Steady Hand robot [23].

A high admittance gain (i.e., low damping) results in high device velocity, which leads to poor user precision. A low admittance gain can be used to achieve the highest level of precision. However, a low admittance gain also causes a reduction in the device velocity and can result in user fatigue when the user exerts higher forces than necessary [23]. This suggests that there is an ideal range of admittance gains and device velocities for optimal user accuracy and that our device's controller must be designed and tuned appropriately to achieve optimal user performance with low fatigue.

The speed and accuracy trade-off in human movements has been studied extensively. The trade-off was first described by Woodworth [24] and later mathematically formalized as Fitts' law [25]. Fitts' law has been observed in a wide variety of tasks and applications (see [26] for a review). The majority of the research on trade-offs between speed and accuracy is related to reaching movements. However, recent analysis has focused on more complicated movement sequences [27] and to tracing tasks [28]. This analysis suggested that the speed-accuracy trade-off function relates to a change in skill level [27]–[29]. In our studies, I assess the effect of different device controller conditions on the skillfulness of user movements during tracing tasks.

<u>3.3 Device Description and Control Strategies</u>

In this section, I describe the development of the E-PAHR and its control strategies.

3.3.1 Enhanced Planar Active Handrest Device Design

The development of the E-PAHR (Figure 3.2) extends the workspace of the currently existing planar solution PAHR and better matches the kinematics of the human arm. The design of the E-PAHR adds a third, rotational DOF to allow lateral and medial arm rotations in the horizontal plane. The E-PAHR is based on a Parker two-axis linear stage with an available translational workspace of 25 x 25 cm, with software and hardware limits of 20 x 20 cm for safety of the device. On top of the Parker stage, I have added a custom rotary stage that uses a capstan drive system with a gear ratio of 34:1. Two ATI Mini40 6-axis force-torque sensors measure user force interactions with our device. The elbow force sensor is placed directly on the center of the rotation axis beneath a padded support. The hand force sensor is placed beneath a second padded support at the end of an adjustable support arm whose length is adjusted to accommodate each user's forearm length between 15 and 30 cm. The two Mini40 force sensors are calibrated to a +/-20 N full scale range in the horizontal direction with a resolution of 0.005 N.

While interacting with the E-PAHR, the user's right hand and/or wrist is rested on the forward padded support and their elbow on the rear padded support. For our tracing tasks, the user also grasps the stylus of a Phantom Premium 1.5 with his or her right hand.

The Active Handrest's position (X, Y, and Theta) is measured by three 1000 count per revolution optical encoders operating in quadrature. A Sensory 626 data acquisition card at a frequency of 2 kHz collects position data. Force input data are collected by two
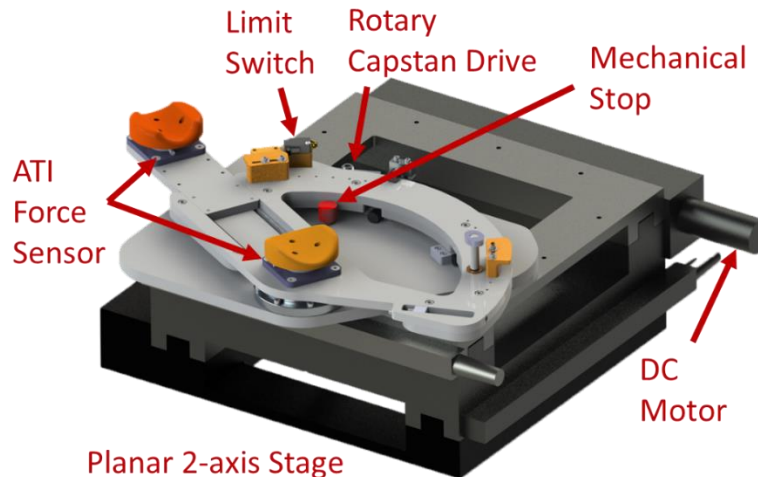
Figure 3.2. Enhanced Planar Active Handrest (E-PAHR) schematic.

National Instruments PCIE-6320 DAQ cards. Position information from the Phantom Premium's stylus is processed using Phantom drivers, version 4.2 and OpenHaptics Academic Edition version 3.0. Our controller on a 2.66 GHz Intel Core2-Quad PC operating in a 32-bit Windows 7 environment, running C++ code with CHAI-3D libraries, processes the input data. The computed motor commands are sent through the Sensory 626 card and amplified by Advanced Motion Controls 12A8 PWM current amplifiers before being sent to the x-y stage's two Maxon RE40 and the rotary axis's Maxon RE36 motors.

I chose to use a capstan drive for the rotational axis to increase the torque of the motor and reduce its speed similar to a gear, but without any backlash that a user could haptically feel. Using such a system allows us to increase the reachable workspace without increasing the overall size of the device, increase robustness to singularities, and increase dexterity [30]. However, adding a third DOF to control a two DOF human arm, assuming that the shoulder is fixed, a widely used assumption in upper limb motion tracking literature [31],[32], results in an overdefined system.

3.3.2 E-PAHR Controller Strategies

The admittance law computes the two desired translational motor velocities. I then implement a closed loop PID controller to achieve this desired translational velocity. The admittance law modified for rotations also computes the desired rotational velocity, ω,

$$\omega \ = \ K_a \ \cdot \ T_{input} \qquad\qquad (3.2)$$

where T_{input} – torque calculated from the user's input forces measured at the two force/torque sensors and not the torque measured directly by the force/torque sensors.

In this case, I first integrate the rotational velocity to achieve a desired rotation position and then implement a PD controller to achieve this desired rotation position. I do not directly control the velocity of the rotational axis due to the back-drivable nature of the capstan drive mechanism.

As shown in [33], human force control ability and precision deteriorates at low forces. However, this deterioration can be avoided by using a deadband to allow the stage to stop at force levels below a certain threshold. Therefore, to increase the stability of the E-PAHR, I added deadbands to the translational and rotational motions such that no motion would occur with input forces less than 0.5 N.

To determine how best to control the E-PAHR, I examined a variety of control strategies in order to obtain a controller that provides the user with the most naturally interaction and accuracy with the device. The six strategies I examined are highlighted in Table 3.1. The first control strategy, "Basic," uses the sum of averages of the two force sensors to determine the device's translational velocity. The torque used to determine the rotational velocity is calculated from the elbow and hand input force components perpendicular to the forearm's axis. This control strategy was examined, as it was

Table 3.1. The controller and support conditions examined.

Controller Condition	Support	Description
Basic	E-PAHR	Sum of applied hand and elbow forces mapped to stage translations. Moment from hand and elbow forces mapped to device rotation
Force Following	E-PAHR	Applied hand forces mapped to stage translations. Elbow moves in the direction of elbow forces while attempting to have no effect on desire hand motion
R-R	E-PAHR	Applied hand force controls stage "rotary joint" motions and rotation axis
R-R + Prismatic	E-PAHR	Applied hand forces control the device's "rotary joint" motions and rotation axis; Elbow moves radially in the direction of the elbow force again a virtual damper
Instantaneous Center of Rotation (ICR)	E-PAHR	Forearm rotational velocity is calculated about a point where the ahnd and elbow force vector normal intersect
Integrated Free Body Acceleration (FBA)	E-PAHR	Applied hand and elbow forces determine free body translational and rotational accelerations, which are then intergrated to determine stage translations and rotations
No Rotation	PAHR	Nonrotating stage. Applied hand forces mapped to stage translations
Freehand	None	Unsupported

computationally the simplest.

The second control strategy, "Force Following," uses the technique often employed by exoskeletons. In this strategy, the hand force sensor determines the position of the device's end effector, i.e., the user's hand. The force input at the elbow force sensor causes stage motion of the user's elbow in the direction of applied force in an attempt to minimize any force generated by the elbow while not affecting the hand's position. This controller strategy was believed to be of value because it would allow for precise end effector control. The third controller strategy, "R-R," uses a planar human arm model with a fixed shoulder position to essentially transform the two prismatic joints of the stage into a second rotary joint (see Figure 3.3 for schematic). The advantage of this control strategy is that the elbow force sensor is not required. The forth strategy, "R-R + Prismatic," is similar to the third but it allows for additional elbow repositioning by allowing elbow movement radially

Figure 3.3. The controller and support conditions examined.

inward and outward (i.e., along l1, as shown in Figure 3.3). In this configuration, movement

of the first rotary joint is no longer fixed to an arc. To achieve this additional motion, only

a single axis of the elbow force sensor is required. Both of these controller strategies could

lead to a less expensive device as the elbow force sensor is either not required or can be

replaced by a single-axis force sensor.

The fifth control strategy calculates the Instantaneous Center of Rotation, or "ICR," of

the stage. The ICR location is calculated as the intersection of the vector normal of the

elbow and hand force inputs. The forearm is then treated as a rigid body rotating about this

ICR. The E- PAHR's motion is calculated to achieve this motion of the forearm relative to

the ICR. This strategy was examined as it allowed for the use of a single admittance gain

(i.e., no difference between rotation and translational admittances).

The final E-PAHR strategy is the integrated Free Body Acceleration model, or "FBA."

In this strategy, I treat the forearm as two point masses connected by a massless rigid bar.

I then calculate the translational acceleration, by solving for a, from

$$m * a = F_{input} - c * V \qquad (3.3)$$

where m – sum of the two point masses

F_{input} – average of the two force inputs

c – damping (inverse of the admittance gain, K_a)

V – actual translational velocity

Similarly the rotational acceleration is calculated by solving for alpha in

$$I * \alpha = T_{input} - c * \omega \qquad (3.4)$$

where I – mass moment of inertia of the 2 point masses

T_{input} – torque measured across the two force inputs

c – damping (inverse of the rotational admittance gain)

ω – actual rotational velocity

This controller strategy had the benefit of not only being able to specify different rotational and translational admittance gains, but different translational and rotational inertias if desired. The nonrotating PAHR and Freehand conditions will be used as references to compare our current strategies to the results obtained with various E-PAHR controller strategies.
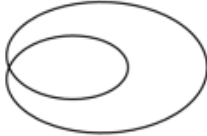
3.4 General Methods

For the purpose of our device evaluation, I examined participants' performance while tracing 2-D shapes over the course of three different experiments. I first compared performance and subjective preferences with the various E-PAHR controller conditions. Based on this analysis, I selected the three best controller methods and then attempted to

improve them by making controller modifications. I finally compared the best-modified E-PAHR configurations to performance under the PAHR and freehand (unsupported) conditions based on performance, subjective feedback, and participant effort/exertion measures.

To evaluate the performance of these strategies, I used similar tracing tasks as used to evaluate the PAHR in [2]. I had participants explore shapes with various spatial features: e.g., open vs. closed/cyclic paths and paths with continuously changing curvature vs. paths with discontinuous changes in curvature. Differences have been found between rhythmic (smooth) and discrete (segmented) movements [34]–[37]. Using a variety of path shapes (see Table 3.2) allows us to assess the performance of the E-PAHR in both smooth and segmented movements.

Table 3.2. Virtual environment shapes and their descriptions.
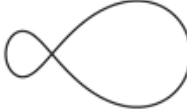
Shape		Description/Properties
Oblate Limacon		Closed, continuous, changing curvature without a change in direction of curvature
Asymmetric Lemniscate		Closed, continuous, changing curvature with a change in direction of curvature
Sine Wave		Open, continuous, changing curvature with a change in direction of curvature
Rectangle		Closed, piecewise linear, discrete changes in curvature (alternating between zero and infinite) without a change in direction of curvature
Line		Open, linear, constant (zero) curvature

3.4.1 Experimental Apparatus

For each experiment, the participant sat in front of the monitor and grasped the Phantom's stylus with his/her right hand as shown in Figure 3.4. For each of the E-PAHR and PAHR conditions, the participant placed his/her right elbow on the rear elbow support and his/her right wrist/hand on the forward hand support. For the PAHR condition, the participant rested only his/her elbow as they would normally, but the rotational axis was held in a fixed orientation. In the Freehand condition, the participant moved in an unsupported manner and did not rest or support his/her right arm. I did not consider either a Fixed Hand or Fixed Elbow support because the size of the shapes being traced by participants often exceeded the limited reach of a fixed support. A Passive support (i.e., a repositionable gravitational support without damping) was also not considered in this experiment as I previously determined this mode of support to be less effective than the freehand (unsupported) condition [1].

Figure 3.4. Experiment setup with target shape displayed on screen.

3.4.2 Experimental Procedures

Before beginning each experiment, the length of the forearm support (i.e., the distance between the elbow and hand supports and force sensors) was adjusted for the participant's comfort. Our controller then automatically adjusted the rotational admittance to accommodate for the longer (or shorter) moment arms. Before starting each controller condition, I asked the participant to navigate the perimeter of the workspace to allow the participant to feel comfortable with each condition and to ensure the Phantom and E-PAHR were able to reach the entire workspace. The E-PAHR and Phantom were repositioned as required for each participant's needs. Participants wore noise-cancelling headphones playing white noise throughout the experiments to reduce distractions.

One of the five virtual environment shapes was presented on the screen as a 2 mm wide black channel with a green centerline. The participants were instructed to "trace the target line as quickly and accurately as possible." Each shape was originally displayed on a red background with a green start block located on an edge for closed shapes or at an end for open shapes. The virtual environment background would change from red to grey when the participant first touched green start block, indicating that experiment data were being recorded. A yellow trace line would be displayed indicating the traced path as the participant navigated the environment. The participant would navigate to the red stop block in order to complete each trial. After completing the trial, the participant would press the space bar to advance to the next trial.

3.4.3 Data Analysis

Experiment data were collected at 2 kHz from when the participant first touched the start block until the participant touched the stop block. The following information was measured for each trial:

- Median Error – median distance from the center-line

- Completion Time – amount of time complete the trial

- Completion Time Per Distance – amount of time to complete the trial normalized per meter of path length (measured in sec/m)

- Total Integrated Force – hand and elbow force inputs summed and integrated over time, as a measure of effort to complete each drawing task

- Total Integrated Force per Distance – Total Integrated Force normalized per meter of path length (measured in N sec/m)

- Total Effective Integrated Force – dot product of force input vectors with the associated hand and elbow velocity vectors

- Efficiency – Total Effective Integrated Force divided by Total Integrated Force *100

- Subjective data***

  – How "natural" each condition felt

  – Participant's perception of accuracy

  – Participant's perception of exertion

  *** Due to the low sampling of subjective data (1 sample per participant per condition), no statistical information other than the mean is presented for each category.

Participants were asked to rate each controller condition on a Likert scale [38] for the

statements "this condition felt natural to use" and "this condition allowed me trace the target accurately." They answered these questions using the following 5 point scale:

1. Strongly disagree

2. Disagree

3. Neither agree nor disagree

4. Agree

5. Strongly agree

When asked to rate their perceived level of exertion, participants responded using Borg's Rating of Perceived Exertion (RPE) scale [39]. They responded using the 6 to 20 point revised RPE [40] as shown in Table 3.3. For a reference, participants were told that "9 - very light" was "equivalent to walking slowly at your own pace," "13 - somewhat hard" was "equivalent to exercise they could sustain at that level of exertion," and "17 - very hard" was "equivalent to exercise where they would eventually fatigue."

For each experiment, I implemented a balanced Latin Squares scheme to control for condition carry-over effects such as learning and fatigue. This scheme presents the experiment conditions in a different order for each participant. I conducted factorial ANOVA on each experiment's resultant data to determine significance of the manipulated variables. Statistical significance was determined at the 0.05 threshold level. All interaction terms were found to be nonsignificant unless specifically stated otherwise. All nonorthogonal post hoc contrasts were evaluated using Tukey's HSD to prevent against family-wise accumulation of Type-I error in multiple comparisons. All participants signed an informed consent form as stipulated by the University of Utah Institutional Review Board before participating in the experiments. All participants self-reported that they were

Table 3.3. Borg's RPE scale.

Rating	Description
6	No exertion at all
7	
	Extremely light
8	
9	Very light
10	
11	Light
12	
13	Somewhat hard
14	
15	Hard
16	
17	Very hard
18	
19	Extremely hard
20	Maximum exertion

right-hand dominant for all experiments.

For each experiment, I implemented a balanced Latin Squares scheme to control for condition carry-over effects such as learning and fatigue. This scheme presents the experiment conditions in a different order for each participant. I conducted factorial ANOVA on each experiment's resultant data to determine significance of the manipulated variables. Statistical significance was determined at the 0.05 threshold level. All interaction terms were found to be nonsignificant unless specifically stated otherwise. All nonorthogonal post hoc contrasts were evaluated using Tukey's HSD to prevent against family-wise accumulation of Type-I error in multiple comparisons. All participants signed

an informed consent form as stipulated by the University of Utah Institutional Review Board before participating in the experiments. All participants self-reported that they were right-hand dominant for all experiments.

3.5 Experiment 1: Preliminary Controller Evaluations

The purpose of our first experiment was to determine the effectiveness of the various E-PAHR controller conditions. In this experiment, I compared participants' performance while tracing sine waves, oblate limacons, asymmetric lemniscates, and rectangles.

3.5.1 Preliminary Controller Methods

Oblate limacons, asymmetric lemniscates, sine waves, and rectangles were presented for each of the controller conditions examined. Six participants (five males and one female, ranging in age from 22 to 33 years) completed the experiment. The time required to complete the experiment was approximately 30 minutes. The main factor of interest in this experiment was the controller condition. Each participant completed eight trials under each of 6 E-PAHR controller conditions shown previously in Table 3.1.

I first used a two-way 8 x 4 factorial ANOVA to predict median error and mean completion time per path length by controller condition and shape type with participant number entered as a random variable. I then used a two-way 8 x 4 factorial ANOVA to predict total integrated force and efficiency by controller condition and shape type with participant number entered as a random variable. Finally, I examined the mean participant preferences for their ratings of how natural each controller felt and how well they thought they performed with each condition.

3.5.2 Preliminary Controller Results and Discussion

Controller condition did not significantly predict median error [$F(5,75) = 1.293$, $p = 0.298$] (Figure 3.5(a)). Shape type did not significantly predict median error [$F(3,75) = 1.201$, $p = 0.343$]. Before conducting completion time analyses, I normalized the completion time per path length. Controller condition also did not significantly predict completion time per path length [$F(5,75) = 2.099$, $p = 0.099$] (Figure 3.5(b)). Shape type, however, did significantly predict completion time per path length [$F(3,75) = 4.274$, $p = 0.023$]. Rectangles took approximately 15.3 s/m less time to complete than asymmetric lemniscates and sine waves.

Controller condition significantly predicted total integrated force per path length, which is an indicator of the effort required during each trial [$F(5,75) = 4.948$, $p < 0.001$] (Figure 3.5(c)). The Basic and FBA controllers had lower total integrated force per path length than the R-R and R-R + Prismatic controllers ($p < 0.010$). Shape type did not significantly predicted total integrated force per path length [$F(3,75) = 1.877$, $p = 0.137$]. Controller condition also significantly predicted efficiency [$F(5,75) = 13.053$, $p < 0.001$] (Figure 3.5(d)). The ICR controller had higher efficiency than any of the other tested controller conditions ($p < 0.001$). Shape type did not significantly predict efficiency [$F(3,75) = 0.139$, $p = 0.936$].

The objective data from this experiment indicated that the Basic and FBA controllers required the least amount of total user effort (in the form of integrated force input) and that the ICR controller was the most efficient controller (had the highest force input efficiency). I also looked to the subjective data to confirm the most preferred conditions. When asked how natural the controller condition felt, participants most preferred the FBA condition
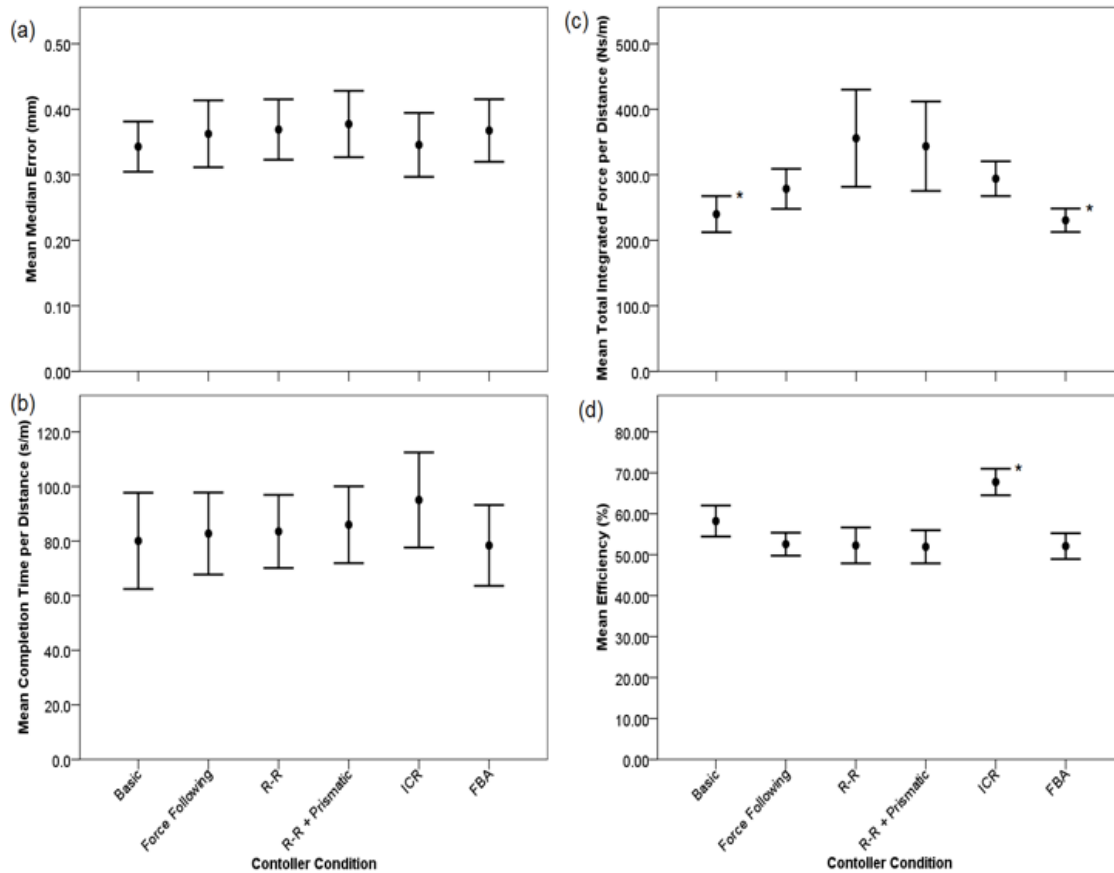
Figure 3.5. Experiment 1 Median Error (a), Completion Time per Distance (b), Total Integrated Force per Distance (c), Efficiency (d), and Subjective Ratings. (Error bars indicate 95% confidence intervals for the estimated mean.)

(4.5/5.0), followed by the ICR and Basic conditions (4.3/5.0 for both). When asked how well they perceived that they performed, participants felt that they did the best with the FBA and ICR conditions (4.2/5.0), followed by the Basic conditions (4.0/5.0). Based on these findings, I decided to only investigate the Basic, ICR, and FBA conditions in our subsequent experiments. I would also like to point out that objectively any of the other three controller conditions could achieve the same accuracy and timing data. Moreover, the two R-R conditions could be used with our device with fewer force sensing inputs, but these had the most total required user effort as seen by the integrated force and were the

least subjectively preferred conditions.

3.6 Experiment 2: Controller Enhancement Comparison

To further refine our choices for the controller options of the E-PAHR, I next made modifications to the three selected controllers from Experiment 1. User comments from our preliminary controller experiments described that the E-PAHR was often more difficult to move in rotation than in translation. I believe this is because I performed torque computations for our Basic and FBA controllers based on locating the center of mass at the midpoint between the elbow and hand. In our second experiment, I chose instead to perform torque computations based on locating the center of mass at a point located at one-quarter of the user's forearm length measured from the elbow position. The longer moment arm from the hand force sensor made the device easier to rotate when subjected to force input on the hand force sensor. This configuration more closely corresponds to human movement as the lateral/medial rotation of the arm occurs along the upper arm's axis through the elbow and not the middle of the forearm. I chose not to place the center of mass at the elbow location, as this would prevent elbow input forces from producing rotations.

For the ICR controller, which does not have a center of mass or torque computation, I chose instead to increase the admittance gain from 10 mm/s/N to 15 mm/s/N. Our hopes here again were that this change would allow easier movement without a degradation in performance. For this second experiment, I asked participants to trace straight lines in eight directions.

3.6.1 Controller Enhancement Comparison Methods

Lines were presented in eight direction increments of 45 degrees: horizontal at 0 degrees, and rotated at 45, 90, 135, 180, 225, 270, and 315 degrees. Six participants (five males and one female ranging in age from 25 to 40 years, completed the experiment. The total time required to complete the experiment was approximately 40 minutes, including time for breaks between experiment conditions.

The main factors of interest in this experiment were the controller condition and the drawing direction. Each participant completed 16 trials (two repetitions of eight directions) for each of six conditions: the three original controllers and three modified controllers for the Basic, ICR, and FBA conditions.

For this experiment, I used a two-way 6 x 8 factorial ANOVA to predict median error by controller condition and drawing direction with participant number entered as a random variable. I examined a two-way 6 x 8 factorial ANOVA to predict mean completion time by controller condition and drawing direction with participant number entered as a random variable. I then used a two-way 6 x 8 factorial ANOVA to predict total integrated force and efficiency by controller condition and drawing direction with participant number entered as a random variable.

3.6.2 Controller Enhancement Comparison Results and Discussion

Controller condition did not significantly predict median error [$F(5,287) = 2.519$, $p = 0.056$] (Figure 3.6(a)). When examining the pairs of controller conditions (original and modified), there was no difference in the median error for the Basic and FBA conditions ($p > 0.549$). However, the modified ICR condition had significantly higher error than the
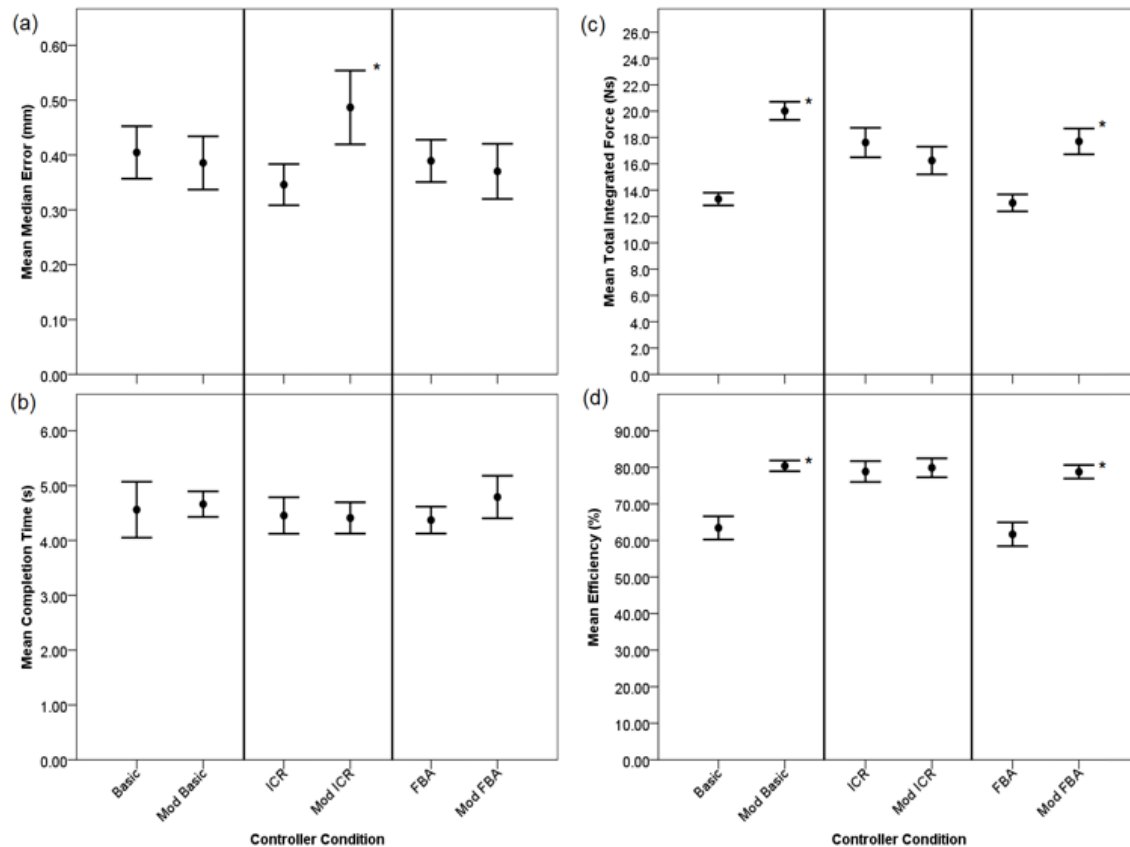
Figure 3.6. Experiment 2 median error (a), completion time per distance (b), total integrated force per distance (c), efficiency (d), and subjective ratings error bars indicate 95% confidence intervals for the estimated mean. * indicates significant differences within each condition pair.

original ICR condition by 0.039 mm (p < 0.001). Drawing direction significantly predicted median error [F(7,287) = 5.542, p < 0.001]. Drawing in the orthogonal directions (bottom to top, top to bottom, left to right, and left to right) had the lower median error than drawing in the nonorthogonal directions by 0.128 mm (p < 0.035).

Controller condition also did not significantly predict completion time [F(5,287) = 0.213, p = 0.953] (Figure 3.6(b)). When examining the pairs of controller conditions, there was no difference in the median error for any of the conditions (p > 0.070). Drawing direction significantly predicted completion time [F(7,287) = 13.520, p < 0.001]. There

were three levels of completion times. Drawing horizontally (left to right or right to left) was significantly faster than the other six directions at an average of 3.89 s. Drawing vertically (top to bottom or bottom to top), drawing from bottom left to top right, and drawing from top right to bottom left was next fastest with an average completion time of 4.54 s (p < 0.001). In addition, drawing from top left to bottom right or from bottom right to top left was the slowest with an average completion time of 5.21 s (p < 0.001).

Controller condition significantly predicted total integrated force, which is an indicator of the effort required during each trial [$F(5,287) = 29.654$, $p < 0.001$] (Figure 3.6(c)). There were three levels of total integrated force. The original Basic and FBA controllers had the lowest total integrated force at an average of 13.18 Ns. The original and modified ICR and the Modified FBA controllers had the next lowest total integrated force at an average of 17.19 Ns (p < 0.001). The Modified Basic controller had the highest total integrated force at 20.02 Ns (p < 0.001). From this it can be seen that the original basic and original FBA controllers had lower total integrated force than their corresponding modified controllers.

Drawing direction also significantly predicted total integrated force [$F(7,287) = 41.079$, $p < 0.001$]. There were three levels of total integrated force as a function of drawing direction. Drawing horizontally had the lowest total integrated force at an average of 12.59 Ns. Drawing from bottom left to top right (on the display screen) and drawing from top right to bottom left had the next lowest total integrated force at an average of 14.98 Ns (p < 0.001). The remaining four directions had the highest total integrated force at an average of 18.86 Ns (p < 0.001).

Additionally, there was a significant interaction between controller condition and drawing direction when predicting total integrated force [$F(35,287) = 12.613$, $p < 0.001$].

Drawing horizontally, drawing from bottom left to top right, and drawing from top right to bottom left took significantly less total integrated force than the other four directions for the original ICR and all three modified controllers. The original Basic and FBA controllers showed no differences in total integrated force by drawing direction.

Controller condition significantly predicted efficiency [$F(5,287) = 30.643$, $p < 0.001$] (Figure 3.6(d)). The original FBA and Basic controllers had lower efficiency than any of the other controller conditions ($p < 0.001$). Drawing direction also significantly predicted efficiency [$F(7,287) = 7.769$, $p < 0.001$]. Drawing horizontally, drawing from bottom left to top right, and drawing from top right to bottom left were significantly less efficient than the other four directions. There was also a significant interaction between controller condition and drawing direction when predicting efficiency [$F(35,287) = 3.450$, $p < 0.001$]. Drawing horizontally, drawing from bottom left to top right, and drawing from top right to bottom left were significantly less efficient than the other four directions for the original Basic and FBA controllers and the modified ICR controller. The modified Basic, FBA, and the original ICR controller showed no differences in efficiency by drawing direction.

I finally examined the subjective data to choose between the pairs of controller conditions (original and modified). When asked how natural the controller condition felt, participants preferred the modified Basic condition (4.0 vs. 3.2/5.0), the original ICR (3.9 vs. 3.2/5.0), and the modified FBA (4.1 vs. 3.7/5.0). When asked how well they perceived that they performed, participants felt that they did better with the modified Basic (3.9 vs. 3.4/5.0) and the modified FBA (3.8 vs. 2.5/5.0). There was no difference between the original and modified ICR. Subjectively participants preferred the modifications for the Basic and FBA controllers, but preferred the original ICR controller.

Based on the efficiency and subjective findings, I decided to use the modifications to the Basic and FBA controller conditions, but to retain the original configuration for the ICR controller in our final experiment.

3.7 Experiment 3: E-PAHR, PAHR, and Freehand Comparison

I conducted our third experiment to compare the performance of the selected E-PAHR controller strategies to the nonrotating PAHR and the freehand (unsupported) conditions. The only factor of interest in this experiment was the controller/support condition. Focusing specifically on the controller/support condition allowed us to examine the error versus completion time trade-off through a hierarchical regression analysis.

3.7.1 E-PAHR, PAHR, and Freehand Comparison Methods

I first desired to confirm the relevant results from Experiment 2 for the data from Experiment 3. For Experiment 3, each support condition of the experiment had participants trace three repetitions of small sine wave, oblate limacon, asymmetric lemniscate, and rectangle shapes and three repetitions of large (where large is 1.5 times wider) of each shape type. 20 participants (17 males and 3 females ranging in age from 21 to 41 years old) completed the experiment of which two were authors of this chapter. The total time required to complete the experiment was approximately 60 minutes, which included time for breaks between experiment conditions.

The main factor of interest in this experiment was the support condition. Each participant completed 16 trials (4 shapes * 2 repetitions * 2 sizes) under each of the five support conditions: three with the E-PAHR, one with the PAHR, and one Freehand. For

this experiment, the smaller shapes were presented as the same size from Experiment 1 and the larger shapes were approximately 1.5 times larger in width. Due to the PAHR's limited workspace, participants were given four repetitions of the smaller shapes and no larger shapes.

For this experiment, I used a two-way 4 x 5 factorial ANOVA to predict median error by shape and support condition with participant number entered as a random variable. I examined a two-way 4 x 5 factorial ANOVA to predict mean completion time per path length by shape and support condition with participant number entered as a random variable. I then used a two-way 4 x 5 factorial ANOVA to predict total integrated force and efficiency by support condition and shape with participant number entered as a random variable. Finally, I used a two-way 4 x 5 factorial ANOVA to predict the perceived level of exertion by support condition and shape with participant number entered as a random variable.

3.7.2 E-PAHR, PAHR, and Freehand

Comparison Results and Discussion

Support condition predicted median error [$F_{(4,454)}$ = 49.489, $p < 0.001$)] (Figure 3.7(a)). The Freehand condition had the greatest amount of median error at 0.76 mm ($p < 0.001$). The PAHR condition at 0.56 mm had less median error than the freehand condition and more median error than any of the E-PAHR conditions by an average of 0.06 mm ($p < 0.001$). Within the E-PAHR support conditions, the FBA controller had more median error than the ICR controller did by 0.03 mm ($p = 0.007$). Shape type also predicted median error [$F_{(7,454)}$ = 13.709, $p < 0.001$)]. Small (0.16 m x 0.08 m) and large (0.24 m x 0.08 m)
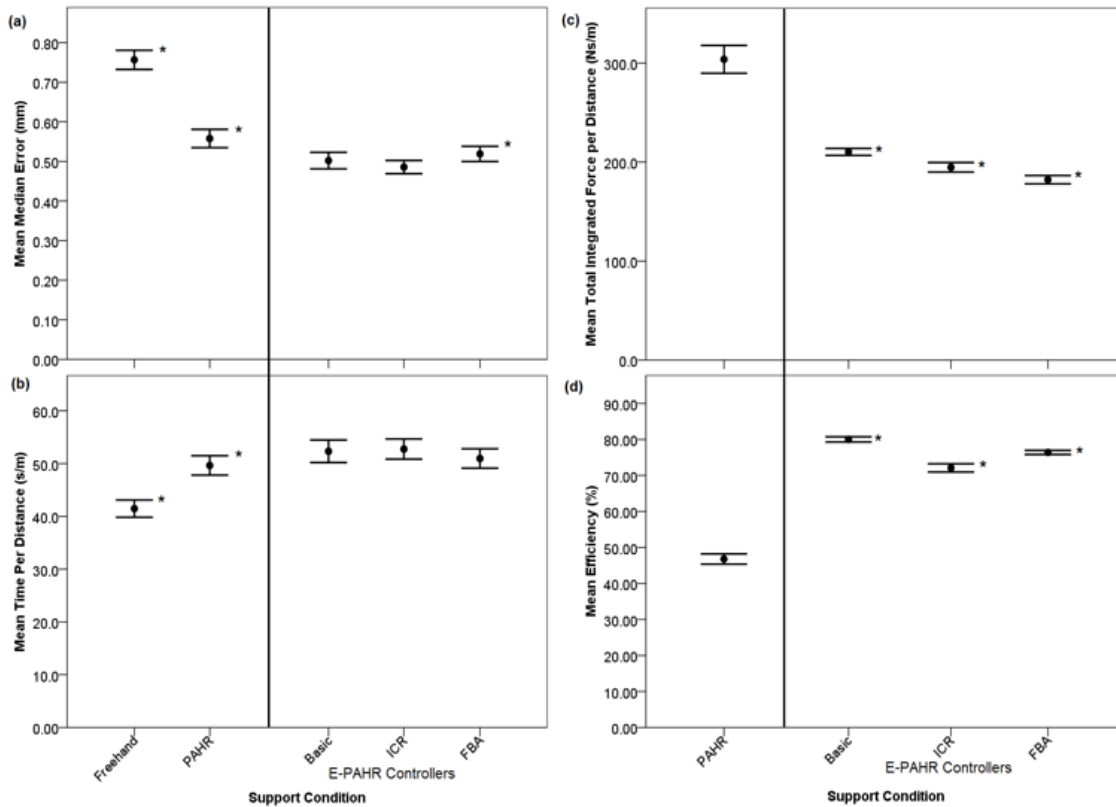
Figure 3.7. Experiment 3 median error (a), completion time per distance (b), total integrated force per distance (c), efficiency (d), and subjective ratings. Error bars indicate 95% confidence intervals for the estimated mean. * indicates significant differences within each condition grouping.

rectangles had less median error than the other shapes ($p < 0.001$).

Before conducting completion time analyses, I again normalized the completion time per path length. Support condition predicted time per path length [$F_{(4,454)} = 6.790$, $p < 0.001$] (Figure 3.7(b)). Freehand had the lowest time per path length at 41.47 s/m ($p < 0.001$). The PAHR condition had less time per path length than Basic and ICR conditions by an average of 2.89 s/m ($p < 0.001$), but the same time per path length as the FBA condition ($p = 0.185$). Shape type predicted time per path length [$F_{(7,454)} = 31.702$, $p < 0.001$]. Small and large sine waves took more time per distance than the other shapes ($p < 0.001$).

All three E-PAHR controller conditions had less median error but higher completion time per path length than the PAHR and Freehand. To test the hypothesis that there is a speed versus accuracy trade-off in our task (cf., [25]), I conducted a hierarchical multiple regression. Due to the general inverse relationship between error and task completion time as found both here and in [1], I first entered the completion time per distance and the inverse of completion time per distance as a set into the hierarchical regression model, followed by use of a device (either the PAHR or E-PAHR), and finally use of the E-PAHR.

Hierarchical regression analysis indicates that the completion time per distance set accounts for a significant 27.1% of the variance in median error [$F_{(2,1583)} = 294.694$, $p < 0.001$]. Use of a device (PAHR or E-PAHR) accounts for an additional significant 9.9% of the variance in median error [$F_{(1,1582)} = 249.901$, $p < 0.001$], leading to an average reduction in error of 0.14 mm, which confirms the findings of [1] and [2] that use of the Active Handrest leads to an increase in user skill level. Use of the E-PAHR accounts for an additional significant, but small 0.6% of the variance in median error [(F 1,1581) = 15.990, $p < 0.001$], leading to an average reduction in error of 0.04 mm. There was no discernable difference in skill level between the three E-PAHR controllers.

Support condition significantly predicted total integrated force [$F_{(3,681)} = 18.410$, $p < 0.001$] (Figure 3.7(c)). The E-PAHR's FBA controller had the lowest total integrated force per distance at 182.18 Ns/m. The ICR controller had the next lowest total integrated force per distance 194.69 Ns/m ($p < 0.001$) followed by the Basic controller at 210.25 Ns/m ($p < 0.001$). The PAHR had the highest total highest total integrated force per distance at 303.76 Ns/m ($p < 0.001$). From this, it can be seen that all of the E-PAHR controllers had significantly lower total integrated force per distance than the PAHR; hence, the user had

lower exertion when using the E-PAHR than PAHR.

Shape type also significantly predicted total integrated force [$F_{(7,681)}$ = 46.239, p < 0.001]. Small (0.1 m wavelength) and large (0.15 m wavelength) sine waves, each of amplitude 0.05 m, had higher total integrated force per distance than the other shapes (p < 0.001). There was a significant interaction between support condition and shape type [$F_{(17,681)}$ = 4.237, p < 0.001]. This interaction was caused by sine waves requiring more total integrated force per distance under the three E-PAHR conditions than with the PAHR.

Support condition significantly predicted efficiency [$F_{(3,681)}$ = 92.405, p < 0.001] (Figure 3.7(d)). The PAHR had lower efficiency than any of the E-PAHR controller conditions at 46.80% (p < 0.001). The ICR controller had the next lowest efficiency at 72.09% (p < 0.001) followed by the Basic controller at 76.40% (p < 0.001). The FBA controller had the highest efficiency at 80.02%.

Shape type also significantly predicted efficiency [$F_{(7,681)}$ = 12.656, p < 0.001]. Drawing the smaller shapes had significantly lower efficiency than the larger shapes. This was caused by the interaction between support condition and shape type when predicting efficiency [$F_{(17,681)}$ = 9.661, p < 0.001]. Small shapes traced using the PAHR had significantly lower efficiency than when traced with any of the E-PAHR conditions.

Lastly, I examined the subjective data ratings for naturalness, performance, and perceived level of exertion. When asked how natural the controller condition felt, participants equally preferred the FBA and Freehand conditions (4.1/5.0). The PAHR condition was perceived to be the least natural condition (2.3/5.0). When asked how well they perceived that they performed, participants felt that they did slightly better with the E-PAHR's ICR controller (4.0/5.0) compared to the FBA and Basic controllers (3.8/4.0).

Participants also felt they performed worse with the PAHR condition (3.2/5.0) and the worst overall with the freehand condition (1.6/5.0). These perceptions were supported by the findings for median error and from the hierarchical regression as discussed earlier in this section.

When asked about their perceived level of exertion, participants found Freehand to have the highest level of perceived exertion (12.9/20). Participants perceived the E-PAHR's FBA controller to require the lowest level of exertion (9.8/20). The measured total integrated force per distance supported the perception that the FBA controller had the lowest exertion. Surprisingly, participants found the PAHR, Basic, and ICR conditions to have about the same level of perceived exertion (10.4, 10.7, and 10.2 out of 20), while the measured total integrated force per distance was actually much higher for the PAHR condition.

Based on the lower perceived and actual (low total integrated force) levels of exertion, participant ratings for Naturalness, relatively high Efficiency, and high skill level, I determined that the FBA controller was the best method for control of the Enhanced Planar Active Handrest. This controller has the additional benefit of being the most flexible by allowing specific virtual masses and damping (inverse of admittance gain) for both translations and rotations.

3.8 Conclusion

In this work, I endeavoured to improve upon the performance of the Active Handrest, a planar device that assists a user in performing precision manipulation tasks over an extended workspace. The results discovered expand on the previous studies of the Active

Handrest [1],[2], which showed a skill level improvement while using the device for large workspace precision tracing tasks. To improve the performance of the device, I explored the effectiveness of a rotational degree-of-freedom to the Active Handrest. Our first experiment helped us to the most effective strategy for the E-PAHR.

After selecting the Basic, ICR, and FBA as the most effective controller strategies for the E-PAHR, I then conducted a second experiment to attempt to improve these three strategies. I decided to use the modifications to the Basic and FBA controllers, but retain the original ICR controller.

Our third and final experiment compared these three E-PAHR controllers to the original PAHR and Freehand support conditions. Through our analysis, I determined that after accounting for the effects of completion time, use of the E-PAHR led to significantly less median error than freehand and slightly less median error than use of the PAHR. Subjective analysis also showed user preference for the E-PAHR over the PAHR. Additional analysis of user force input showed a large reduction in the total integrated force required to complete a task and an almost doubled efficiency for the E-PAHR over the PAHR. These findings along with the E-PAHR's increased workspace underscores the potential benefit for the Active Handrest's use in conducting large workspace precision tasks.

Through our experimentation, I demonstrated that the E-PAHR is a useful device for assisting users in performing precision tasks over a large workspace. I have confirmed the finding that the E-PAHR improves user skill level, and I established that the E-PAHR reduces user effort when compared to our previous device prototype. Based on these results, I anticipate that the Active Handrest will be useful in many practical applications, such as medical tasks, artistry, machining, upper limb rehabilitation, or other tasks

requiring dexterous manipulation of tools while preforming precision tasks over a large workspace. In the future, I intend to develop a Spatial Active Handrest that will allow for support in the vertical direction and increased precision as a user performs tasks in a three-dimensional large workspace.

3.9 Acknowledgment

3.10 References

[1]   M. Fehlberg, B. Gleeson, and W. Provancher, "Active Handrest: a large workspace tool for precision manipulation," *Int. J. Robotics Res.*, vol. 31, no. 3, pp. 289-301, 2012.

[2]   M. Fehlberg, A. Doxon, W. Provancher, "Improved Active Handrest performance through use of adaptive admittance and virtual fixtures," *IEEE Trans. Human-Mach. Syst.*, vol. 44, no. 4, pp. 484–498, 2014.

[3]   S. Ito and Y. Yokokohji, "Maneuverability of master control devices considering the musculo-skeletal model of an operator," *Proc. World Haptics*, pp. 57–62, 2009.

[4]   A. Erdelyi, T. Sihvonen, P. Helin, and O. Hanninen, "Shoulder strain in keyboard workers and its alleviation by arm supports," *Int. Arch. Occup. Environ. Health*, vol. 60, pp. 119–124, 1998.

[5]   Equipois. ZeroG. Available: http://www.equipoisinc.com.

[6]   S. B. Chyatte, C. Long 2nd , and P. J. Vignos Jr., "The balanced forearm orthosis in muscular dystrophy," *Arch. Phys. Med. Rehabil.*, vol. 46, pp. 633–636, 1965.

[7]   Y. L. Yasuda, K. Bowman, and J. Hsu. "Mobile arm supports: criteria for successful use in muscle disease patients," *Arch. Phys. Med. Rehabil.*, vol. 67, pp. 253–256, 1986.

[8]   R. Beer, C. Naujokas, B. Bachrach, and D. Mayhew, "Development and evaluation of a gravity compensated training environment for robotic rehabilitation of post-stroke reaching," *Proc. IEEE RAS & EMBS Int. Conf. Biomed. Robo. Biomech.*, pp.

205–210, 2008.

[9] Kwakkel, R. C. Wagenaar, T. W. Koelman, G. J. Lankhorst, and J. C. Koetsier. "Effects of intensity of rehabilitation after stroke: a research synthesis." *Stroke*, vol. 28, no. 8, pp. 1550–1556, 1997

[10] R. Riener, T. Nef, and G. Colombo. "Robot-aided neurorehabilitation of the upper extremities." *Med. Bio. Eng. Comp.*, vol. 43, no. 1, pp. 2–10, 2005.

[11] B. Langhammer, B. Lindmark, and J. K. Stanghelle. "Stroke patients and long-term training: is it worthwhile? A randomized comparison of two different training strategies after rehabilitation." *Clinical Rehabil.*, vol. 21, no. 6, pp. 495–510, 2006.

[12] R. F. Beer, M. D. Ellis, B. G. Holubar, J. P.A. Dewald. "Impact of gravity loading on post-stroke reaching and its relationship to weakness." *Musc. Nerve*, vol. 36, no. 2, pp. 242–250, 2007.

[13] R. Taylor, P. Jensen, L. Whitcomb, A. Barnes, R. Kumar, D. Stoianovici, P. Gupta, Z. Wang, E. Dejuan, and L. Kavoussi. "A steady-hand robotic system for microsurgical augmentation," *Int. J. Robotics Research*, vol. 18, no. 12, pp. 1201–1210, 1999.

[14] J. Colgate, W. Wannasuphoprasit, and M. Peshkin, "Cobots: robots for collaboration with human operators," *Proc. Int. Mech. Eng. Cong. Exhib.*, vol. DSC-58, pp. 433–440, 1996.

[15] N. Hogan, H. I. Krebs, A. Sharon, and J. Charnnarong, "Interactive robotic therapist," US Patent 5,466,213, Massachusetts Institute of Technology, 1995.

[16] R. Loureiro, F. Amirabdollahian, M. Topping, B. Driessen, and W. Harwin. "Upper limb robot mediated stroke therapy—GENTLE/s approach." *Auto Robots*, vol. 15, no. 1, pp. 35–51, 2003.

[17] P. S. Lum and C. G. Burgar, "Robot-assisted movement training compared with conventional therapy techniques for the rehabilitation of upper-limb motor function after stroke," *Arch. Phys. Med. Rehabil.*, vol. 83, no. 7, pp. 952–959, 2002.

[18] T. Nef, M. Guidali, and R. Riener. "ARMin III – Arm therapy exoskeleton with an ergonomic shoulder actuation," *Applied Bio. Biomech.*, vol. 6, no. 2, pp. 127–142, 2009.

[19] S. Moubarak, M. Pham, R. Moreau, and T. Redarce. "Gravity compensation of an upper extremity exoskeleton." *Proc. Int. Conf. IEEE Eng. Med. Bio. Soci. (EMBC)*, pp. 4489–4493, 2010.

[20] N. Hogan, "Impedance control: an approach to manipulation: part III applications."

J. Dynamic Syst. Meas. Control, vol. 107.2, p. 17, 1985.

[21] R. Q. Van der Linde, P. Lammertse, E. Frederiksen, and B. Ruiter, "The HapticMaster, a new high-performance haptic interface," *Proc. EuroHaptics*, pp. 1–5, 2002.

[22] R. Colombo, F. Pisano, S. Micera, A. Mazzone, C. Delconte, M. C. Carrozza, P. Dario, and G. Minuco, "Robotic techniques for upper limb evaluation and rehabilitation of stroke patients," *IEEE Trans. Neural Syst. Rehabil. Eng.*, vol. 13, no. 3, pp. 311–324, 2005.

[23] S. P. Wise and R. Shadmehr. "Motor control," *Encycl. Human Brain,* vol. 3, pp. 137–157, 2002.

[24] R. S. Woodworth, "Accuracy of voluntary movement," *Psych. Review: Monograph Suppl.*, vol. 3, no. 3, pp. 1, 1899.

[25] P. Fitts. "The information capacity of the human motor system in controlling the amplitude of movement." *J. Exp. Psych.*, vol. 47, no. 6, pp. 381–391, 1954.

[26] R. Plamondon and A. M. Alimi, "Speed/accuracy trade-offs in target-directed movements," *Behav. Brain Sci.*, vol. 20, no. 2, pp. 279–303, 1997.

[27] J. Reis, H. M. Schambra, L. G. Cohen, E. R. Buch, B. Fritsch, E. Zarahn, P. A. Celnik, and J. W. Krakauer, "Noninvasive cortical stimulation enhances motor skill acquisition over multiple days through an effect on consolidation," *Proc. Natl. Acad. Sci.* U.S.A., vol. 106, no. 5, pp. 1590–1595, 2009.

[28] L. Shmuelof, J. W. Krakauer, and P. Mazzoni, "How is a motor skill learned? Change and invariance at the levels of task success and trajectory control," *J. Neuro.*, vol. 108, no. 2, pp. 578–594, 2012.

[29] J. W. Krakauer and P. Mazzoni, "Human sensorimotor learning: adaptation, skill, and beyond," *Current Opinion Neuro.*, vol. 21, no. 4, pp. 636–644, 2011.

[30] M. Ueberle, N. Mock, and M. Buss. "VISHARD10, a novel hyper-redundant haptic interface." *Proc. 12th Int. Symp. Haptic Interfaces Virtual Environ. Teleop. Syst.*, pp. 58–65, 2004.

[31] L. Goncalves, E. Di Bernardo, E. Ursella, and P. Perona, "Monocular tracking of the human arm in 3D," *Proc. Fifth Int. Conf. Comp. Vision,* pp. 764–770, 1995.

[32] T. B. Moeslund and E. Granum, "Multiple cues used in model-based human motion capture," *Proc. Fourth IEEE Int. Conf. Auto. Face and Gesture Recognition,* pp. 362–367, 2000.

[33] M. Nambi, W. Provancher, and J. Abbott, "On the ability of humans to apply

controlled forces to admittance-type devices," *Adv. Robo.*, vol. 25, pp. 629–650, 2011.

[34] S. Schaal, D. Sternad, R. Osu, and M. Kawato, "Rhythmic arm movement is not discrete," *Nature Neurosci.*, vol. 7, no. 10, pp. 1136–1143, 2004.

[35] N. Hogan and D. Sternad, "On rhythmic and discrete movements: reflections, definitions and implications for motor control," *Exp. Brain Research*, vol. 181, no. 1, pp. 13–30, 2007.

[36] S. Levy-Tzedek, M. Ben-Tov, and A. Karniel, "Early switching between movement types: indication of predictive control?" *Brain Res. Bulletin*, vol. 85, no. 5, pp. 283–288, 2011.

[37] M. Ben-Tov, S. Levy-Tzedek, and A. Karniel, "The effects of rhythmicity and amplitude on transfer of motor learning," *PloS One,* vol. 7, no. 10, p e46983, 2012.

[38] R. Likert, R. "A technique for the measurement of attitudes," *Arch. Psych.*, vol. 22, 1932.

[39] G. Borg, "Psychophysical bases of perceived exertion." *Med. Sci. Sports Exercise*, vol. 14, no. 5, pp. 377–381, 1982.

[40] G. Borg, "Psychophysical scaling with applications in physical work and the perception of exertion," *Scandinavian J. Work, Environ. Health*, pp. 55–58, 1990.

CHAPTER 4

SPATIAL ACTIVE HANDREST: ADDING GRAVITY COMPENSATION

AND LOCAL SUPPORT FOR 3D TASKS

The Spatial Active Handrest (SAHR) is a human-robot cooperative device that improves a user's accuracy over a three-dimensional workspace and is an extension of prior work on the planar, Enhanced Planar Active Handrest (E-PAHR). Potential applications of the SAHR include assistive robotic surgery, surgery training and simulation, and upper extremity rehabilitation. In this chapter, I studied human arm movements within a three-dimensional workspace and designed the SAHR to closely match the kinematics of the human arm and provide an ergonomic support throughout its workspace. A series of experiments evaluated various control strategies and virtual fixtures and tested the SAHR's utility through a surgery simulation experiment. I also measured participants' surface electromyography (EMG) signal at four locations on the shoulder and upper arm to investigate changes in muscle activity with and without use of the SAHR. Compared to unassisted support conditions, the SAHR improves participants' performance and reduces strain on large muscles in the shoulder, i.e., trapezius and lateral deltoid.

4.1 Introduction

The original Planar Active Handrest (PAHR) was developed at the University of Utah to assist with large workspace precision manipulations in the horizontal plane [1]. This device had two degrees-of-freedom (DOF) and only provided planar horizontal support to the user's arm. Fehlberg et al. have shown that using the PAHR improves participants' performance and skill levels compared to unsupported support conditions like freehand and fixed elbow [1]. In a later study, Fehlberg demonstrated that adding virtual fixtures to the PAHR could further improve participants' skill levels [2]. However, the PAHR did not match the kinematics of a human arm due to its Cartesian, two DOF kinematics, which resulted in uncomfortable arm postures. To alleviate this problem, Fehlberg and the authors developed the Enhanced Planar Active Handrest (E-PAHR) by adding a rotational third DOF to better match the planar kinematics of human arm and increase participant's comfort levels [3]. There have also been prior studies on a single-axis gravity compensation device, the Vertical Active Handrest (VAHR), which investigate the complications of adding gravity compensation and ergonomic support [4]. In the research presented herein, I will combine all our previous findings, and further extend the workspace of the E-PAHR to the third dimension. This is done to provide three-dimensional gravity compensation and ergonomic support to improve the device's utility and to reduce fatigue.

Tasks that require dexterous motions, precision control, and/or holding a heavy tool for an extended period could result in muscle fatigue and deterioration in user's motor control. Traditionally, humans have used static supports, such as a wrist support while writing, to stabilize their arm motions and improve accuracy. Ito and Yokokohji have shown that resting the arm on a surface reduces muscle fatigue [5]. However, using static

wrist supports limit the task to the wrist's workspace. When dealing with tasks that require a larger three-dimensional workspace, an intermittent repositioning of the wrist support is required to improve accuracy while reducing muscle fatigue.

For our research, I developed the Spatial Active Handrest (SAHR) (Figure 4.1), a human-robot cooperative device that provides ergonomic support and matches the kinematics of the human arm over a large three-dimensional workspace. I intend to achieve this goal by studying the kinematics of the human arm through a motion capture study and adding a vertical DOF support. This device will improve upon the currently available Enhanced Planar Active Handrest (E-PAHR) to allow elevation of a user's arm through elbow flexion and extension. The SAHR can be used to increase the accuracy of able-bodied users while performing dexterous tasks such as robotic-assisted surgery, surgery simulation, painting, or to rehabilitate or help disabled users regain lost motor function.

Figure 4.1 Spatial Active Handrest (SAHR).

This chapter presents three main studies: a motion capture study of the human arm while reaching and sweeping, the control strategy and virtual fixture selection through a three-dimensional line-tracing task, and a device utility experiment using a simple surgery simulator. I used the motion capture study to finalize the SAHR's device design and to track the participants' arm movements to determine whether to independently move the elbow and hand supports' elevation axis. In the second study, I investigated the performance of various SAHR control strategies and virtual fixtures in a three-dimensional line-tracing task. The third and last study compared participants' performance and muscle activity during a simple surgery simulation task. I used surface electromyography (EMG) signals from the trapezius, deltoid, biceps, and triceps muscle groups to empirically measure changes in muscle activity and compare participants' fatigue during assisted and unassisted support conditions. Neurobiology literature suggests that muscles comprised of motor units with small innervation ratios are more adept at delivering precise motions and that muscles with large innervation ratios are better at large scale coarse motions [6]. Therefore, our hypothesis is that the SAHR will allow for more agile force input control compared to unassisted support conditions by using the smaller muscle groups of the hand and wrist rather than the large groups of the shoulder and arm while also helping to reduce a user's shoulder fatigue.

In the following section, I provide a review of related literature. I review the benefits of providing support to the user, available passive and active assistive devices, control strategies used in human interactive devices, and virtual fixtures. Next, I present the motion capture study of the human arm and the corresponding results. Section 4.4 describes how I used the motion capture findings to design the SAHR and explains the details of the

selected SAHR control strategy and virtual fixture. Section 4.5 illustrates the general experimental methods used in our experiments. Lastly, I describe in more detail the specific methods, obtained results, and discussions for each experiment, followed by conclusions and future work.

4.2 Background

The lack of gravitational support while performing a task that requires dexterous motions or holding a heavy object for an extended period of time could result in muscle fatigue. Various studies have linked muscle fatigue with a decrease in accuracy and velocity when throwing [7], passing [8], and hitting [9] an object. Many researchers have studied the effect of using static or repositionable supports on muscle fatigue. For instance, Cook and Burgess found that while using a mouse and keyboard, a forearm support is preferable and reduces musculoskeletal discomfort compared to a nonsupported floating posture [10]. Furthermore, the addition of a simple armrest to a chair is shown to reduce arm, shoulder muscle load [11], and reduce the amount of applied force while typing [12]. Ito and Yokokohji have shown that in addition to lowering the gravity load on the user, an armrest reduces muscle fatigue by decreasing the grip force [6]. Studies have shown repositionable static supports to further reduce muscle fatigue over a larger workspace by eliminating the weight of the arm while typing [13] or using tools [14].

In order to utilize the aforementioned, many devices with passive and active supports are designed to reduce muscle fatigue and provide gravitational compensation to the user. Disabled and able-bodied users can use passive support devices to offload the weight of user's arm or a heavy tool within its workspace. Three popular examples are Equipois'

zeroG [14], Balanced Forearm Support [15], and Mobile Arm Support [16]. On the other hand, robotic devices with active support are commonly used for assisting in tasks that require dexterous motions or rehabilitation purposes.

Common designs of rehabilitation robots include end point manipulation and powered exoskeletons. Exoskeletons are anthropomorphic robots that are tightly connected to the human arm, and its joint angles fully define a human arm's pose. An example of such a robotic device is the ARMin III [17], which can be attached to a chair or wheelchair to provide gravity compensation. Similarly, endpoint manipulation devices guide a user's arm along a predefined trajectory and could assist disabled users with regaining lost motor skills in their arm. A few popular examples of endpoint manipulators are MIT Manus [18], GENTLE/S [19], and PUMA 560 [20].

Another area of related research is the use of robotic devices to assist able-bodied users in performing dexterous tasks. The Steady Hand, a robotic system developed at Johns Hopkins University, helps users with submillimeter manipulation tasks by simultaneously taking force input from the user and a robot to move the tool accordingly [21].

Another consideration that is highly coupled with device design of a human interactive device is the control paradigm that is implemented. The most common control paradigms for human-robot interaction robotics are impedance and admittance control [22]. Impedance devices tend to be lightweight, highly backdrivable, and impede user's movements by applying force feedback [23]. On the other hand, admittance control is often used on heavier and nonbackdrivable devices that can render high stiffness. The admittance control paradigm was used previously on the E-PAHR as well as by many other researchers in robotic applications, such as the Steady Hand surgery robot [21] and rehabilitation [24].

When it comes to controlling an admittance-type device, Nambi demonstrates that although the velocity limit and admittance gain of a device affects the force control accuracy, the input force is the most important factor in user accuracy [25]. In order to achieve the highest level of force control precision, a low admittance gain is required, which results in a reduction in device's velocity. Consequently, a sluggish device can cause operator fatigue as the user exerts higher forces than necessary [26]. These findings suggest that there is an ideal range of forces, admittance gains, and velocities for optimal human control using an admittance control strategy. Furthermore, every control strategy needs to be tuned appropriately to provide an optimal performance without tiring the user.

Another general approach to assist in human-robot cooperative robots is the use of virtual fixtures. Researchers have used virtual fixtures to guide a user along a preknown path [27] or to prevent the user from entering a forbidden region [28]. In a previous study, Fehlberg has shown that by adding a virtual fixture that the user's accuracy could be improved beyond other tested control strategies. Additionally, the same study has shown that adding a stylus virtual fixture significantly increases accuracy of each hand/arm support condition.

4.3 Motion Capture Study of Human Arm

Our goal with the SAHR is to design a device that provides ergonomic support and gravity compensation while closely matching the kinematics of human arm within a large three-dimensional workspace. Researchers from the University of Pennsylvania have derived an inverse kinematics of a seven DOF human arm model [29]. However, such models have been shown to lack a well-founded theory for generating and evaluating

natural postures. There have been multiple studies investigating elbow elevation angle with respect to the target coordinates [30], but Seungsu et al. have shown that the hand location is not the only factor that affects the elbow position and elevation angle [31]. Hence, I designed our own motion capture study that is geared toward SAHR's application, workspace, and experimental tasks. More specifically, our goal was to investigate how participants' elbow height varies as a function of hand or grasped tool height and if there is a correlation between the two, in order to better inform the desired kinematics of the SAHR. I used the results of this study to decide whether to couple the height of SAHR's elbow and hand or to allow for an independent control of each.

4.3.1 Methods

The designed motion capture study consisted of three tasks selected to represent possible applications of SAHR. The first and second tasks involved reaching, precision manipulation, and relocation. Fifteen Ping-Pong balls were used as targets and placed at various locations and heights within a rectangular box workspace (1200 W x 600 H x 600 D mm), which was much larger than the workspace of the prior designed E-PAHR. Each Ping-Pong ball had a distinct shape and number drawn onto it. In the first task, I asked the participants to start from a pre-set location and hand posture, reach toward one of the targets, trace the corresponding shape on the target, and return to the known starting position. Once a trial was completed, I instructed the participant to move to the next random target. The second task was similar to the first, but with the difference that I asked participants to not return to the known starting position and continue to the next random target until all 15 targets were traced. In the third and last task, I asked the participants to

slowly sweep the space of a smaller three-dimensional rectangular box (500 mm x 300 mm x 300 mm), which more closely matched the workspace of E-PAHR and our intended size of the SAHR.

This experiment included 10 participants and used 10 Flex13 OptiTrack motion capture cameras to record the participants' arm motions at 120 Hz. While the focus of this experiment was to compare the elbow and hand height changes relative to each other, I used 18 markers to fully track the participants' arm movements and postures. These markers were placed on grasped tool and participants' hand, forearm, elbow, upper arm, shoulder, and upper body.

4.3.2 Results and Discussion

The first and main finding of this experiment was to observe a linear correlation between elbow and hand height within the tested workspace (Figure 4.2). Using regression
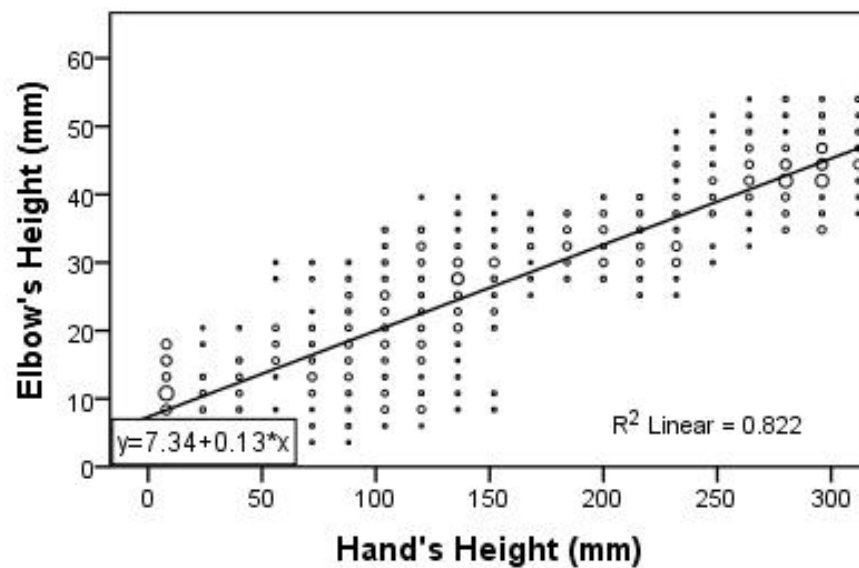

Figure 4.2 Human arm movement study and the linear correlation between the elbow and hand height within the tested workspace.

analysis, it is clear that hand height is a significant predictor of elbow height within the tested workspace, and it accounts for 82.2% of the variance ($R^2 = 0.822$, $F(1, 4327) = 6178.9$, $p < 0.001$). Another insignificant predictor was how far the participant's hand was in front of him, which accounted for only 3.9% of the variance in elbow height (Figure 4.3 bottom). The results also indicated that how far the participant's elbow was across from him was not a significant predictor and only accounted for 0.3% of the variance (Figure 4.3 top). Based on these results, I concluded that while independent elevation control of elbow and hand may be ideal, it is not necessary. The device design can be simplified by coupling the elevation of two locations such that the elbow elevates 1 mm for every 7.3 mm of hand elevation. I believe that a user's shoulder girdle elevation and decompression can compensate for the variance in elbow height observed in the regression.

Our second finding was with regard to Donders' law and its extension to human arm movement. According to this law, there is a unique shoulder and elbow angle for every hand posture in a three-dimensional workspace. However, there have been multiple studies with contradicting results of this law's accuracy [32, 33]. In our limited study of 10 subjects and 15 targets, I found Donders' law to hold true as no significant different between the participant's shoulder and hand angles during the first and second tasks was observed. However, this is not conclusive due to our small sample size.

4.4 Device Description, Control Strategy, and Virtual Fixtures

I designed the Spatial Active Handrest (SAHR) with four DOF to provide an ergonomic support over a large three-dimensional workspace that closely matches the kinematics of the human arm. A user can control this device through inputs from two force sensors, each
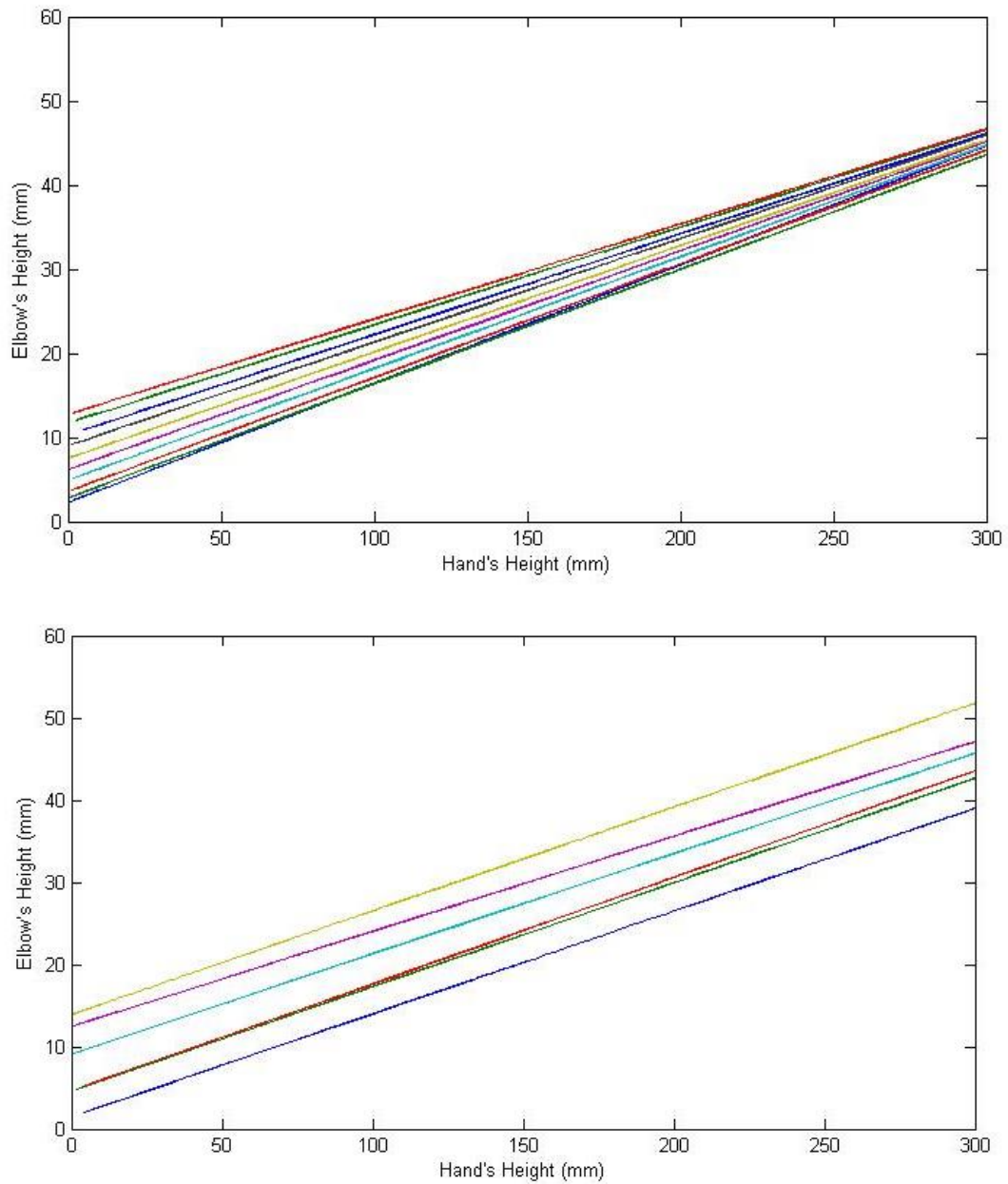
Figure 4.3 Linear correlation between the elbow and hand height as a factor of change in the hand location along Cartesian planar axis.

located under the user's wrist and elbow. An admittance control strategy calculates the desired velocity based on the applied force and outputs appropriate commands to the motors. I also implemented virtual fixtures to improve participants' performance and reduce complexities of a three-dimensional task.

4.4.1 SAHR Mechanical Design

The SAHR (Figure 4.4) was built on top of the existing E-PAHR. SAHR uses a Parker motorized two-axis lead screw linear stage to control the x-y position of the elbow. The absolute workspace of this linear stage is 250 x 250 mm, but the elbow workspace is limited to 200 x 200 mm in software to protect the device. This covers the workspace of an average human's elbow (average human upper arm length is 250 mm [34]) as long as the upper body remains stationary and the user does not lean. The stage has a custom-made rotary capstan drive with a gear ratio of 34:1 to allow lateral and medial arm rotations within the horizontal plane. I used a single antibacklash lead screw stage with 12.7 mm pitch to actuate a 4-bar mechanism to provide elevation changes of hand and elbow. The two rotation axes for the horizontal and elevation rotations were designed to be offset from each other based on the findings of the motion capture study. A 500 count per revolution incremental encoder is attached to the shaft of each motor to provide an approximate 4 μm position feedback resolution when operated in quadrature. The overall workspace of SAHR for a user with an average forearm length of 310 mm [34] is approximately 450 W x 200 H x 200 D mm, which is slightly smaller than our targeted device workspace.

Two input strategies, force and position/motion input, can be used to control the SAHR's position. The SAHR uses two six-axis ATI mini-40 force-torque sensors to
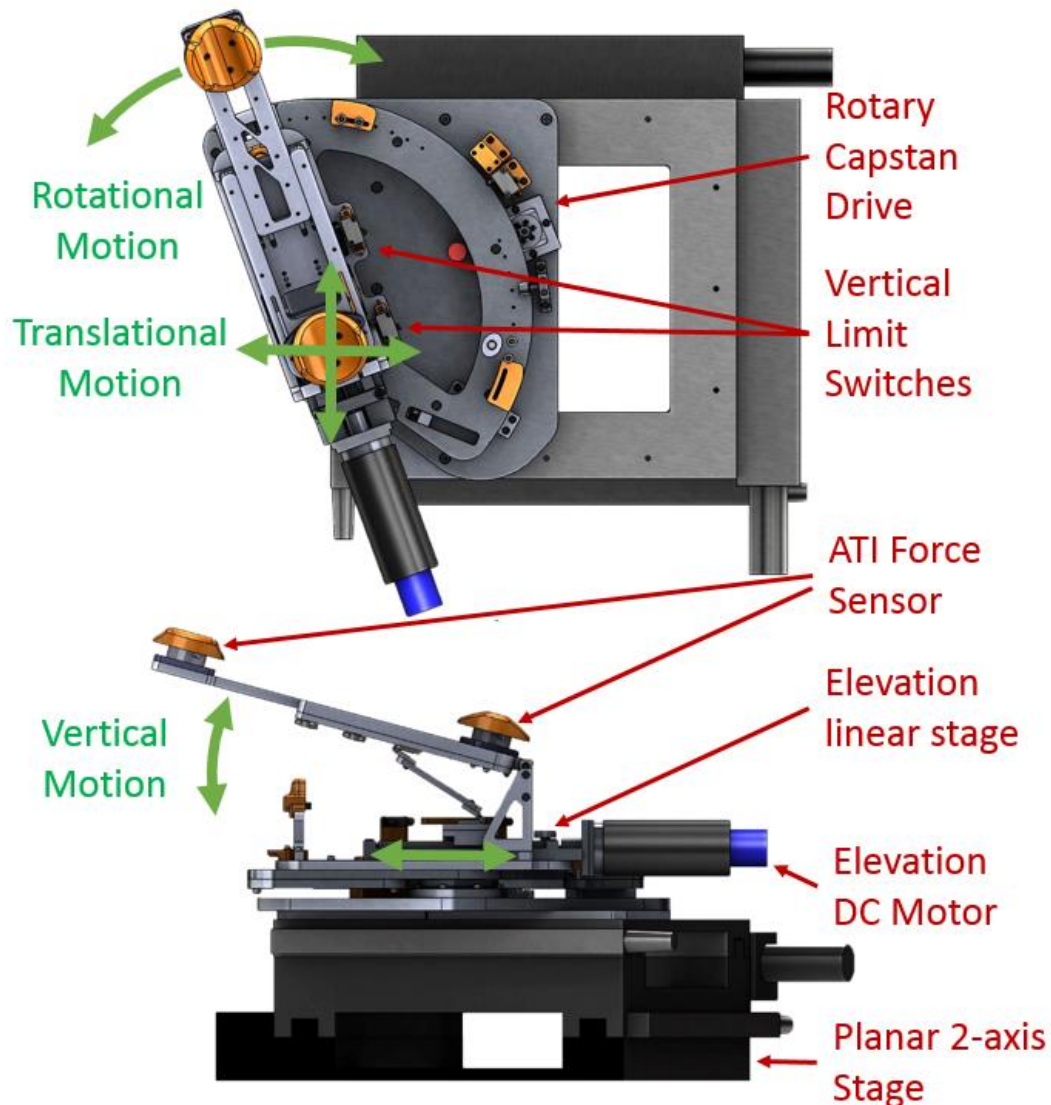
Figure 4.4 Spatial Active Handrest (SAHR) and its respective components.

measure user's applied force. While the ATI sensors are capable of measuring applied torque, I only used the force sensor readings and converted the force readings across two of the sensors (i.e., a force couple) to an input torque as needed. Both force sensors were calibrated to 20 N full scale in the horizontal direction (40 N vertically) and have a resolution of 0.005 N. The distance between the hand and elbow supports can be adjusted from 150 to 300 mm to accommodate for variation in user forearm length. Furthermore,

the upper portion of the SAHR and the elbow force sensor can be moved to ensure a 7.32 ratio between hand and elbow elevation while keeping the elbow at the capstan drive's center of rotation. A SensAble Phantom 1.5 was used both as the position input method and for evaluating the participant's position accuracy while manipulating with the use of the SAHR. A phantom premium was chosen for its low inertia and large workspace (581 W x 267 H x 191 D mm) that matches SAHR's.

A National Instruments PCIE-6320 X-Series card collects the applied force from the ATI force sensors at a 2 kHz frequency. The remaining sensors and switches are sampled at 1 kHz using a Sensory Model 626 PCI Multifunction I/O Board. I used Microsoft Visual C++ and Chai3D libraries [35] to send/receive information to/from Phantom premium and calculate the corresponding output to the motor based on the current control strategy. Advanced Motion Controls 12A8 Brush-Type PWM amplifier, calibrated to a maximum of 5 Amps full scale, sends the appropriate current commands to the motors.

4.4.2 Control Strategy

Motion of the SAHR was driven by input from the elbow and wrist force sensors. Equation (4.1) shows the admittance law used to calculate the elbow's desired translational velocities based on the applied force to the force sensors. I used a PID controller with encoder position feedback to achieve desired translational velocities. Similarly, I used (4.2), a modified version of the admittance law, to calculate the desired rotation velocities based on the applied torque across the two force sensors. The desired velocity was then integrated to obtain a desired position, and a PD controller with encoder position feedback was used to maintain this position.

$$V = K_a * F_{input} \qquad (4.1)$$

$$\omega = K_a * T_{input} \qquad (4.2)$$

where K_a is the admittance gain, F_{input} is the input force from the ATI force sensors, and T_{input} is the calculated input torque based on the applied force at the two force sensors. I limited the maximum velocity of the stage to ±90 mm/sec for safety purposes. According to Nambi et al., the most important factor in controlling an admittance type device is the input force [25] due to a deterioration of human force control at very low input forces. Based on his findings and recommendations, I used a force deadband of ±0.5 N to increase SAHR's stability by preventing the stage from moving at low input force levels.

In a previous study, I investigated and tested various control strategies using the E-PAHR [3]. The results highlighted three control strategies for having the least tracing error and the most natural arm movements. I plan to implement these control strategies on the SAHR and compare their performance in a three-dimensional workspace to determine how to best control the SAHR.

The first tested control strategy is called "Basic" due to its simple and intuitive nature. In this control strategy, all axes are decoupled from each other for simplicity (which resembles a control strategy previously used with the E-PAHR). The applied hand and elbow forces are averaged together and used to calculate the desired translational x-y velocities of the SAHR. The hand and elbow force inputs perpendicular to the forearm axis are used to determine the applied torque and desired rotational velocity of the SAHR.

The second control strategy, "Poinsot," uses the Poinsot's theorem to transform all the applied forces into a single force along a screw axis and a torque about the same axis. I used the derived equations by Murray et al. to locate this screw axis and the respective

forces and torques about it [36]. The screw axis can be calculated by

$$l = \begin{cases} \left\{ \frac{f \times \tau}{\|f\|^2} + \lambda f : \lambda \in \mathbb{R} \right\}, & if\ f \neq 0 \\ \{0 + \lambda \tau : \lambda \in \mathbb{R}\}, & if\ f = 0 \end{cases} \quad (4.3)$$

where l is the screw axis, f is the applied total force, and τ is the total applied torque. Once the axis is calculated, the force along and the torque about the axis can be calculated using the magnitude and pitch equations:

$$M = \begin{cases} \|\ f\ \|, & if\ f \neq 0 \\ \|\ \tau\ \|, & if\ f = 0 \end{cases} \quad (4.4)$$

$$h = \frac{f^T \tau}{\|f\|^2} \quad (4.5)$$

where M is the magnitude and h is the pitch of the screw. I implemented this control strategy as it uses a single admittance gain and eliminated the need for having different translational and rotational admittance gains.

The third and last control strategy is called the integrated Freebody Acceleration (FBA) controller. This strategy assumes that the SAHR is a massless rigid body with point masses at its ends. The desired translational acceleration can then be calculated:

$$m \cdot a = F_{input} - c \cdot V \quad (4.6)$$

where m is the total mass of the two equal point masses, a is the desired translation acceleration, F_{input} is the average applied force to the SAHR, c is the translational damping, and V is the SAHR's instantaneous velocity. Similarly, the desired rotational acceleration can be calculated by solving for alpha:

$$I \cdot \alpha = T_{input} - c \cdot \omega \quad (4.7)$$

where I is the total mass moment of inertia of the two point masses, T_{input} is the average applied torque to the SAHR, c is the rotational damping, and ω is the SAHR's

instantaneous rotational velocity.

4.4.3 Virtual Fixture

I implemented three virtual fixtures on the SAHR. The underlying control strategy used in these fixtures was the Freebody Acceleration (FBA) described earlier. As the SAHR is a four DOF device, a fourth input or restriction is needed to fully constrain the device. To solve this matter I employed a technique often used in exoskeletons to allow elbow position rotations about the user's hand to minimize the applied elbow force while not changing the position of the stylus or end effector. The combination of this method and the virtual fixture allowed for an accurate position control of the stylus and comfortable elbow movements.

The first implemented virtual fixture, "Tangent Support," keeps the user and the SAHR a pre-set distance away from a known operating surface. When the user applies forces to the SAHR, this fixture only allows movements that are tangential to the operating surface by masking the input forces normal to the surface. The goal of this fixture is to simplify a three-dimensional task into two-dimensions and provide improved task performance.

The second fixture, "3D Virtual Spring," allows the user to freely move the SAHR along a preknown trajectory and adjusts its position in an attempt to direct user's drawing path onto the targeted trajectory. This virtual fixture applies an attracting force proportional to the normal distance between the user's stylus position and the targeted trajectory:

$$F = -K_F(\vec{X} - \vec{X}_0) \qquad (4.8)$$

where F is the applied virtual force to the stage, K_F is the virtual fixture's spring constant (400 N/m), $\vec{X}$ is the Phantom Premium's stylus position in three-dimensional space, and $\vec{X}_0$ is the normal projection of the stylus onto the target trajectory.

The third and last implemented virtual fixture, "Tangent Support + Virtual Spring," combines the first virtual fixtures with a planar virtual spring fixture (similar to that used with the E-PAHR). As a result, the SAHR stays within a pre-set distance from an operating surface and guilds the user's hand toward the targeted trajectory within that instantaneous plane.

4.5 General Methods

This section provides a general description of how our experiments were conducted and the virtual environments used. Later sections provide specific methods, results, and discussion for each experiment.

I conducted two sets of experiments to evaluate SAHR's performance and utility using the control paradigms and fixtures outlined in Section 4.4. In all experiments, I asked participants to sit on a stool, hold the Phantom Premium's stylus, keep a natural writing posture with their hands, and maintain a good sitting posture. I then asked participants to place their right arm on the device to adjust the length of forearm, reposition the elbow location to maintain the ratio between hand and elbow height from the arm motion study, and move the top portion of SAHR to ensure that elbow force sensor is at the center of rotation. Once everything was adjusted, I strapped the participant's hand to the device to allow participants to apply upward forces and give each participant a few minutes to try out each support condition/control strategy until they felt comfortable operating the device. All participants wore noise-canceling headsets and listened to white noise for the duration of the experiment to prevent any distractions and to mask ambient noise. In order to minimize the effect of test order, such as fatigue and learning, I used a Latin squares to

balance test order. Once a support condition was completed, a 3-minute break was given to prevent eye and muscle fatigue, make necessary changes for the new support condition if necessary, and to ask a few questions. A questionnaire was used to subjectively measure how natural the movements of each support condition felt, how well the participant thought he/she performed, and participants' perceived level of exertion before and after each support condition based on Borg's Rating of Perceived Exertion (RPE) scale [37]. They responded using the revised RPE, which scales from 6 to 20 [38]. I used the mean of subjective answers from the questionnaire to evaluate the each support condition.

Once the experiment was over, I used a factorial two-way repeated measures ANOVA model to evaluate the results. Based on ANOVA results, I used Bonferroni's post hoc analysis to further investigate the different between each condition by performing a t-test on all pairs. I sampled information throughout the trials at 1 kHz, such as stylus position, closest point on the target trajectory, SAHR's position, and applied hand/elbow force. I used the following three metrics to analyze each trial: 1) mean of absolute tracing error, 2) maximum absolute tracing error, and 3) completion time. For simplicity and ease of reading, I use the following abbreviations for these metrics: mean error, maximum error, and completion time.

4.5.1 Experiment 1: Control Strategy and Fixture Selection

The first set of experiments used a three-dimensional line-tracing task and was broken into two sections to A) determine the best SAHR control strategy, and B) experiment with multiple virtual fixtures. I selected the three-dimensional line-tracing task as it provided a quick way to methodically test SAHR's performance in a three-dimensional workspace,

and its results could be compared to prior studies [2], [3]. In this experiment, the participants were asked to trace a line in the three-dimensional space while keeping a balance between completion time and accuracy. The line could be along the eight cardinal directions in three possible planes: horizontal, vertical, and 45 degrees plane. I realized the complications of presenting a three-dimensional task on a two-dimensional monitor. To alleviate this issue, I presented two different views to the participants. The camera in the secondary view was always fixed and showed a cube that represented the workspace, the drawing surface, and the target line. The camera in the main view was always normal to the drawing plane so the view and perspective did not change based on the drawing plane. Furthermore, the location of the stylus was updated in the main view as a sphere with a 1 mm radius. The trial would begin when the stylus position crossed the starting location, which was represented as a green square. The line was displayed in green and the stylus's trace line was shown in red. The trial ended when the stylus crossed the end location, marked with a red square.

4.5.2 Experiment 2: SAHR utility

The second set of experiments combined a line tracing and a simplified surgery simulation task to mimic the potential application of SAHR and compare its utility against unsupported conditions. These experiments were broken into two sections that resembled A) vein harvesting and B) melanoma removal surgical procedures. In both experiments, a model of the upper thigh (a truncated cone) and a line representing the incision path was displayed. A 26" monitor was rotated to the portrait orientation to allow for a simultaneous front and top views of the upper thigh. Furthermore, this allowed us to scale the leg such

that it roughly matched the dimensions of an average upper thigh while having a one-to-one correlation between the actual and rendered stylus positions. The participants were asked to start each trial by making an incision close to the start location, which was marked by a green square. The participant would then "cut" through the start location and along a black line that represented the marking done by the surgeon before making an incision. The trial would end when the stop location, marked by a red square, was crossed. I displayed a trace of stylus location of the surface of the thigh in color red when each trial was completed.

The first task, the vein harvesting procedure, was used to evaluate SAHR's utility during long continuous motions (Figure 4.5). The participant was presented with one of the four long sinusoidal lines on the top or front of the upper thigh that marked the path of
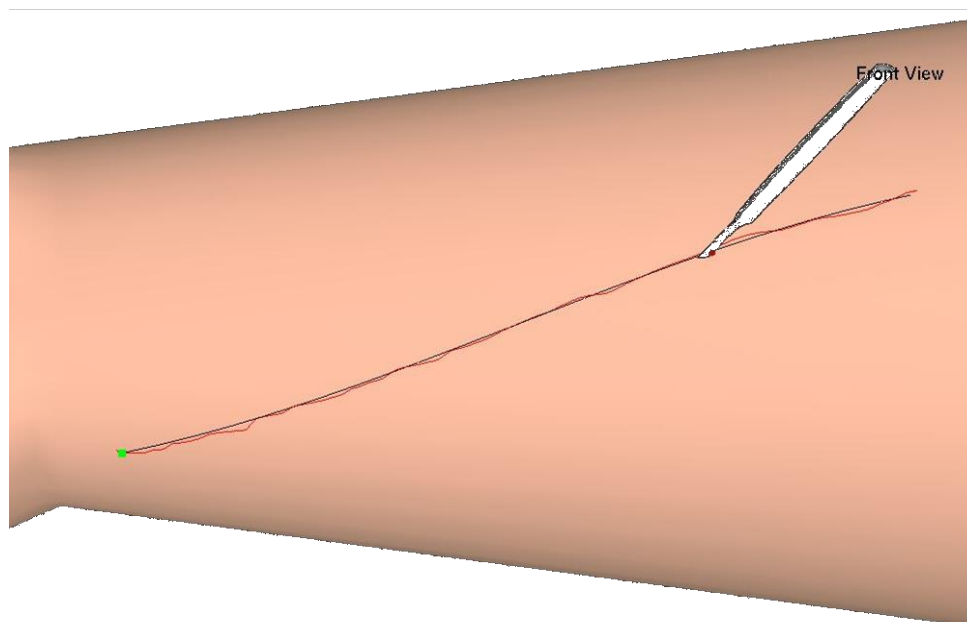

Figure 4.5 Rendered vein-harvesting simulation. The scalpel tip marked stylus position and could be moved by the participant. Note that this is a cropped section of what was displayed and the top view, which was displayed above this model, which was cropped to allow increased visibility.

the incision. I selected sinusoidal incision paths to resemble the path of the great saphenous vein. This path had a period of 2x the upper thigh length and an amplitude slightly less than the smallest rendered cross-section of the upper thigh. The stylus location was represented by a scalpel and a red dot on the tip of the scalpel signified the required depth of the incision that participants were instructed to maintain.

The second task, a simulated melanoma removal procedure, was used to evaluate the SAHR's utility during tasks that required multiple short and delicate movements at different locations (Figure 4.6). The diameter of each melanoma cancerous region was 15 or 22.5 mm, and these regions were located on a grid across the upper thigh model. The stylus was represented as a cauterizer and a red dot on the tool marked the required depth of cut.
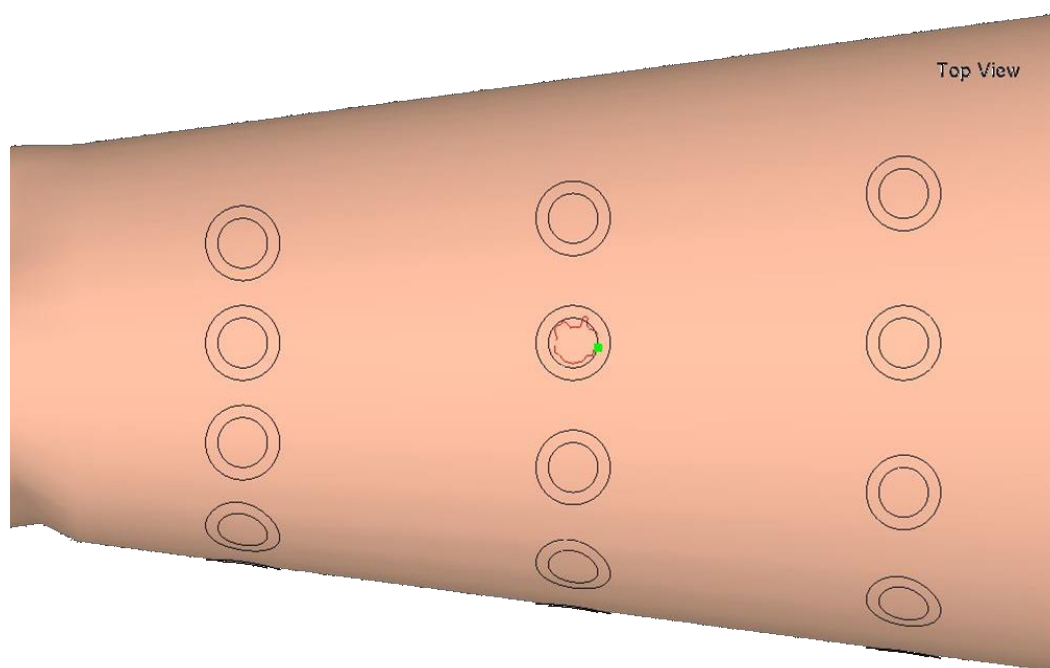

Figure 4.6 Rendered melanoma removal simulation. Note that this is a cropped section of what was displayed and the front view, which was displayed below this model and was cropped to allow increased visibility.

During Experiment 2, I measured participant's EMG muscle activities under both assisted and unassisted support conditions. I sampled EMG data at 1000 Hz, which is considered the functional Nyquist rate for surface EMG data analysis [39]. The following four muscles were used in our study: trapezius, lateral deltoid fiber, anterior deltoid fiber, and biceps. Research has shown that fatigue can typically be distinguished by a reduction in maximum voluntary contractions and/or a shift in the EMG's power spectrum though Fast Fourier Transform analysis (FFT) [40]. However, I do not expect large muscle exertions and lactic acid build up as our experiments involve low-level static contractions. Based on the findings of Jorgensen et al. on muscle activities during prolonged low-level static contractions [41], I looked at the changes in the root mean squared (RMS) EMG signals and mean spectral frequency muscle activity over the length of our experiment.

4.6 Experiment 1-A: Control Strategy Selection

Our goal in the first section of Experiment 1 was to evaluate multiple SAHR control strategies and select the control strategy that improves participants' overall performance beyond other control input strategies. I were interested in identifying a control strategy with the best balance of low mean error, low maximum error, and fast completion time. Furthermore, I used questionnaire data for subjective evaluation.

4.6.1 Methods

The support conditions used in Experiment 1-A were Basic, Poinsot, and FBA. A quick study was done to see the effect of rendering the drawing surface (stylus fixture) against not rendering it, which showed a reduction in accuracy without the rendered drawing

surface but no change in the trend between conditions. Hence, all control strategies in this experiment have stylus fixture rendering the drawing surface for participant's convenience and to help keep participants within the drawing plane for this spatial drawing task.

Twelve participants (three female), with an average age of 23 (ages 19 to 29), all right-hand dominant, took part in this experiment. Each participant completed 16 lines for each drawing plane per support condition. This experiment took an hour on average to complete.

4.6.2 Results and Discussion

Our analysis showed that control strategy was a significant predictor of mean error $(F[2,1620] = 5.508, p = 0.024)$ (Figure 4.7). The Basic control strategy had significantly higher mean absolute tracing error than the other two tested control strategies $(p < 0.001)$. The Freebody Acceleration (FBA) control strategy had lower numerical mean error, but
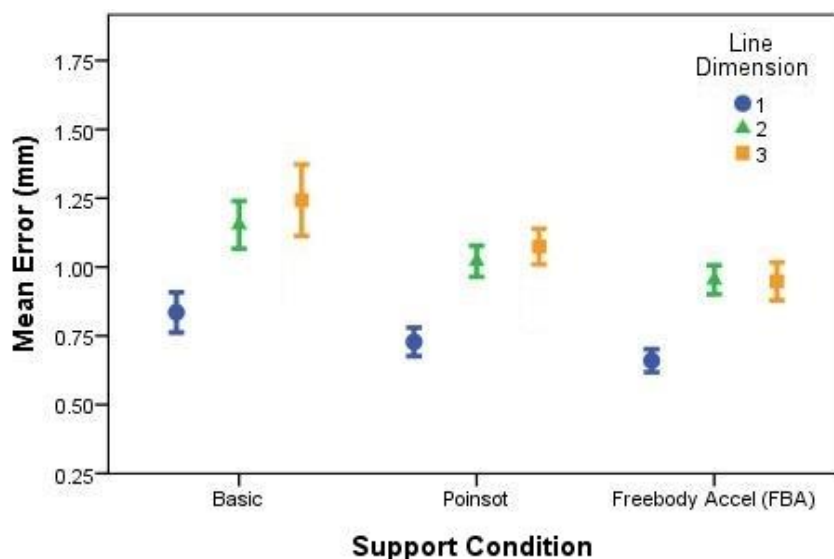

Figure 4.7 Mean absolute error categorized based on the tested control strategy and dimension of the tracing line. Three-dimensional lines spanned the body diagonal of a cube. All three tested control strategies have a stylus fixture (drawing surface) rendered for user's comfort.

the post hoc analysis showed no significant difference between the Poinsot and FBA control strategies (p = 0.417). Furthermore, the dimension of the tracing line was also found to be a significant predictor of the mean error (F[2,1620] = 50.932, p < 0.001), with lines that are parallel to one of the coordinate axes (one dimensional line) having significantly less mean error than lines that spanned 2 or 3 dimensions (p < 0.001), see Figure 4.8. The obtained data for maximum error show a possible trend, but did not highlight any control strategy as significant over others.

Similarly, I found the type of control strategy to be a significant predictor of trial completion time (F[2,1692] = 5.954, p < 0.001) (Figure 4.8). The time that it took participants to complete a trial using the Basic control strategy was significantly slower that FBA (p < 0.001). Once again I found FBA to have numerically faster, though not statistically significant completion time relative to Poinsot (p = 0.462).

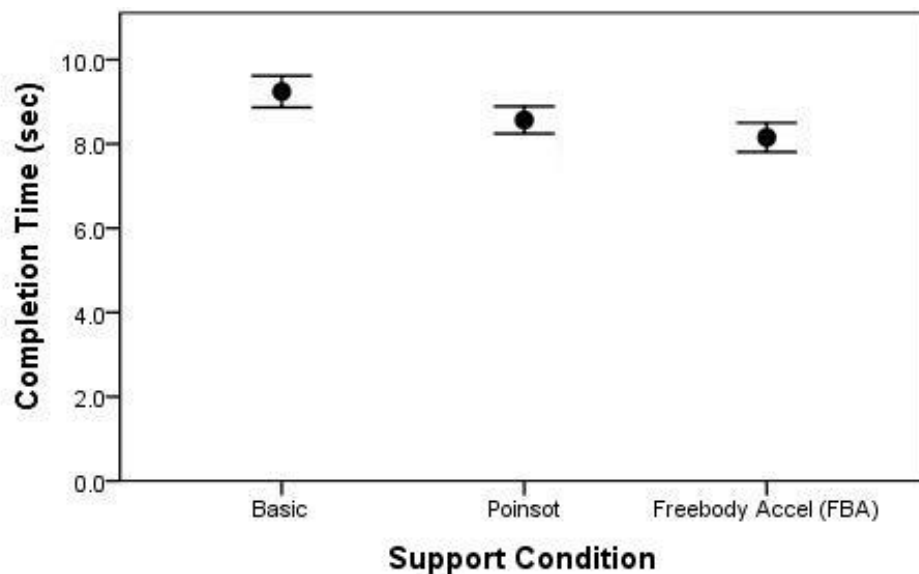Based on the questionnaire results, participants ranked FBA to have the most natural

Figure 4.8 Trial completion time across tested control strategies. All three control strategies have a stylus fixture (drawing surface) rendered for user's comfort.

movements (4.3 out of 5) and to allow them to perform the best (4.1 out of 5). Participants selected Poinsot control strategy as the second best control strategy on both accounts (4.0 out of 5 on natural movements, 3.8 out of 5 on performance). All participants felt slight to no exertion with all three tested control strategies (average of 1.2 point change in Borg scale).

The obtained results show that the Basic control strategy has the worst performance compared to the other two. Although no significant difference between FBA and Poinsot control strategies was observed, I selected the FBA to be the best control strategy to be used in subsequent experiments based on its numerically lower mean error, faster completion time, and perceived preference by participants.

4.7 Experiment 1-B: Virtual Fixture Selection

Experiment 1-B investigated virtual fixtures and their performance compared to each other in combination with the best SAHR control strategy from Experiment 1-A.

4.7.1 Methods

The support conditions used for the second section were 1) FBA (selected condition from Experiment 1-A minus the rendered of a drawing surface with a stylus fixture), 2) FBA + drawing surface stylus fixture (selected condition from Experiment 1-A), SAHR virtual fixtures, 3) Tangent Support fixture, 4) 3D Virtual Spring fixture, and 5) Tangent Support + Virtual Spring fixture. As it is a more realistic scenario to not have stylus fixtures in SAHR's potential future applications, no stylus fixtures or drawing surfaces were rendered in any of the support conditions with the exception of FBA + stylus fixture. This

exception was due to the need for a baseline of comparison between experiments 1-A and 1-B.

Ten participants (two females), average age of 23 (ages 19 to 30), all right-hand dominant, were used in this experiment. Each participant completed 16 lines for each drawing plane per support condition. This experiment took an hour and a half on average to complete.

4.7.2 Results and Discussion

I found support condition to be a significant predictor of mean error ($F[4,2368] = 13.207$, $p < 0.001$) (Figure 4.9). The FBA control strategy with no rendered (stylus fixture) drawing surface has a significantly higher mean error than the other tested support conditions ($p < 0.001$). Furthermore, adding a rendered drawing surface as a stylus fixture to the FBA or adding a Tangent Support fixture significantly reduces participant's mean error ($p < 0.001$). Lastly, adding a 3D Virtual Spring fixture to the FBA or Tangent Support
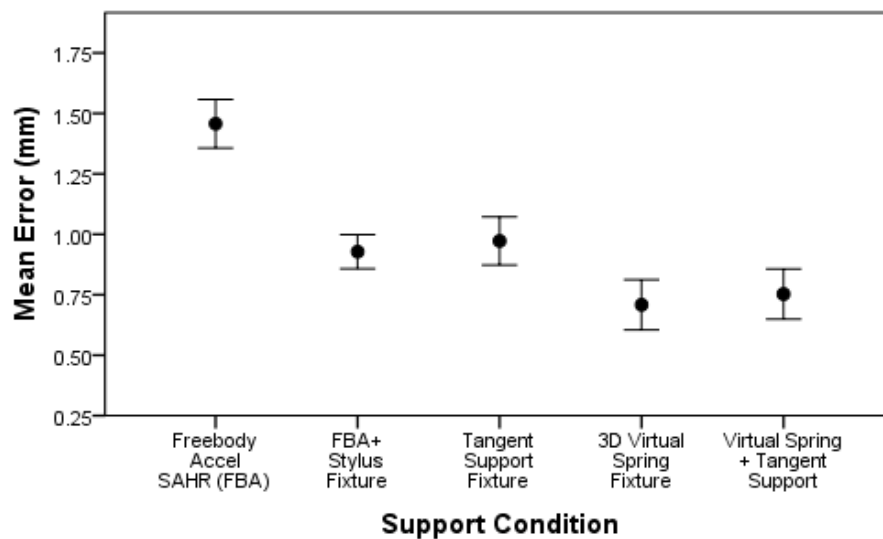

Figure 4.9 Mean absolute error categorized based on tested controllers.

fixture results in a further significant reduction of mean error (p < 0.001). Similar to Experiment 1-A, one-dimensional lines and lines along the four cardinal directions had a significantly lower mean error (p < 0.001). Maximum error results show no further distinction compared to the mean error.

I found the support condition to be a significant predictor of completion time (F[4, 2368] = 8.084, p < 0.001) (Figure 4.10). The FBA with no stylus fixture had a significantly slower completion time compared to the other tested support conditions. No significant differences between the other four support conditions' completion time were noticed. The questionnaire results showed that most participants rated FBA to have the most natural movements (4.2 out of 5) and FBA with stylus fixture as the second (3.9 out of 5). Participants perceived all three SAHR virtual fixtures to be unnatural (≤ 2.3 out of 5). On the other hand, participants reported that the SAHR's virtual fixtures allowed them to perform better (≥ 3.9 out of 5). This is expected, as the goal of virtual fixtures is to increase precision.
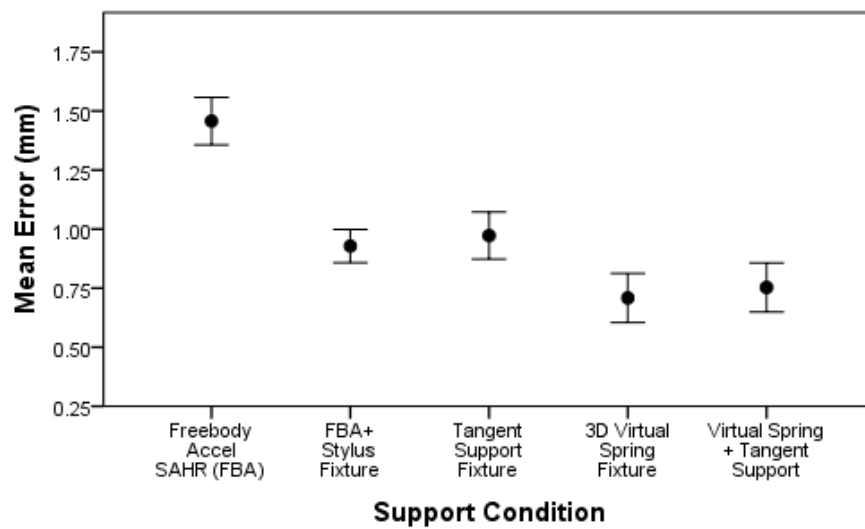

Figure 4.10 Mean absolute error categorized based on tested controllers.

These results agree with the previous study [2], that adding stylus fixture to a control strategy would increase a participant's tracing accuracy. Furthermore, I found that adding virtual fixture to the FBA in three-dimensional space also decreases participants' completion time. Based on this result, I plan to use Tangent Support and 3D Virtual Spring fixtures among the testing virtual fixtures for our next experiment. The Tangent Support + Virtual Spring support condition was eliminated, as it showed no further improvements over the 3D Virtual Spring fixture. I also eliminated the FBA + stylus fixture as having a drawing surface rendered on the stylus for the duration of a surgery or procedure was not a realistic scenario.

4.8 Experiment 2

Experiment 2 involved two simulated surgery simulation tasks that were matched to the design of the SAHR. These tasks were 1) vein harvesting surgery that requires a long continuous incision and 2) melanoma removal procedure that requires multiple short and delicate cuts at various locations. Our goal was to evaluate the performance of the SAHR in assisting in completing these tasks relative to nonrobotic support conditions.

4.8.1 Methods

The support conditions used in both experiments were freehand, table support, FBA (with no stylus fixture), Tangent Support fixture, and 3D Virtual Spring fixture. I used the same support conditions in both experiments to allow for a cross-comparison between the two. In the freehand support condition, the participant was completely unsupported throughout the experiment. The table support condition provided a table that the participant

could use to rest his/her elbow on as desired. I chose not to render any haptic forces to the user when the stylus (scalpel) and the leg model interacted to eliminate any possible unstudied effects. Furthermore, prior studies have shown the same general trends between active handrest support conditions with and without a stylus virtual fixture [2].

Each experiment took an average of an hour and a half to complete. Ten participants completed both experiments with each session on a separate day. The participants were asked to refrain from going to gym or doing anything strenuous before the experiment. All subjects were male and right-hand dominant with an average age of 25 (22 to 32).

4.8.2 Results and Discussions

I found support condition to be a significant predictor of mean error for both vein harvesting ($F[4,2361] = 12.928$, $p < 0.001$) and melanoma removal surgery simulations ($F[4,5268] = 11.773$, $p < 0.001$) (Figure 4.11). No significant difference between freehand
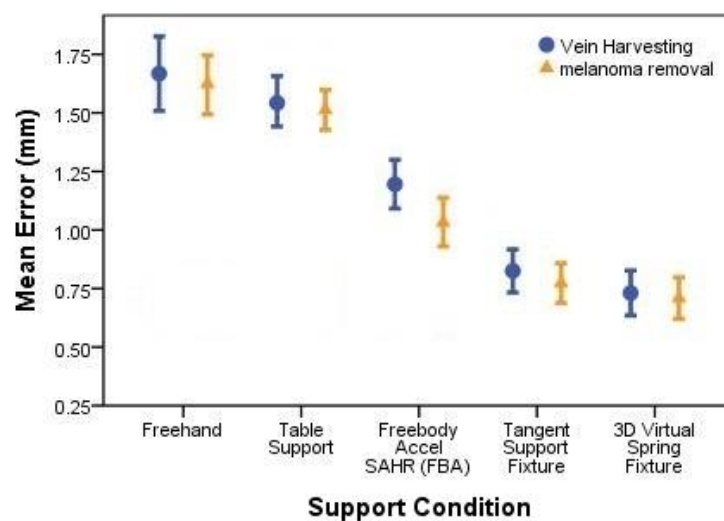

Figure 4.11 Mean absolute error categorized based on tested controllers and simulation task.

and table support condition was found in either surgery task (p = 1.000), and both

conditions had the highest mean error among the tested support conditions. Using the

SAHR's FBA control strategy significantly reduced participants' mean error (p < 0.001).

Adding virtual fixtures to the motion of the SAHR resulted in a further significant reduction

in the participants' mean error (p < 0.001). No significant difference in mean error between

vein harvesting and melanoma removal surgery tasks was observed. Maximum error results

show a similar trend to the mean error but have larger variance. The range of maximum

error values spanned from 5.23 mm on average for freehand and 2.58 mm for the SAHR

with 3D Virtual Spring fixture.

I found support condition to be a significant predictor of mean error for both vein

harvesting (F[4,2361] = 12.928, p < 0.001) and melanoma removal surgery simulations

(F[4,5268] = 11.773, p < 0.001) (Figure 4.12). No significant difference between freehand

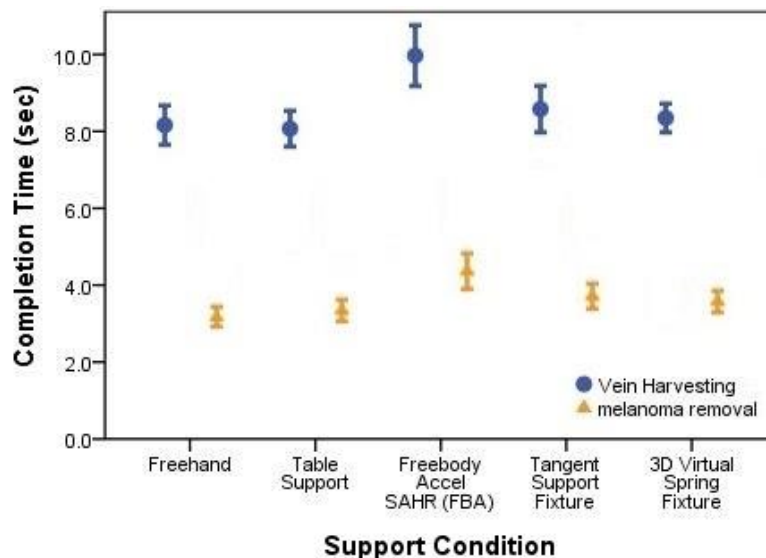and table support condition was found in either surgery task (p = 1.000), and both

Figure 4.12 Trial completion time across tested controllers and simulation tasks.

conditions had the highest mean error among the tested support conditions. Using the SAHR's FBA control strategy significantly reduced participants' mean error (p < 0.001). Adding virtual fixtures to the motion of the SAHR resulted in a further significant reduction in the participants' mean error (p < 0.001). No significant difference in mean error between vein harvesting and melanoma removal surgery tasks was observed. Maximum error results show a similar trend to the mean error but have larger variance. The range of maximum error values spanned from 5.23 mm on average for freehand and 2.58 mm for the SAHR with 3D Virtual Spring fixture.

Table 4.1 presents the questionnaire results in a tabular form. Similar to our previous findings, participants perceive FBA to have the most natural movements among the SAHR support conditions (4.1 out of 5). Most participants expressed a large increase in perceived exertion levels when using the freehand (8.2) and table support (7.6) conditions compared to assisted SAHR conditions (< 2.9).

From the four measured muscle activities, the EMG signal from the trapezius and lateral deltoid muscles showed a significant increase in root mean squared of EMG signal over 15 minutes for both freehand and table support conditions (p < 0.001) (Figure 4.13). On the other hand, no increase in muscle activity was observed when using the SAHR

Table 4.1 Participant's average perceived questionnaire answers.

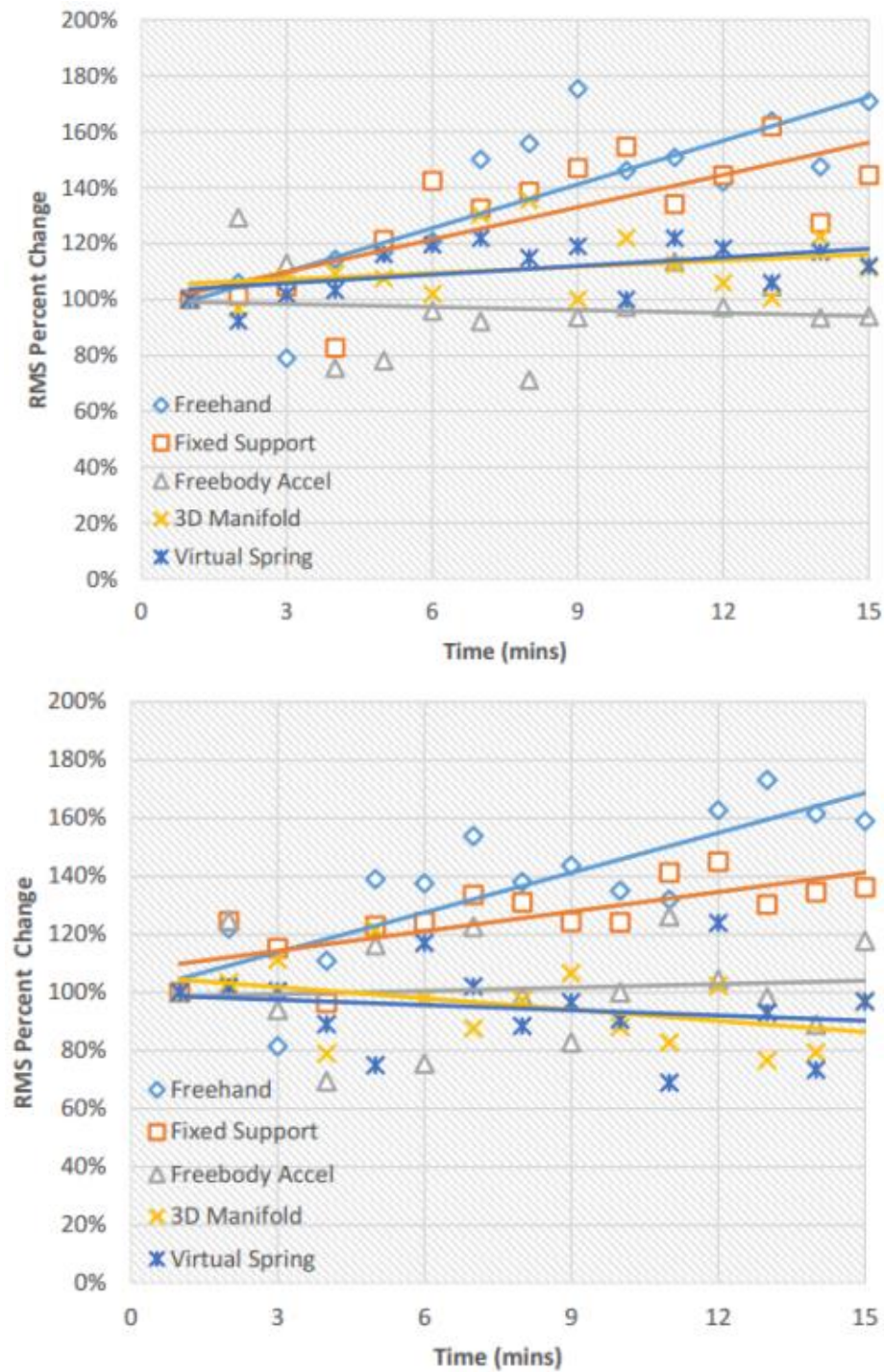| Question / Support Condition	How natural were movements?	How well did you perform?	Change in borg's scale fatigue
Freehand	5	1.3	8.2
Table Support	5	1.4	7.6
Freebody Accel SAHR (FBA)	4.1	3.1	1.7
Tangent Support Fixture	1.9	4.2	2.9
3D Virtual Spring Fixture	2.2	4.5	2.1

Figure 4.13 EMG signal from trapezius (top) and lateral deltoid fiber (bottom) over a 15-minute period for each tested support condition.

assisted conditions. The EMG muscle activities of the interior deltoid and biceps muscles showed no significant difference between the tested support conditions and was hence not shown in Figure 4.13. Furthermore, the FFT analysis showed no change in muscle motor rate of fire. I think that this is due to the short length of our experiment and its low-level task exertion, which results in no lactic acid build up. These results support our hypothesis that the SAHR reduces muscle activity of larger muscle groups in the shoulder, which could allow for smaller muscles groups and joints to be involved in operating the device that is shown to be desired [6].

The obtained results demonstrate that the SAHR can improve participant's accuracy performance beyond unassisted support conditions. Furthermore, adding a virtual fixture further improves a user's accuracy while matching the completion time of unassisted support conditions. However, virtual fixtures do have their disadvantages. The 3D Virtual Spring fixture requires knowing the position of the grasped tool, which could be costly to implement. Similarly, the Tangent Support fixture also requires geometric knowledge of the operating surface. However, it should be noted that emergence of consumer 3D scanners may make this more practical in the future.

4.9 Conclusion and Future Work

I presented the Spatial Active Handrest (SAHR), a novel assistive device that provides gravity compensation and ergonomic support over a large three-dimensional workspace. Possible applications of this device are assistive robotic surgery, surgery training and simulation, and upper extremity rehabilitation. The Freebody Acceleration (FBA) control strategy was selected between two other control strategies for having significantly higher

accuracy and faster completion time in a three-dimensional line tracing experiment. The same experiment was used to evaluate various virtual fixtures. Finally, I used a simple surgery simulation task to compare assisted SAHR support conditions with unassistedconditions. The results show that the Freebody Acceleration control strategy significantly decreases participants' absolute mean tracing error ($p < 0.001$) beyond freehand and table support conditions. Furthermore, the addition of virtual fixtures to the SAHR significantly reduced participants' mean absolute error over other tested assisted and unassisted conditions ($p < 0.001$) while having no significant reduction in completion time ($p > 0.2$). An electromyography analysis of four muscle groups confirms our hypothesis that the SAHR reduces fatigue in contrast to unassisted support conditions, which exhibited an increase in root mean squared of muscle activity over 15 minutes.

In future work, I would like to investigate the following modifications: 1) redesign the SAHR to be more portable and accommodating of users of different sizes and heights, 2) improve the surgery simulator to allow for more experiments to demonstrate the SAHR's benefits as a surgery training device, and 3) conduct a clinical study with patients in need of rehabilitation to investigate rehabilitation capabilities of the device.

4.10 Acknowledgment

4.11 References

[1]   M. Fehlberg, G. Gleeson, and W. Provancher, "Active Handrest: A large workspace tool for precision manipulation," *Int. J. Robotics Research,* vol. 31, no. 3, pp. 289-

301, 2012.

[2]   M. Fehlberg, R. King, A. Doxon, and W. Provancher. "Evaluation of Active Handrest performance using labyrinths with adaptive admittance control and virtual fixtures." *IEEE Haptics Symposium*, pp. 273–80, 2012.

[3]   M. Fehlberg, H. N.Sani, and W. Provancher, "Enhancement to the Planar Active Handrest," *J. Human-Robot Interactions*, 2015.

[4]   C A. Stewart, "A Vertical Active Handrest to Aid in Dexterous Tasks and to Provide Gravitational Support," M.S. thesis, Mech Eng., Univ. Utah., Salt Lake City., UT, 2012.

[5]   S. Ito and Y. Yokokohji, "Maneuverability of master control devices considering the musculo-skeletal model of an operator," Proc. World Haptics, 2009.

[6]   N. Forestier, and V. Nougier. "The Effects of Muscular Fatigue on the Coordination of a Multijoint Movement in Human," Neuro. Letters 252, no. 3, pp. 187–190, 1987.

[7]   J. Knierim. "Motor units and muscle receptors" *Neuro. Online*. [On-line]. Available: http://neuroscience.uth.tmc.edu/s3/chapter01.html, 2012.

[8]   T. McMorris, and T. Rayment, "Short-duration, high-intensity exercise and performance of a sports-specific skill: a preliminary study," *Percep. Motor Skills*, vol. 105, no. 2, pp. 523–530, 2007.

[9]   D. Hornery, D. Farrow, I. Mujika, and W. Young, "Fatigue in tennis: Mechanisms of fatigue and effect on performance." *Sports Med.* vol. 37, no. 3 pp. 199–212, 2007.

[10]   C. Cook and R. Burgess-Limerick, "The effect of forearm support on musculoskeletal discomfort during call centre work." *App. Ergo*, vol. 35, no. 4 pp. 337–342, 2004.

[11]   Y. Feng, W. Grooten, P. Wretenberg, and U. P. Arborelius. "Effects of arm support on shoulder and arm muscle activity during sedentary work." *Ergo*, vol. 40, no. 8 pp. 834–848, 1997.

[12]   M. J. Rose, "Keyboard operating posture and actuation force: implications for muscle over-use." *Applied Ergo*, vol. 22, no. 3, pp. 198–203, 1991.

[13]   A. rdelyil, T. Sihvonen, P. Helin, and O. Hänninen. "Shoulder strain in keyboard workers and its alleviation by arm supports." Int. Arch. Occup. Environ. Health. vol. 60, no. 2, pp. 119–124, 1998.

[14]   Equipois   zeroG   Demonstration,   2011.
www.youtube.com/watch?v=UOk3hIt_SZY&feature=youtube_gdata_player.

[15]   S. B. Chyatte, C. Long, and P. J. Vignos. "The balanced forearm orthosis in
muscular dystrophy." *Arch. Phys. Med. Rehab*, vol. 46, no. 9, pp. 633–636, 1969.

[16]   Y. Yasuda, K. Bowman, and J. D. Hsu. "Mobile arm supports: Criteria for
successful use in muscle disease patients." *Arch. Phys. Med. Rehabil.*, vol. 67, no.
4, pp. 253–56, 1986.

[17]   T. Nef, G. Marco, and R. Riener. "ARMin III – Arm therapy exoskeleton with an
ergonomic shoulder actuation." *Applied Bio. Biomech.*, vol. 6, no. 2, pp. 127–42,
2009.

[18]   N. Hogan, H. I. Krebs, A. Sharon, and J. Charnnarong. "Interactive Robotic
Therapist," U.S. Patent 5466213 A, issued Nov 14, 1995.

[19]   L. Rui, F. Amirabdollahian, M. Topping, B. Driessen, and W. Harwin. "Upper limb
robot mediated stroke therapy—GENTLE/s approach." *Auto. Robots,* vol. 15, no.
1, pp. 35–51, 2003.

[20]   P. S. Lum, C. G. Burgar, P. C. Shor, M. Majmundar, and M. Van der Loos, "Robot-
assisted movement training compared with conventional therapy techniques for the
rehabilitation of upper-limb motor function after stroke," *Arch. Phys. Med.
Rehabil.*, vol. 83, no. 7, pp. 952–959, Jul. 2002.

[21]   R. Taylor, P. Jensen, L. Whitcomb, A. Barnes, R. Kumar, D. Stoianovici, P. Gupta,
Z. Wang, E. Dejuan, and L. Kavoussi, "A steady-hand robotic system for
microsurgical augmentation," *Int. J. Robotics Research*, vol. 18, no. 12, pp. 1201–
1210, Dec. 1999.

[22]   G. Zeng and A. Hemami, "An overview of robot force control," *Robotica*, vol. 15,
no. 05, pp. 473–482, 1997.

[23]   N. Hogan, "Impedance control: an approach to manipulation," in *American Control
Conf.,* 1984, pp. 304–313.

[24]   R. Colombo, F. Pisano, S. Micera, A. Mazzone, C. Delconte, M. C. Carrozza, P.
Dario, and G. Minuco, "Robotic techniques for upper limb evaluation and
rehabilitation of stroke patients," *IEEE Trans. Neural Syst. Rehabil. Eng.*, vol. 13,
no. 3, pp. 311–324, 2005.

[25]   M. Nambi, W. R. Provancher, and J. J. Abbott, "On the ability of humans to apply
controlled forces to admittance-type devices," *Adv. Robotics*, vol. 25, no. 5, pp.
629–650, 2011.

[26]   S. P. Wise and R. Shadmehr, "Motor Control," in *Encyclopedia of the Human Brain*, vol. 3, pp. 137–157, 2002.

[27]   A. Bettini, P. Marayong, S. Lang, A. Okamura, and G. D. Hager, "Vision-assisted control for manipulation using virtual fixtures," *IEEE Trans. Robotics*, vol. 20, no. 6, pp. 953–966, Dec. 2004.

[28]   J. J. Abbott, P. Marayong, and A. M. Okamura, "Haptic virtual fixtures for robot-assisted manipulation," *Robotics Res.*, pp. 49–64, 2007.

[29]   D. Tolani and N. I. Badler, "Real-time inverse kinematics of the human arm," *Presence (Camb)*, vol. 5, no. 4, pp. 393–401, 1996.

[30]   T. Kang, Y. Shimansky, and J. He, "Angle of elbow elevation depends on the reach target coordinates," *Eng. Med. Bio., 2002. Proc. Second Joint*, 2002, vol. 3, pp. 2571–2572, 2002.

[31]   S. Kim, C. H. Kim, and J. H. Park, "Human-like arm motion generation for humanoid robots using motion capture database," in *2006 IEEE/RSJ Int. Conf. Intelli. Robots Syst.*, pp. 3486–3491, 2006.

[32]   D. Straumann, T. Haslwanter, M.-C. Hepp-Reymond, and K. Hepp, "Listing's law for eye, head and arm movements and their synergistic control," *Exp Brain Res*, vol. 86, no. 1, pp. 209–215, Aug. 1991.

[33]   J. F. Soechting, C. A. Buneo, U. Herrmann, and M. Flanders, "Moving effortlessly in three dimensions: does Donders' law apply to arm movement?," *J. Neurosci.*, vol. 15, no. 9, pp. 6271–6280, Sep. 1995.

[34]   S. Plagenhoef, F. G. Evans, and T. Abdelnour, "Anatomical data for analyzing human motion," *Res. Quarterly Exer. Sport*, vol. 54, no. 2, pp. 169–178, 1983.

[35]   F. Conti, F. Barbagli, D. Morris, and Sewell, "CHAI three-dimensional: an open-source library for the rapid development of haptic scenes," *IEEE World Haptics*. 2005.

[36]   R. M. Murray, Z. Li, and S. S. Sastry, A mathematical introduction to robotic manipulation. Boca Raton: CRC Press, 1994.

[37]   G. Borg, "Psychophysical bases of perceived exertion." *Med. Sci. Sports Exercise*, vol. 14.5, pp. 377-381, 1982.

[38]   G. Borg, "Psychophysical scaling with applications in physical work and the perception of exertion," *Scandinavian J. work, environ. health*, pp. 55-58, 1990.

[39]   J. C. Ives and J. K. Wigglesworth, "Sampling rate effects on surface EMG timing and amplitude measures," *Clinical Biomechanics*, vol. 18, no. 6, pp. 543–552,

2003.

[40] B. Bigland-Ritchie, E. F. Donovan, and C. S. Roussos, "Conduction velocity and EMG power spectrum changes in fatigue of sustained maximal efforts," *J Appl Physiol Respir Environ Exerc Physiol*, vol. 51, no. 5, pp. 1300–1305, Nov. 1981.

[41] K. Ito and Y. Hotta, "EMG-based detection of muscle fatigue during low-level isometric contraction by recurrence quantification analysis and monopolar configuration," *2012 Ann. Int. Conf. IEEE Eng. Med. Bio. Society (EMBC)*, pp. 4237–4241, 2012.

CHAPTER 5

CONCLUSION

This research presented three studies to demonstrate a three-dimensional human-robot cooperative manipulator that assists users with tasks that require dexterous motions. The first study investigates the improvements of the force-based admittance controller beyond other tested support conditions with the help of gravity compensation and localized support. The first experiment fine-tuned the admittance gain of the force controller and found an admittance gain of 10 mm/s/N to have the best user accuracy and skill level improvements. Further investigation on position-based controllers also demonstrated that adding a high elastic isometric controller further improves position-based controllers. In the next experiment, the force-based admittance controllers were compared to the best elastic controller. Some modifications were added to improve the force-based admittance performance. The results showed that adding a forearm support significantly improved participants mean median tracing error ($p < 0.001$). Furthermore, strapping the user's arm to the stage allowed for applying upward force or using an admittance gain that scaled based on the user's arm weight. This modification could further improve the force-based controller's accuracy to match the isometric elastic controller. Due to these findings and the elastic controller's significantly slower trial completion time ($p < 0.001$), the force-based controller with a strap was selected as the best controller to use in the final evaluation

of the VAHR. The last experiment compared the best stage support condition to unassisted conditions (freehand and fixed elbow). The results show that a force-based admittance controller improves a user's skill level beyond the unassisted cases.

The second study enhanced the planar workspace of the planar active handrest by adding a third degree-of-freedom to allow forearm rotation and better match the kinematics of the human arm. The main goal was to improve the devices comfort and workspace but maintain the accuracy improvements that the planar active handrest controllers provided. With this goal in mind, seven control strategies were proposed to allow users to naturally control the stage through the two available force sensors. Two studies were conducted to improve and compare these controllers, which showed the simplest controllers, Instantaneous Center of Rotation, and Freebody Acceleration to have the best balance of accuracy, completion time, and comfort. Lastly, these best controllers were compared to performance when completing a task via freehand and while assisted by the PAHR. The results show that the E-PAHR controllers outperform freehand's accuracy and match the performance of Planar Active Handrest with the added benefit of an enhanced and more natural workspace.

The third and last study combined our findings from the previous studies and developed a four-degree-of-freedom stage that further enhanced the workspace of E-PAHR to the third dimension. A motion capture study was conducted to improve the understanding of the human arm motion and to design a device that provided an ergonomic support throughout its workspace. The results showed a high linear correlation ($R^2 = 0.822$) between the elbow and hand elevation. This result was used to design the Spatial Active Handrest (SAHR) by adding a single elevation degree-of-freedom to the E-PAHR. Three

control strategies and virtual fixtures were proposed and evaluated. To test the device utility, a surgical simulation was used to evaluate users' performance when aided by the SAHR. The results showed that the Spatial Active Handrest was able to improve users' accuracy and skill level beyond other unassisted support conditions. Furthermore, an EMG analysis of the upper arm and shoulder muscles showed no changes in muscle activities while using the SAHR and an increase in root mean square absolute muscle activity during unassisted support conditions, which is a sign of fatigue.

5.1 Future Work

The active handrest's utility was demonstrated throughout this research. Future work should focus on simplification and testing the device for possible future applications. The first and most important change is to redesign the stage to be smaller and better able to accommodate various users' height, size, and shapes. The second objective would be to test this device for other possible applications such as surgery simulations or rehabilitation. The implemented surgery environment that was developed in this research can be expanded upon and tested by medical students. In addition, our device could be modified slightly to accommodate users with disabilities or users that require rehabilitation. Clinical trials with users that require rehabilitation can be beneficial to demonstrate the device's ability to help users regain lost motor skills or assist them with daily tasks.